論文 / 著書情報
Article / Book Information

題目(和文)	マイクロ流路とエマルションを用いた機能性アルギン酸カルシウムハイドロゲル粒子の生成とその応用
Title(English)	Microfluidic emulsion-based synthesis of functional calcium-alginate hydrogel particles and their applications
著者(和文)	LIUYingzhe
Author(English)	Yingzhe Liu
出典(和文)	学位:博士(工学), 学位授与機関:東京工業大学, 報告番号:甲第11741号, 授与年月日:2022年3月26日, 学位の種別:課程博士, 審査員:西迫 貴志,初澤 毅,進士 忠彦,柳田 保子,石田 忠
Citation(English)	Degree:Doctor (Engineering), Conferring organization: Tokyo Institute of Technology, Report number:甲第11741号, Conferred date:2022/3/26, Degree Type:Course doctor, Examiner:,,,,
学位種別(和文)	博士論文
Category(English)	Doctoral Thesis
種別(和文)	要約
Type(English)	Outline

東京工業大学

令和 4 年 2 月 博士論文

Microfluidic emulsion-based synthesis of functional calcium-alginate hydrogel particles and their applications

指導教員： 西迫 貴志 准教授

工学院 機械系 機械コース

劉英哲 Yingzhe LIU

Table of Contents

Chapter 1. Introduction

Chapter 2. Microfluidic emulsion-based synthesis of calcium-alginate hydrogel particles

Chapter 1
Introduction

1.1 Background

This thesis is focusing on the microfluidic generation of different kinds of functional alginate-based hydrogel particles that have great potentials in the physical, chemical, and biological fields. Such hydrogel microparticles have attracted great attention because of their ability to realize specific applications in functional coating, oil recovery, drug delivery, cell encapsulation, tissue engineering, cosmetics, personal care, and foods.

Microfluidic devices are a kind of extremely small-scale systems that may be used to make monodisperse, homogenous hydrogel microbeads along with single and double emulsions. for laboratory-scale testing. Up to date, various microfluidics technology has been used for preparing functional alginate-based hydrogel particles.

However, the previously reported microfluidic methods for synthesizing alginate hydrogel microbeads are more or less existing certain shortages, such as the clogging issues, polydispersity, and deformation of obtained gel particles, difficulties in achieving a large-scale production output. In addition, the applications of alginate hydrogels (e.g. microencapsulation) still have great uncovered potentials that are worth further exploration and research.

In this thesis, a novel microfluidic emulsion-based external gelation applied in a diverse microfluidic device was presented to produce monodisperse highly spherical calcium alginate (Ca-alginate) microparticles, Janus Ca-alginate microbeads, Ca-alginate microspheres with functional coatings, and Ca-alginate microbeads with a high-volume output. Further, a new application of the Ca-alginate microcapsules for the antifouling coatings is also demonstrated.

This chapter briefly introduces the background and recent researches of hydrogel particles and microfluidics technology. Also, the main objectives of this thesis are described.

1.2 Hydrogel

1.2.1 Definition

A nonfluid colloidal network or polymer network that is extended across its whole volume by a dispersion solution is referred to as gel [1]. Considering the type of dispersion medium, the gel materials can be classified into hydrogel and aerogel. An aerogel is a solid made from a gel that has been dried without shrinking. Aerogels typically have a high proportion of pores (15–50%) and a relatively tiny mesh size (1–10 nm), as well as a large surface area (150–900 m^2/g). The network does not shrink when the solvent is removed under supercritical circumstances, resulting in a highly porous, low-density material. On the other hand, A hydrogel, also known as a colloidal gel, is a network of polymer chains in which water acts as the dispersion medium (**Fig. 1.1**). The hydrophilic polymer chains are bound together by cross-links, resulting in a three-dimensional solid. The structural integrity of the hydrogel network is not dissolved by the high concentration of water because of the intrinsic cross-links. Hydrogels are natural or manmade polymeric networks that are very absorbent (they may hold over 90% water).

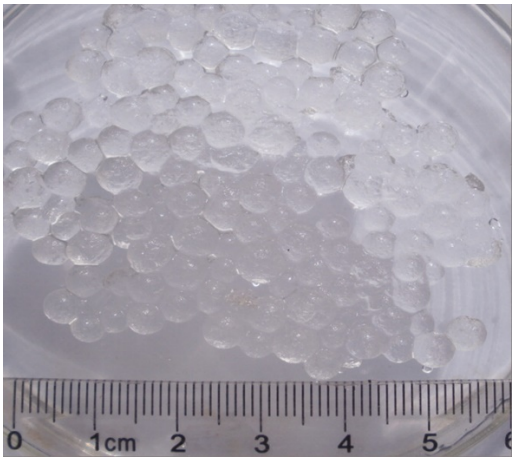

Fig. 1.1 A photograph of hydrogel balls. Reproduced with permission [2]. Copyright 2011 Wiley-VCH.

1.2.2 Application

Polymer gels have several applications in a number of industries. Diverse varieties of polymer (crosslink) gels are likely to see increased demand due to their distinct and discrete features that

meet the needs of various end-users such as sanitation, medication delivery systems, packaging, tissue engineering, and others [3]. The growing global population, as well as increased attention to healthcare, will fuel demand for polymer gels. Healthcare reforms have been towards the top of many national agendas to meet the needs of the people for sustainable and safe living. Such developments indicate that crosslink gels will be in more demand in the near future [3].

Hydrogels are the leading segment of the polymer gel market which is expected to grow by more than 6.7% (**Fig. 1.2**). The hydrogel market is promising due to its high absorption capabilities, they are used in medical applications, personal care and electronics, agriculture, and other fields. Soft contact lenses and agricultural uses, for example, will be emerging areas of investigation for hydrogels. The eye-care sector has been working hard to develop treatments that improve corneal oxygenation. Silicone hydrogels are in high demand because of their improved oxygen permeability, comfort, and wettability.

Fig. 1.2 An insight of the polymer gel market [4].

In addition, hydrogel materials have great prospects in the treatment of dry chronic wounds. They will form a moist protective layer on the wound to promote wound healing. Hydrogel-based wound dressings have the advantages like quick absorption of wound debris and exudate, removal of devitalized tissue, and the ability to soften dry tissues. Because of their cooling and moisturizing properties, these cross-linked gels are especially useful in the treatment of acute burns. It is worth noting that particle forms such as granules, micro-particles, and powders

accounted for a sizable portion of the polymer gel market, because of their broad usage in a wide range of fields such as agriculture, personal care, and so on.

1.2.3 Classification

The hydrogel products may be classed on a variety of criteria. The hydrogels in this chapter are classified according to their composition and kind of chemical reaction [5] (**Fig. 1.3**).

1.2.3.1 Polymeric composition

(1) Homopolymer hydrogel

The hydrogel could be formed from only one species monomer which is called homopolymers. It is the most basic structural unit in any polymer network [6]. Determined by the nature of the monomer and the polymerization process, homopolymers might just have a cross-linked skeletal structure. The typical homopolymer materials include polyvinyl alcohol (PVA), polyacrylic acid (PAA), polyvinyl pyrrolidone (PVP), and polyethyleneglycol (PEG),.

(2) Co-polymeric hydrogel

Co-polymeric hydrogels are made up of two or more kinds of monomer species, one of which is natively hydrophilic and is organized in a random, block, or alternating pattern along the chain of the polymer network [7]. The examples of the co-polymeric hydrogel are PEG-PVA, PEG-PVP, and so on.

(3) Multi-polymer interpenetrating polymer network (IPN) hydrogels

IPN hydrogels are a kind of hydrogel that is composed of two separate native and/or synthesized polymer materials that are contained in a cross-linking shape [5]. Typically, a hydrogel is added to the mixture of monomers as well as a polymerization trigger. Furthermore, A cross-linked polymer makes up one part of semi-IPN hydrogels, while a non-cross-linked polymer makes up the other. The key benefits of IPNs are that they can build thick hydrogel networks with stiffer and harder mechanical characteristics, tunable physical features, and effective loading of drugs [8].

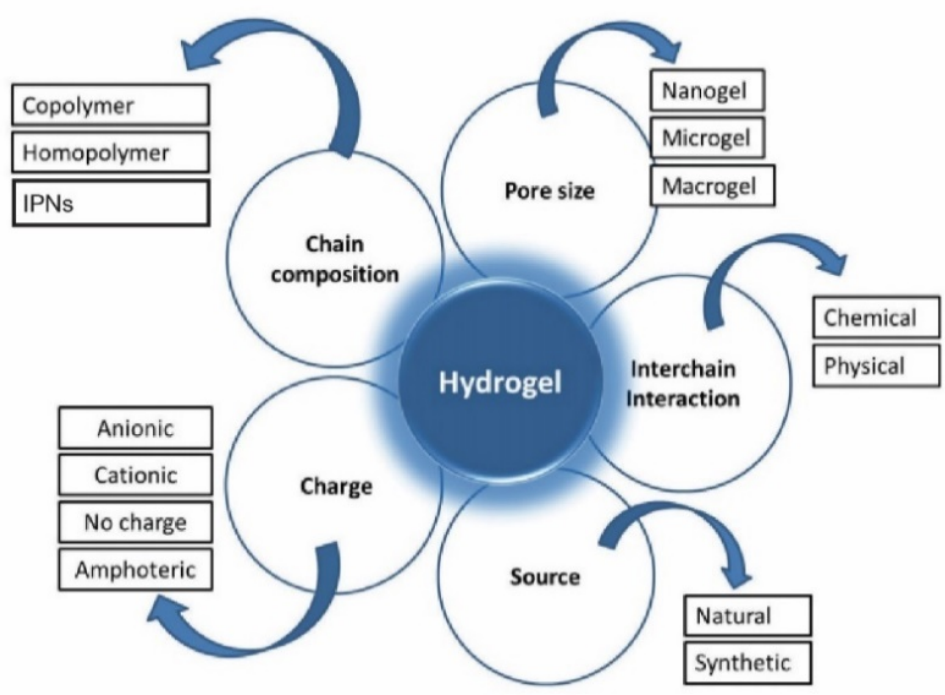

Fig. 1.3 Classification of polymer hydrogels based on composition and chemical reaction. Reproduced with permission [9]. Copyright 2019 SciELO.

Polysaccharides are a kind of polymer that may be employed as a building component in IPN hydrogels. They are used for the construction of IPN having specialized qualities because of their availability, cheap cost of manufacture, unusual and complicated features. Furthermore, the functional groups found in polysaccharides may be exploited for chemical transformation, which results in novel polymer materials, such as structures formed via chain crosslinking. Alginate and hyaluronic acid are the most researched polysaccharides that are extremely appropriate for the creation of IPN hydrogels.

1.2.3.2 Cross-linking type

There are two kinds of hydrogels based on the composition of their cross-linked reactions. Permanent junctions exist in chemically cross-linked networks, while transitory junctions occur in physical networks as a result of polymer chain interconnections or physical reactions such as ionic contacts, hydrophilic or hydrophobic interactions. **Table 1.1** depicts typical ways of producing chemical and physical hydrogels.

Table 1.1 Typical ways for producing chemical and physical hydrogels [10]

Methods	Example
Physical hydrogels	
· Heat a polymer solution	· Poly(ethylene oxide)-poly(propylene oxide)-poly(ethylene oxide) (PEO-PPO-PEO) in H_2O
· Cool a polymer solution	· Gelatin or agarose
· Freeze-thaw cycles	· PVA
· Forming bonded gel at low pH	· PEO and poly(acrylic acid)
· Polyanion + polycation	· Na-alginate + polylysine
· Polyelectrolyte liquids with ions	· alginate$^-$ + Ca^{2+}
Chemical hydrogels	
· Radiation	· PEO
· Multi-functional reactive compounds	· Poly(ethylene glycol) + diisocyanate
· Crosslinkers	· Glutaraldehyde + collagen
· Copolymerize a monomer + crosslinker	· Hydroxyethyl methacrylate + ethylene glycol dimethacrylate
· Copolymerize a monomer + multifunctional macromer	· Poly(lactic acid)- PEO- Poly(lactic acid) + photo-sensitizer + light radiation

1.2.4 Alginate-based hydrogel

1.2.4.1 Alginate

Alginate, typically in the form of Na-alginate, is a natural polymer present in all brown algae species, including *Macrocystis pyrifera*, *Ascophyllum nodosum*, *Laminaria hyperborean*, *Laminaria digitate*, and *Laminaria japonica* [11] by treatment with an aqueous alkaline solution, usually using sodium hydroxide. Alginate has piqued the interest of researchers in the biological and chemical fields due to its biocompatibility, biodegradability, and non-toxic property.

The most important part of alginate is D-mannuronate and L-guluronate residue. Alginates are basically bulk polymers, according to the fractions of precipitation with calcium salts and manganese, and the guluronate-mannuronate proportion changes determined by the natural source. Alginate is currently understood to be a class of polymers composed of (1,4)-linked β-D-mannuronate (M) and α- L-guluronate (G) residues (**Fig. 1.4**).

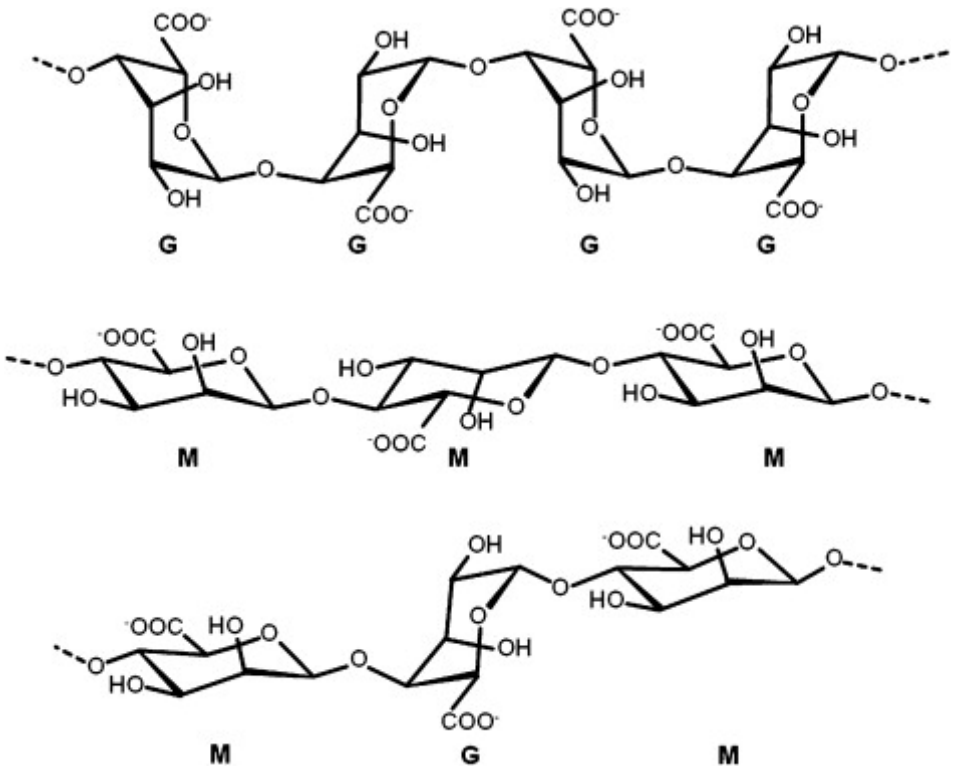

Fig. 1.4 M-block, G-block, and alternating block in alginate. Reproduced with permission [11]. Copyright 2012 Elsevier.

G-blocks are thought to contribute to the formation of hydrogels by cross-linking reaction with metal cations (e.g., Ca^{2+}). The sequence, constitution, molecular mass, and G-block length are therefore essential parameters influencing the physical characteristics and formed hydrogel properties of alginate.

1.2.4.2 Alginate-based hydrogel

In contrast to other polysaccharides like agar or gelatin, alginate can create hydrogel regardless of temperature. Alginate hydrogels are categorized into two types based on the method of crosslinking: “physical/reversible” hydrogels or “chemical/permanent”.

(1) Physical alginate hydrogels

Metal ionic crosslinking

Alginate-based hydrogels with a cross-linked structure comparable to extracellular matrices in tissues are now extensively exploited as useful instruments for controlled drug administration

[16,17], tissue healing [14,15], and biomedical sensing [12,13]. The most popular method for producing alginate hydrogel is to mix alginate aqueous solution with divalent cations (e.g., calcium ions Ca^{2+}, **Fig. 1.5**). The development of alginate-based hydrogels offers various benefits 18,19. The cross-linking response is quick. (ii) Na-alginate polymer is inexpensive and simple to produce. (iii) Alginate hydrogels are readily digestible and can be eliminated by chelators such as ethylenediaminetetraacetic acid (EDTA). (iv) The gelation may be controlled at room temperature, resulting in a simple operating system that is safe and mild. (v) Alginate hydrogels are thermostable and their mechanical properties are easily adjustable.

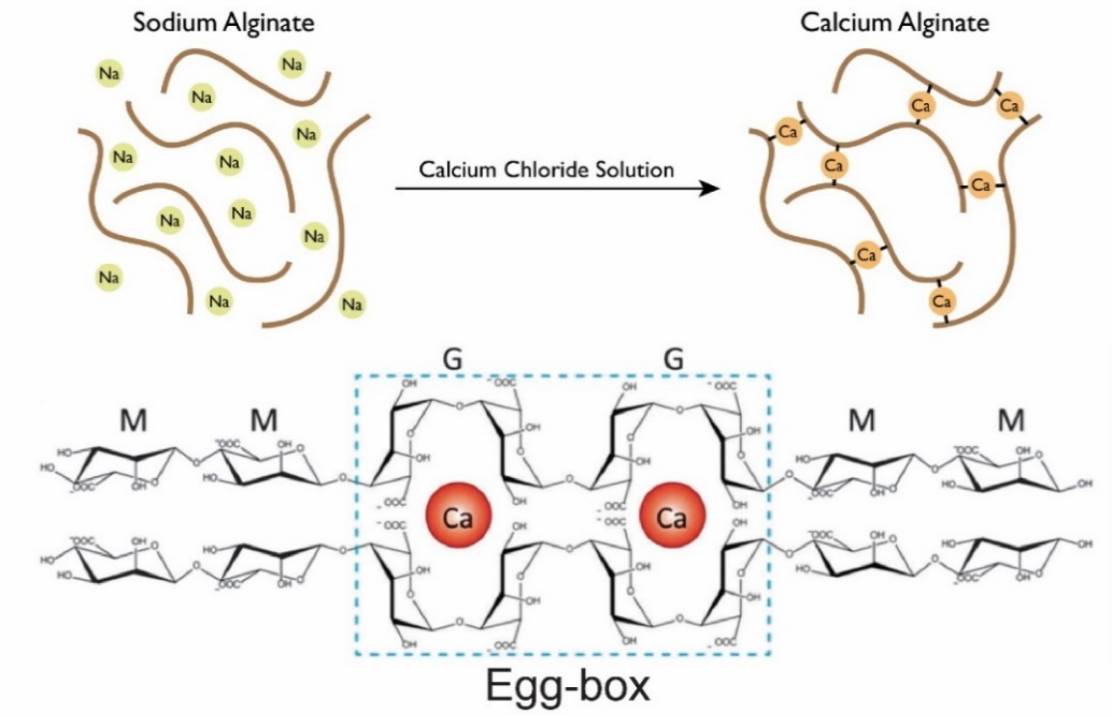

Fig. 1.5 Ionic cross-linking (egg-box model) of alginate. Reproduced with permission [20]. Copyright 2014 RSC.

Alginic Acidic hydrogels

When the pH of the alginate polymer suspension falls lower than the acid disconnection constant (pKa), alginic acid gels develop. A quick drop in pH causes alginic molecules to precipitate into aggregates, but a long and constant decrease of pH causes the creation of a macro-sized gel of alginic acid. Because of their restricted applicability, alginic acid gels have received less attention than ionic gels [21].

Phytic acid crosslinking

Nita, L.E. et al., reported a preparation method of alginate-phytic acid (alginate-PA) hydrogels using PA as the cross-linker (**Fig. 1.6**) [22]. The PA molecules have a large number of anions and hydroxyl groups that are capable to react with the alginate molecules to form ionic and hydrogen bonds. Compared to ionic crosslinking alginate hydrogels utilizing metal ions, the alginate-PA hydrogel had better mechanical properties. However, this approach needs a specific concentration of PA to trigger the gelation. Because the PA is a kind of strong acid, this might limit its application in some fields such as cells encapsulation. Besides, when mixing the PA and alginate solution, the reaction needs agitation and the speed is also slow (e.g. 24 h).

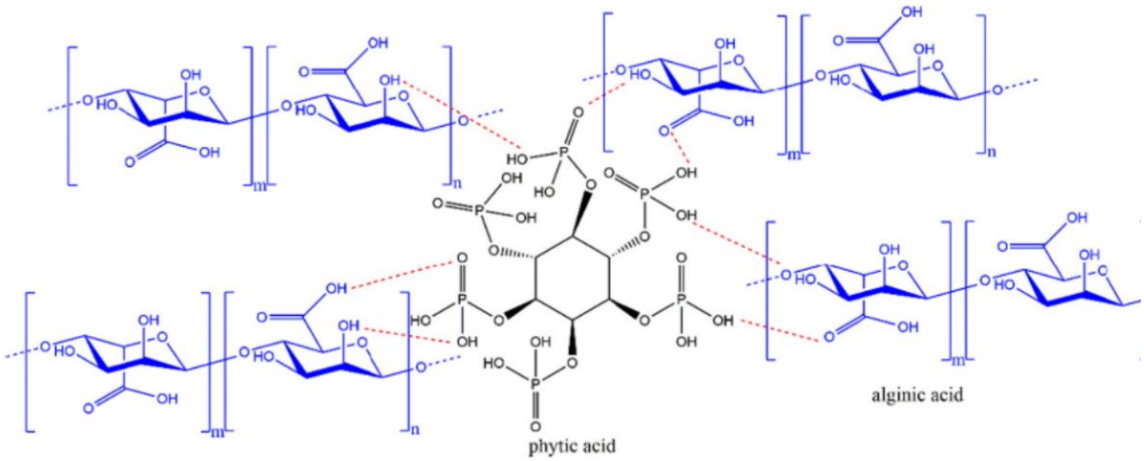

Fig. 1.6 Schematic graph of the formation of alginate-PA hydrogel. Reproduced with permission [22]. Copyright 2021 Elsevier.

(2) Chemical alginate hydrogels

The most normal method to prepare covalent alginate hydrogels is utilizing a crosslinking agent such as poly(ethylene glycol)-diamine, glutaraldehyde, and adipic acid dihydrazide (AAD) [23]. Alginate polymers might be crosslinked by reacting their functional groups (e.g., -OH) with bi-functional molecules (**Fig. 1.7**). To promote the amidation reaction, a catalyst agent is often required [24]. Compared to the ionic crosslinking, the covalently crosslinked alginate hydrogels had a slower reaction speed but strong and stable covalent bonds [25].

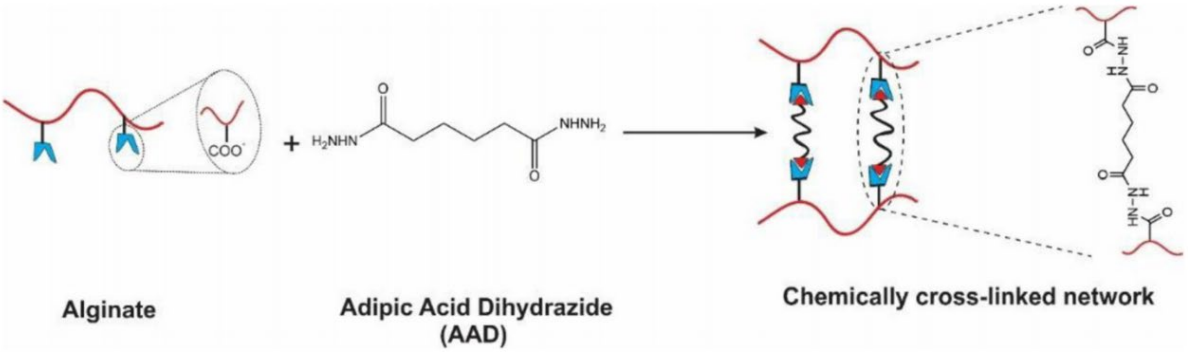

Fig. 1.7 Schematic graph showing covalent crosslinking of alginate using adipic acid dihydrazide (AAD) as cross-linker. Reproduced with permission [23]. Copyright 2020 Springer.

1.3 Production techniques of alginate hydrogel beads

When selecting an effective encapsulation technique for most purposes, the diameter of the alginate microspheres is a crucial issue. Macrogels and microgels are gel particles with a diameter more than and less than 1 mm, respectively. Nanogels are alginate gel particles whose size is around submicron (typically < 500 nm). In general, the method's complexity is inversely dependent on the particle dimension of the produced alginate gel particles. During gelation, these procedures are designed to split the macro-size alginate hydrogel into smaller beads.

1.3.1 Extrusion

1.3.1.1 Simple dripping

The most frequent method to make alginate beads of macro-size is simple dripping, which has been extensively described [26-29] (**Fig. 1.8a**). A droplet forms at the needle tip as the alginate aqueous solution runs out of the syringe hole. The drop expands until it separates from the tip of the needle and falls into the gelling water. The surface tension of the solution causes a round alginate droplet to develop during this period.

The stickiness of the alginate, the size of the needle aperture, the alginate exits flow rate, and the height of departure position from the gelation reservoir may all affect the dimension and morphology of the gel beads. The length between the tip of the needle and the gelation bath

determines particle sphericity. In addition, because of the high reaction speed, the droplets' spherical shape may be distorted as they touch the surface of the gelation bath.

Although syringe extrusion is the easiest technique for manufacturing homogenous alginate gel particles, it creates large particles and has limitations on throughput. Furthermore, owing to pumping problems and needle obstruction, this approach is confined to alginate solutions with low viscosity (< 200 mPa·s). Because of the large particle size, newly manufactured particles must be cured in the gelation bath for some time.

1.3.1.2 Jet break-up extrusion

A laminar flow of polymer is created in this technique by driving the liquid through the tip of the needle. Electrostatic atomization (**Fig. 1.8b**), vibrating nozzle (**Fig. 1.8c**), or jet-cutting (**Fig. 1.8d**) is then used to break the jet into separate droplets.

(1) Electrostatic atomization

This approach generates alginate droplets by using the influence of an external electric force on the parameters of a fluid jet [30-33]. An electric field is applied to an alginate solution flowing from a nozzle. The electric field puts an electrical charge on the liquid, causing the liquid flow to distort and elongate. When the distorted liquid is disturbed, droplets form. This process produces gel particles with diameters ranging from 50 to 350 μm. The intensity of the external field has a substantial impact on the dimensions of the generated hydrogel microspheres.

(2) Vibration technique

The alginate liquid stream is exposed to automatic vibration in the vibration method [34,35]. The quantity of vibrational energy created is determined by the frequency of the wave generator, while the displacement of the nozzle interrupts the flow pattern out of the tip, resulting in the creation of distinct sodium alginate droplets. This approach yields alginate microgels ranging in size from 300 μm to 5 mm. The size of the drops is affected by the vibration intensity, nozzle size, flow rate, viscosity as well as the voltage of the electric field.

(3) Jet cutter method

A revolving device made of tiny cables in a container is positioned underneath a nozzle in this manner [36-38]. The cutter's rotation interrupts the flow of the alginate liquid jet into cylindrical parts, which form alginate droplets and descend into a gelling bath afterward. As the cable tears through the liquid jet, the revolving cutting motion might lead to a loss of alginate substance (cutting loss). This approach yields microgels with great homogeneity (coefficient of variation = 7%) with diameters ranging from 200 μm to 5 mm. The nozzle size, rotating speed, and flow velocity all influence the dimensions and morphology of the hydrogel microspheres.

1.3.1.3 Spinning disk or nozzle

A revolving disk or spinning multi-nozzle arrangement can be used to atomize the alginate solution (**Fig. 1.8e**) [39-43]. The alginate liquid is supplied onto a revolving circle or via spinning nozzles in both arrangements. When the centrifugal force of spinning deteriorates the liquid stream out of the tip or the surface of the spinning plate, discrete particles develop. The dimensions of the produced droplets are determined by the rotational speed. At low rotating speeds, distinct droplets develop right at the nozzle's or plate's periphery. At normal velocities, a consistent fluid laminar stream forms when the fluid exits the disc or nozzle. The ligament disintegrates into separate droplets after a certain length. When the solution exits the disk or nozzle at high rotating rates, a fluid film forms, causing the film to disintegrate rapidly into droplets.

The formation of satellite microgels is a significant drawback of this approach. Nonoptimal manufacturing circumstances induce the existence of satellite microgel particles, which may account for up to 50% of the total weight of microspheres produced.

1.3.1.4 Spray nozzle

Pneumatic nozzles are also be used to prepare hydrogel microparticles (**Fig. 1.8f**) [44-48]. Pressurized sodium alginate is produced by pneumatic nozzles orifice.

When alginate solution leaves the aperture, it comes into contact with a pressured atmosphere (typically air), which causes sodium alginate to atomize. After that, the alginate-based droplets are gathered in a gelation bath. The size of the alginate droplet may be regulated by many factors

using stationary nozzles, including delivery speed, alginate concentration. spraying distance and air pressure.

The usage of fixed nozzles is better suited for small-scale manufacturing and batch processes. Another downside of this approach is that nozzle obstructions may develop, particularly with polymer liquids that have a high viscosity.

1.3.2 Gel formation by impinging

The impinging technique produces alginate microparticles by ionizing alginate and reactant phase in a container in opposing directions (**Fig. 1.8g**) [49,50]. The alginate solution is ionized into tiny droplets through the nozzles compressed by gas. In the meanwhile, a second nozzle at the chamber's bottom atomizes calcium solution as a mist. When the small droplets of Na-alginate come into touch with the $CaCl_2$ mist, they instantly gel. Ca-alginate microcapsules that have just developed settle and run out of the chamber.

The impinging aerosol approach has certain benefits over other technologies now in use. This approach is continuous because the Na-alginate and $CaCl_2$ solutions may be continually supplied into the reaction chamber by a pump. The system's modular architecture allows for the use of several nozzle types, and adjustable factors such as liquid and air pressure, and distance between nozzles allow for the production of alginate microgels with a narrow size distribution.

1.3.3 Emulsification technique

Alginate microgels are generated in a continuous phase during the emulsification technique [51-55]. An alginate solution is distributed and homogenized in the outer oil phase forming a water-in-oil emulsion (**Fig. 1.8h**). By mixing, the gelation solution is gradually incorporated into the emulsion. Gelling happens when alginate droplets combine with a gelling solution. The emulsification method is often employed in combination with the previously mentioned internal gelation process.

Factors influencing the diameter and CV values of prepared hydrogel microparticles include the type and concentration of surfactant, the ratio of water and oil phase, and the shearing force of the homogenizer. The use of surfactant is not required, although it will assist reduce the average sizes of the obtained hydrogel beads. A surfactant such as Span 80 has allegedly been

used to generate microgels with diameters ranging from 1 to 150 m. A higher alginate solution-to-oil ratio results in smaller alginate microgel sizes.

The emulsification approach has the benefit of being a low-cost method for manufacturing alginate microgels. Internal gelation results in a more uniform structure. The fundamental limitation of this approach is that the unpredictable merging of drops in the process usually results in hydrogel microbeads with a broad range of sizes and morphologies. In controlled release investigations, this might lead to poor repeatability.

1.3.4 Templating method

Nanogels may be made by starting with nanocrystals or emulsion droplets as templates. [56-58]. The Na-alginate solution is encapsulated inside liposomes during micellar templating (**Fig. 1.8i**). The porosity of the lipid layer increases as the temperature approaches the melting point, allowing external Ca^{2+} to seep into the liposome structure for alginate gelation to commence. When a detergent is added, the lipid bilayer is removed, revealing the freshly produced calcium alginate nanogel.

Although these approaches so far have only been used to encapsulate proteins, the capacity to create nanogels offers up new possibilities for cellular drug delivery. Nonetheless, these technologies are complicated and offer relatively low throughput, rendering them become difficult for scale-up. For instance, because of the liposome system's poor encapsulation effectiveness, the nanogel output from this approach is less than 10%. Furthermore, recovering nanogels is challenging and often needs ultracentrifugation. This technique has yet to be used in any application. The use of hazardous chemicals and solutions also restricts their applicability in biological, medicinal, and food fields.

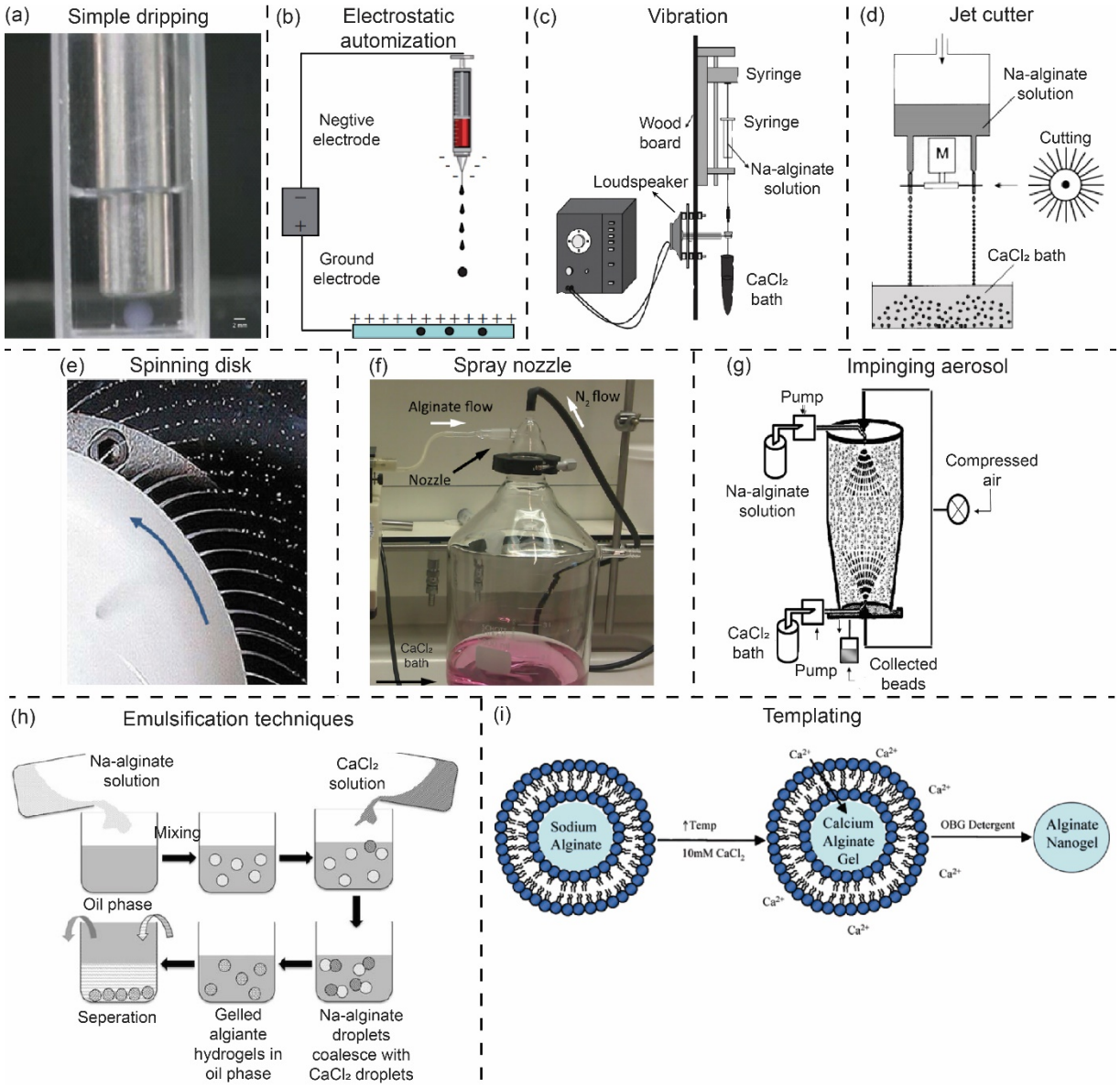

Fig. 1.8 Alginate hydrogels formation by (a) simple dripping (Reproduced with permission [26]. Copyright 2011 Elsevier), (b) electrostatic automization (Reproduced with permission [30]. Copyright 2009 Informa), (c) vibration (Reproduced with permission [34]. Copyright 2009 Scientific Research), (d) jet cutter (Reproduced with permission [36]. Copyright 1998 Wiley-VCH), (e) spinning disk [39], (f) spray nozzle (Reproduced with permission [44]. Copyright 2015 PLOS), (g) impinging aerosol (Reproduced with permission [49]. Copyright 2011 Elsevier), (h) emulsification techniques (Reproduced with permission [51]. Copyright 2006 Wiley-VCH) and (i) templating (Reproduced with permission [56]. Copyright 2008 ACS).

1.3.5 Microfluidics

The alginate hydrogel particles can also be prepared by the microfluidic method. The details of this technique will be further discussed in the next section. The comparison of the above fabrication methods (except the microfluidics) is shown in **Table 1.2**.

Table 1.2 Summary of the procedure used to create alginate hydrogel beads

Method	Particle size	Mono-dispersity	Uniformity	Roundness	Scalability
Simple dripping	1–2 mm	Normal	High	Low	–
Electrostatic	1–500 μm	Normal	High	Low	+
Vibration	< 500 μm	Low	Low	Low	+
Jet cutter	0.2–5 mm	High	High	Low	+
Spinning	0.3–2 mm	High	High	High	–
Spray nozzle	80–130 μm	Low	Low	High	–
Impinging aerosol	10–50 μm	Low	Low	High	+
Emulsification	0.1–1 mm	Low	High	High	+
Templating	< 200 nm	Low	High	High	–

1.4 Microfluidic droplet-based technique

Microfluidics is the study of techniques and equipment that allow for the control and domination of fluids at micron or nanoflow sizes. Microfluidic systems have traditionally been used in DNA analysis, fluid dynamics, PCR, protein analysis, and cell culture.

The generation of gel particles is generally accomplished by dispersed phase formation. Before the production of hydrogel particles, the polymer solution without gelation is broken up into a discrete droplet in this procedure. As a result, the microfluidic droplet-based technique might be a perfect approach for synthesizing functional facile alginate hydrogel microparticles, because microfluidic devices allow for greater control of the flow pattern, monodisperse droplets with a CV value in diameter below 10% could be created, that is critical for the creation of subsequent hydrogels.

A detailed discussion comparison of the previous works on the microfluidic alginate microbeads production will be presented in **Chapter 2, Section 1**. This chapter will focus on the concept and mechanism of the existed microfluidic droplet-based technology.

1.4.1 Physical ingredients

Droplet production in a microfluidics system is generally accomplished by passive approaches that produce a consistent and continuous flow. These methods use the liquid stream field to distort the interface and encourage the spontaneous evolution of the instabilities of the interface. As a result, the local external actuation can be avoided. A number of dimensionless characteristics are utilized to assess the significance of each force applied to the droplet breakup.

(1) Capillary number

The capillary number (Ca) is the most essential parameter in microfluidic droplet generation, describing the competition of viscous stress and interfacial tension. The two's relative strength is represented as:

$$Ca = \frac{\mu \upsilon}{\gamma} \tag{1-1}$$

where μ is the viscosity of continuous phase, γ represents the tension of the interface and υ is the characteristic velocity scale.

A low Ca value suggests that the flow field is dominated by stresses induced by interfacial tension. Droplets flowing in this circumstance almost completely decrease their surface area by creating spherical ends. When the Ca value is quite high, however, the viscous impact is larger than the interfacial tension impacts, and substantial deformations of the drops and asymmetric forms may be seen. Droplets of uniform size were generated only within a narrow range of Ca value, as in other constrained micro geometries (typically between 10^{-3} and 10) [59].

The proportion of flow rates is another dimensionless element that is crucial in droplet formation [60]:

$$\varphi = \frac{Q_d}{Q_c} \tag{1-2}$$

the Q_d and Q_c represent the flow rate of disperse and continuous phases respectively.

(2) Reynolds number

The Reynolds number (*Re*) is the proportion of inertial forces to viscous forces inside a fluid subjected to relative internal movement owing to varying fluid velocities. The *Re* is formulated as having:

$$Re = \frac{\rho \upsilon D}{\mu} \tag{1-3}$$

where ρ is the density of the fluid and D means the diameter of the channel. However, in a microfluidic device, the value of D is on the micro-scale. For microfluidics, small geometric dimension scales often result in $Re \ll 1$. As a result, only the small Reynolds number condition will be considered that the flows tend to be dominated by laminar.

(3) Weber number

The Weber number compares inertia to interfacial tension defined as:

$$We = \frac{\rho \upsilon^2 l}{\gamma} = Ca \cdot Re \tag{1-4}$$

where l represents the characteristic length, typically the droplet diameter. Because the inertia force of the droplet in the microchannel is generally small, the Weber number in microfluidics is usually ignored.

(4) Bond number

Finally, the effects of gravity on the generation of droplets in microfluidic devices are often overlooked, which may be estimated by the Bond number, that relates the tension of interface to gravity:

$$Bo = \frac{\Delta \rho g l^2}{\gamma} \tag{1-5}$$

where g is the acceleration of gravity, $\Delta\rho$ is the difference in fluid densities. The value of the Bond number in an oil and water microfluidic device is usually small than 10^{-5}.

1.4.2 Droplet production in microchannels

Droplet-based microfluidic systems should provide a regular and steady monodisperse droplet flow and be adaptable enough to deliver droplets of a certain volume at a specified pace. Three key techniques based on various physical processes have been developed to achieve this

goal: (1) split in a co-flowing stream; (2) split in a cross-flowing stream; and (3) split in a flow-focusing stream.

The dispersion phase is forced into the microchannel in all of these circumstances, where it encounters the immiscible continuous phase. The connector is intended to improve droplet manufacturing repeatability. The design of the junction, flow rates, and physical features like the tension of interface and viscosity influence the flow pattern, which changes the interface and finally results in droplet formation. Indeed, the conflict between the pressures caused by external flow and viscous shear forces, as well as the capillary pressure preventing fluid deformation, determines droplet size.

1.4.2.1 Co-flowing

Figure 1.9 is a typical example of the structure of the co-flow device. A co-flow device typically consists of a round tube matched with a rectangular or square outside channel, with the two parallel flows running at the tip. The Rayleigh-Plateau instability is readily recognized as the physics of droplet formation in co-axial injectors.

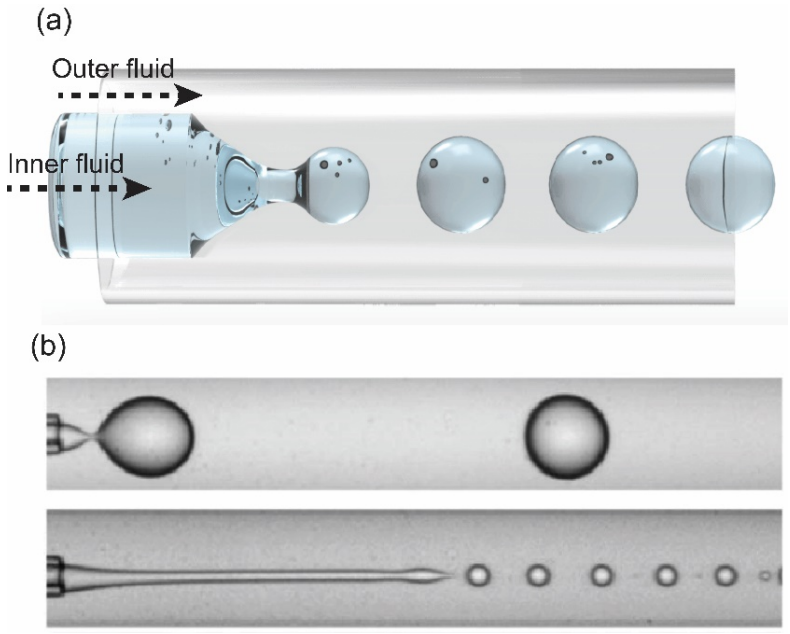

Fig. 1.9 A typical droplet manufacturing example in a co-flow device. (a) A schematic graph of co-flow device [61]. (b) Microscopic images of droplet formation. Reproduced with permission [62]. Copyright 2007 APS.

A fully unstable setup in co-axial infusion devices should result in the self-sustained development of droplets at the device inlet, while a convectively unsteady flow should result in droplets that form a limited distance downstream only after the instability has had time to expand. As a result of the viscosity ratio, *Ca*, and equilibrium confinement value, the transition is explained in further depth [63,64].

1.4.2.2 T-junctions

A typical structure of a T-junction droplet-based device consists of two orthogonal channels in which two immiscible phases flow through and the droplets form when they meet (**Fig. 1.10**).

In a confined channel geometry, the droplets formation regimes could be distinguished as the capillary number and proportion of flow rate varied [65]. Up to now, many numerical and experimental works have been presented demonstrating that the viscosity ratio, flow rate ratios, and channel width ratios are essential for the generation process of the droplet [66].

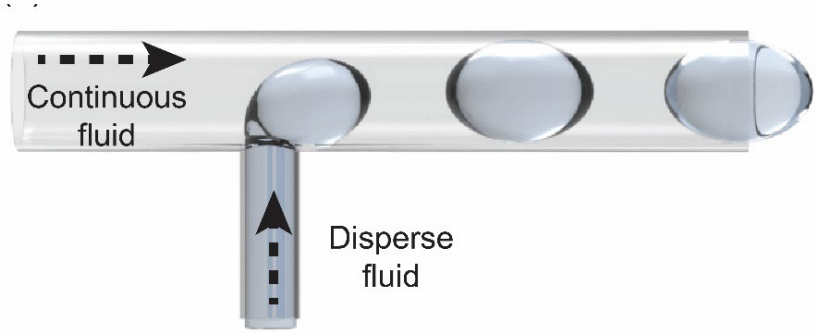

Fig. 1.10 Example of typical generation of the droplet in T-junction device. (a) A schematic graph T-junction device [61].

1.4.2.3 Flow-focusing

The dispersion phase is compressed by two flowing flows of the continuous phase in a standard flow concentrating configuration (**Fig. 1.11**).

The conventional microfluidic flow-focusing geometry can be classified into two types: the first kind has a small, constricted shape that leads to a suddenly enlarged downstream region. (**Fig. 1.11a**), this kind of geometry can be designed in both three-dimensional and two-

dimensional ways; the second type having a cross-junction were the disperse phase encounter with an orthogonal continuous co-flow (**Fig. 1.11b**).

However, due to the huge variety of spatial aspect proportions that characterize flow-focusing devices, simple scaling formulas to forecast the diameter of droplets, CV values, and production efficiency as a function of critical factors have not been developed. As a consequence, no specific scaling rules for the transition of droplets generation mechanism, nor the dimension and production frequency of droplet generation [67]. Although it is widely recognized that the diameter of a droplet is defined by the flow rate relationship between the dispersed and continuous phase for a particular microchannel design, this is not always the case [68].

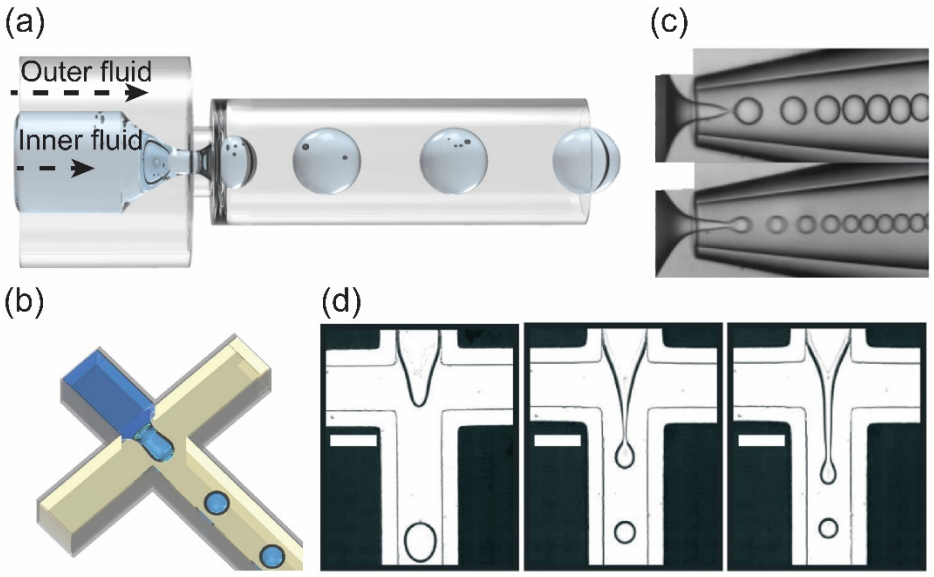

Fig. 1.11 Example of typical generation of the droplet in a flow-focusing device. Schematic graphs of flow-focusing geometry in (a) capillary device [61] and (b) 2-dimensional microchannel device (Reproduced with permission [69]. Copyright 2020 ACS). Microscopic images of droplet formation in (c) capillary device (Reproduced with permission [70]. Copyright 2015 ACS) and (d) microchannel device (Reproduced with permission [71]. Copyright 2014 RSC).

1.5 Objectives

As discussed in the above sections. The droplet-based microfluidics approach is unquestionably ideal for the production of hydrogel microbeads. However, the existing microfluidic researches on the generation of alginate-based microgels still have, more or less, a deficiency in mechanical, physical, or chemical aspect. This discussion will be extended in the following chapters respectively.

As a result, in this thesis, a novel microfluidic emulsion-based external gelation (μFEEG) strategy was developed to produce different types of functional calcium alginate (Ca-alginate) hydrogel microparticles. Further, to meet the practical industry requirements, a paralleled microfluidic platform was put forward for the mass generation of Ca-alginate microparticles. Finally, a new application of the Ca-alginate microcapsules for antifouling biocide encapsulation was demonstrated.

The main objectives of this thesis are as follows:

(1) To design and testify a novel μFEEG for synthesizing highly spherical calcium alginate hydrogel microparticles and investigate the key parameters behind this strategy (**Chapter 2**).

(2) To utilize this μFEEG preparing functional Ca-alginate microparticles including the magnetic and/or fluorescent Janus beads (**Chapter 3**) and hydrogels with magnetic and/or fluorescent coatings (**Chapter 4**).

(3) To design and fabricate a microfluidic device for synthesizing monodispersed and facile shaped Ca-alginate hydrogels in a high-volume output for industrial application (**Chapter 5**).

(4) To use the highly spherical hydrogel particles to encapsulate the anti-fouling drug Irgarol and further investigate their release mechanism and antifouling effects (**Chapter 6**).

1.6 Outline of thesis

Chapter 1 Introduction

Introduces the background of hydrogel and alginate materials, existing methods for producing alginate hydrogel particles. In the meanwhile, the background of droplet-based microfluidic techniques is briefly demonstrated.

Chapter 2 Highly spherical calcium alginate hydrogel

Carries out a novel μFEEG method for synthesizing highly spherical calcium alginate microparticles. The mechanism and important parameters of this gelation approach are reported.

Chapter 3 Functional Janus calcium alginate hydrogel

Introduces the production of functional magnetic and/or fluorescent Janus calcium alginate hydrogel microspheres using the μFEEG. The prepared Janus particles were used for the mammal cells encapsulation.

Chapter 4 Surface coating of the alginate hydrogel particles

Introduces the formation of calcium alginate hydrogel microbeads with magnetic and/or fluorescent surface coatings using the μFEEG.

Chapter 5 Mass production of calcium alginate hydrogel particles

Presents an innovative microfluidic module consisting of a PDMS chip and stainless holders for the high-throughput preparation of cell-laden calcium alginate hydrogel microcapsules with facile shapes through the μFEEG.

Chapter 6 Microencapsulation of hydrophobic antifouling biocide

Introduces and investigates a new application of the alginate hydrogel microcapsule for encapsulation of hydrophobic antifouling biocides that can be used for antifouling coating paints.

Chapter 7 Conclusions and outlook

Describes the conclusions and points out the outlook of this thesis.

The connection between the above chapters is shown in **Fig. 1.12**.

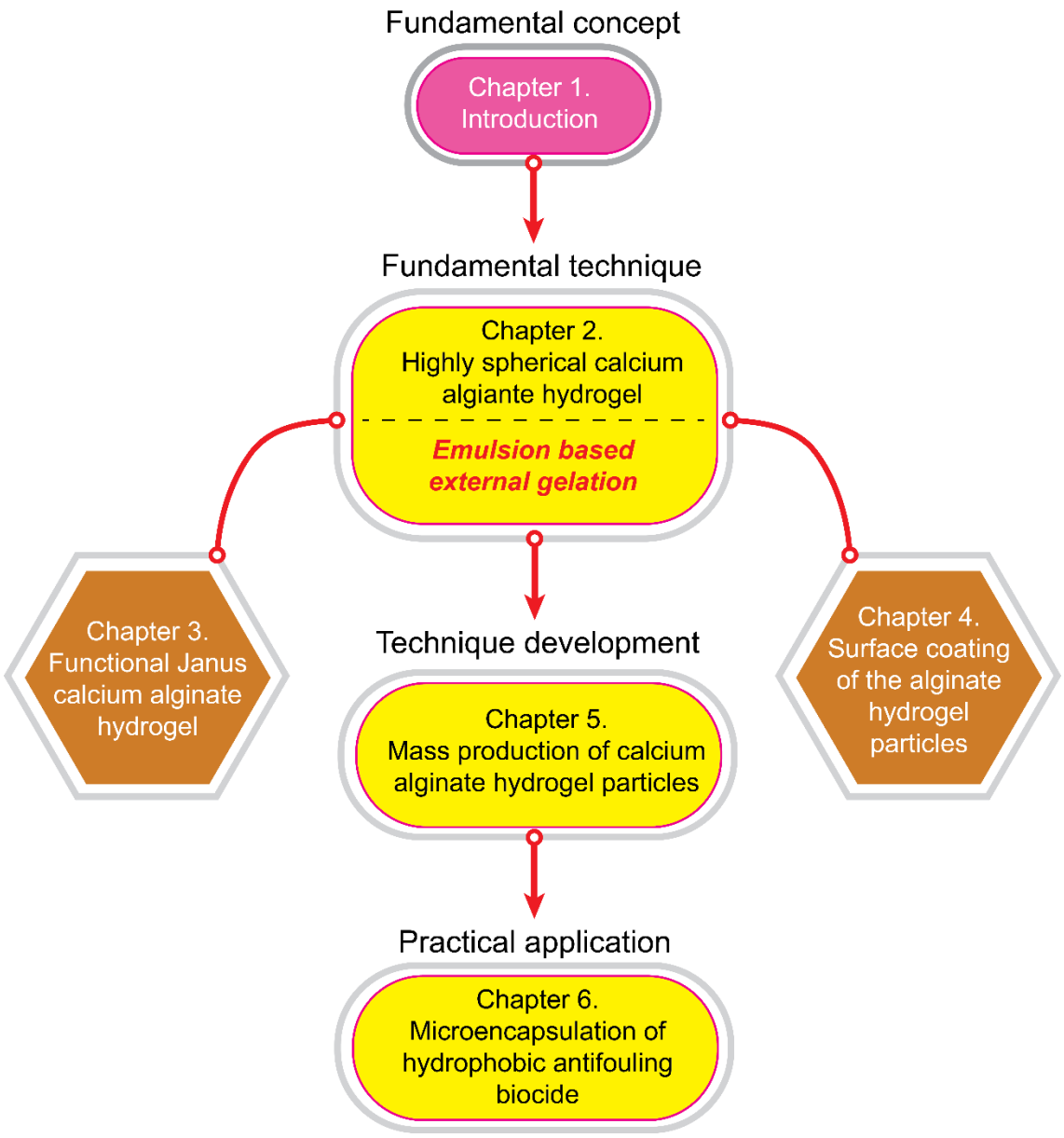

Fig. 1.12 The flow chart showing the connection between each chapter in this thesis.

References

[1] Khademhosseini, A. and Demirci, U. *Gels Handbook: Fundamentals, Properties and Applications*; World Scientific: Singapore, 2016.

[2] Yang, S., Fu, S., Liu, H., Zhou, Y., Li, X. Hydrogel beads based on carboxymethyl cellulose for removal heavy metal ions. *J. Appl. Polym. Sci*. **2011**, 119, 1204–1210.

[3] Pilidindi, K. and Pandey, H. *Polymer Gel Market Size report*; Global Market Insights: USA, January 2018.

[4] Mohite, S. and Prasad, E. *Hydrogel Market Outlook-2027*; Allied Market Research: USA, January 2020.

[5] Ahmed, E.M. Hydrogel: Preparation, characterization, and applications: A review. *J. Rev. Res.* **2015,** 6, 105–121.

[6] Lizawa, T.; Taketa, H.; Maruta, M.; Ishido, T.; Gotoh, T.; Sakohara, S. Synthesis of porous poly(N-isopropylacrylamide) gel beads by sedimentation polymerization and their morphology. *J. Appl. Polym. Sci.* **2007,** 104, 842–850.

[7] Yang, L.; Chu, JS. and Fix, JA. Colon-specific drug delivery: new approaches and in vitro/in vivo evaluation. *Int. J. Pharm.* **2002,** 235, 1–15.

[8] Mohamadnia, Z.; Zohuriaan-Mehr, M.J.; Kabiri, K.; Jamshidi, A.; Moberi, H. pH-sensitive IPN hydrogel beads of carrageenan-alginate for controlled drug delivery. *J. Bioact. Compat. Polym.* **2007,** 22, 342–356.

[9] Frachini, E.C.G. and Petri, D.F.S. Magneto-responsive hydrogels: preparation, characterization, biotechnological and environmental applications. *J. Braz. Chem. Soc.* **2019,** 30, 2010–2028.

[10] Hoffman, A.S. Hydrogels for biomedical applications. *Adv. Drug Deliv. Rev*. **2012,** 64, 18–23.

[11] Kuen, Y.L. and David, J.M. Alginate: Properties and biomedical applications. *Prog. Polym. Sci.* **2012,** 37, 106–126.

[12] Chen, Z.; Wang, T. and Yan, Q. Building a polysaccharide hydrogel capsule delivery system for control release of ibuprofen. *J. Biomater. Sci. Polym. Ed*. **2018,** 29, 309–324.

[13] Chen, K.; Merkel, T.J.; Pandya, A.; Napier, M.E.; Luft, J.C.; Daniel, W.; Sheiko, S. and DeSimone, J.M. Low modulus biomimetic microgel particles with high loading of hemoglobin. *Biomacromolecules* **2012,** 13, 2748–2759.

[14] Chen, L.; Shen, R.; Komasa, S.; Xue, Y.; Jin, B.; Hou, Y.; Okazaki, J. and Gao, J. Drug-loadable calcium alginate hydrogel system for use in oral bone tissue repair. *Int. J. Mol. Sci.* **2017,** 18, 989.

[15] Rowley, J.A.; Madlambayan, G. and Mooney, D.J. Alginate hydrogels as synthetic extracellular matrix materials. *Biomaterials* **1999,** 20, 45–53.

[16] Xie, X.; Zhang, W.; Abbaspourrad, A.; Ahn, J.; Bader, A.; Bose, S.; Vegas, A.; Lin, J. Tao, J.; Hang, T.; et al. Microfluidic fabrication of colloidal nanomaterials-encapsulated microcapsules for biomolecular sensing. *Nano Lett.* **2017,** 17, 2015–2020.

[17] Le Goff, G.C.; Srinivas, R.L.; Hill, W.A. and Doyle, P.S. Hydrogel microparticles for biosensing. *Eur. Polym. J.* **2015,** 72, 386–412.

[18] Yamada, M. and Seki, M. Multiphase microfluidic processes to produce alginate-based microparticles and fibers. *J. Chem. Eng. Jpn*. **2018,** 51, 318–330.

[19] Leong, J.Y.; Lam, W.H.; Ho, K.W.; Voo, W.P.; Lee, M.F.X.; Lim, H.P.; Lim, S.L. Tey, B.T.; Poncelet, D.; Chan, E.S. Advances in fabricating spherical alginate hydrogels with controlled particle designs by ionotropic gelation as encapsulation systems. *Particuology* **2016,** 24, 44–60.

[20] Yoon, J.; Oh, D.X.; Jo, C.; Lee, J. and Hwang, D. Improvement of desolvation and resilience of alginate binders for Si-based anodes in a lithium ion battery by calcium-mediated cross-linking. *Phys. Chem. Chem. Phys.* **2014,** 16, 25628.

[21] Pawar, S.N. and Edgar, K.J. Alginate derivatization: A review of chemistry, properties and applications. *Biomaterials* **2012,** 33, 3279–3305.

[22] Nita, L.E.; Chiriac, A.P.; Ghilan, A.; Rusu, A.G.; Tudorachi, N. and Timpu, D. Alginate enriched with phytic acid for hydrogels preparation. *Int. J. Biol. Macromol.* **2021**, 181, 561–571.

[23] Abasalizadeh, F.; Moghaddam, S.V.; Alizadeh, E.; Akbari, E.; Kashani, E.; Fazljou, S.M.B.; Torbati, M. and Akbarzadeh, A. Alginate-based hydrogels as drug delivery vehicles in cancer treatment and their applications in wound dressing and 3D bioprinting. *J. Biol. Eng.* **2020**, 14, 1–22.

[24] Hashemnejad, S.M. and Kundu, S. Rheological properties and failure of alginate hydrogels with ionic and covalent crosslinks. *Soft Matter* **2019**, 15, 7852–7862.

[25] Yang, J.; Steck, J. and Suo, Z. Gelation kinetics of alginate chains through covalent bonds. *Extreme Mech. Lett.* **2020**, 40, 100898.

[26] Chan, E.S. Effect of formulation of alginate beads on their mechanical behavior and stiffness. *Particuology* **2011,** 9, 228–234.

[27] Thu, B.; Smidsrod, O. and Skjak-Brek, G. Alginate gels-some structure-function correlations relevant to their use as immobilization matrix for cells. *Progr. Biotechnol.* **1996,** 11, 19–30.

[28] Krasaekoopt, W.; Bhandari, B. and Deeth, H. The influence of coating materials on some properties of alginate beads and survivability of microencapsulated probiotic bacteria. *Int. Dairy J.* **2004,** 14, 737–743.

[29] Krasaekoopt, W.; Bhandari, B. and Deeth, H. Survival of probiotics encapsulated in chitosan-coated alginate beads in yogurt from UHT-and conventionally treated milk during storage. *Food. Scie. Technol.* **2006,** 39, 177–183.

[30] Suksamran, T.; Opanasopit, P.; Rojanarata, T.; Ngawhirunpat, T.; Ruktanonchai, U. and Supaphol, P. Biodegradable alginate microparticles developed by electrohydrodynamic spraying techniques for oral delivery of protein. *J. Microencapsul.* **2009,** 26, 563–570.

[31] Bugarski, B.; Li, Q.; Goosen, M.F.A.; Poncelet, D.; Neufeld, R.J. and Vunjak, G. Electrostatic droplet generation: Mechanism of polymer droplet formation. *AIChE J.* **1994,** 40, 1026–1031.

[32] Manojlovic, V.; Djonlagic, J.; Obradovic, B.; Nedovic, V. and Bugarski, B. Immobilization of cells by electrostatic droplet generation: A model system for potential application in medicine. *Int. J. Nanomed.* **2006,** 1, 163–171.

[33] Klokk, T. and Melvik, J.E. Controlling the size of alginate gel beads by use of a high electrostatic potential. *J. Microencapsulation* **2002,** 19, 415–424.

[34] Yan, Z.; Kajiyama, S.; Masuhara, H. Hosokawa, Y. Kaji, T. and Fukui, K. A new size and shape controlling method for producing calcium alginate beads with immobilized proteins. *J. Biomed. Sci. Eng.* **2009,** 2, 287–293.

[35] Gaudio, P.D.; Auriemma, G.; Mencherini, T.; Porta, G.D.; Reverchon, E. and Aquino, R.P. Design of alginate-based aerogel for nonsteroidal anti-inflammatory drugs

controlled delivery systems using prilling and supercritical-assisted drying. *J. Pharm. Sci.* **2013,** 102, 185–194.

[36] Prube, U.; Fox, B.; Kirchhoff, M.; Bruske, F.; Breford, J. and Vorlop, K.D. New process (jet cutting method) for the production of spherical beads from highly viscous polymer solutions. *Chem. Eng. Technol.* **1998,** 21, 29–33.

[37] Prusse, U.; Bilancetti, L.; Bucko, M.; Bugarski, B.; Bukowsko, J.; Gemeiner, P.; Lewinska, D.; Manojlovic, V.; Massart, B.; Nastruzzi, C.; et al. Comparison of different technologies for alginate beads production. *Chem. Pap.* **2008,** 62, 364–374.

[38] Tran, V.T.; Benoit, J.P. and Venier-Julienne, M.C. Why and how to prepare biodegradable, monodispersed, polymeric microparticles in the field of pharmacy. *Int. J. Pharm.* **2001,** 407, 1–11.

[39] Southwest Research Institute. *Micro/Nano Encapsulation*; Southwest Research Institute: San Antonio, Texas, 2011.

[40] Ogbonna, J.C.; Matsumura, M.; Yamagata, T.; Sakuma, H. and Kataoka, H. Production of micro-gel beads by a rotating disk atomizer. *J. Ferment. Bioeng.* **1989,** 68, 40–48.

[41] Nagata, R.; Koga, K.; Gondo, S.; Uemura, Y. and Hatate, Y. Preparation of calcium alginate micro-gel beads using a rotating nozzle. *Kagaku Kogaku Ronbunshu.* **2001,** 27, 648–651.

[42] Prube, U.; Jahnz, U.; Wittlich, P.; Breford, J. and Vorlop, K.D. Bead production with jetcutting and rotating disc/nozzle technologies. *Landbauforschung Volkenrode Sonderheft.* **2002,** 241, 1–10.

[43] Senuma, Y.; Lowe, C.; Zweifel, Y.; Hilborn, J.G. and Marison, I. Alginate hydrogel microspheres and microcapsules prepared by spinning disk atomization. *Biotechnol. Bioeng.* **2000,** 67, 616–622.

[44] Elk, M.V.; Ozbakir, B.; Barten-Rijbroek, A.D.; Storm, G.; Nijsen, F.; Hennink, W.E.; Vermonden, T. and Deckers, R. Alginate microspheres containing temperature sensitive liposomes (TSL) for MR-Guided embolization and triggered release of doxorubicin. *PLOS One* **2015,** 10, 1–19.

[45] Kwok, K.K.; Groves, M.J. and Burgess, D.J. Production of 5–15 μm diameter alginate-polylysine microcapsules by an air-atomization technique. *Pharm. Res.* **1991,** 8, 341–344.

[46] Cui, J.H.; Goh, J.S.; Park, S.Y.; Kim, P.H. and Lee, B.J. Preparation and physical characterization of alginate microparticles using air atomization method. *Drug Devel. Ind. Pharm.* **2001,** 27, 309–319.

[47] Yeo, Y.; Baek, N. and Park, K. Microencapsulation methods for delivery of protein drugs. *Biotechnol. Bioprocess Eng.* **2001,** 6, 213–230.

[48] Strasdat, B. and Bunjes, H. Incorporation of lipid nanoparticles into calcium alginate beads and characterization of the encapsulated particles by differential scanning calorimetry. *Food Hydrocolloids.* **2013,** 30, 567–575.

[49] Sohail, A.; Turner, M.S.; Coombes, A.; Bostrom, T. and Bhandari, B. Survivability of probiotics encapsulated in alginate gel microbeads using a novel impinging aerosols method. *Int. J. Food Microbiol.* **2011,** 145, 162–168.

[50] Hariyadi, D.M.; Wang, Y.; Lin, S.C.Y.; Bostrom, T.; Bhandari, B. and Coombes, A.G.A. Novel alginate gel microspheres produced by impinging aerosols for oral delivery of proteins. *J. Microencapsul.* **2012,** 29, 250–261.

[51] Zhang, F.J.; Cheng, G.X.; Gao, Z. and Li, C.P. Preparation of porous calcium alginate membranes/microspheres via an emulsion templating method. *Macromol. Mat. Eng.* **2006,** 291, 485–492.

[52] Poncelet, D. Production of alginate beads by emulsification/internal gelation. *Ann. N Y Acad. Sci.* **2001,** 944, 74–82.

[53] Chan, L.W.; Lim, L.T. and Heng, P.W. Microencapsulation of oils using sodium alginate. *J. Microencapsul.* **2000,** 17, 757–766.

[54] Reis, C.P.; Neufeld, R.J.; Vilela, S.; Ribeiro, A.J. and Veiga, F. Review and current status of emulsion/dispersion technology using an internal gelation process for the design of alginate particles. *J. Microencapsul.* **2006,** 23, 245–257.

[55] Zhao, Y.; Carvajal, M.T.; Won, Y.Y. and Harris, M.T. Preparation of calcium alginate microgel beads in an electrodispersion reactor using an internal source of calcium carbonate nanoparticles. *Langmuir* **2007,** 23, 12489–12496.

[56] Hong, J.S.; Vreeland, W.N.; Lacerda, S.H.D.; Locascio, L.E.; Gaitan, M. and Raghavan, S.R. Liposome-templated supramolecular assembly of responsive alginate nanogels. *Langmuir* **2008,** 24, 4092–4096.

[57] Santis, S.D.; Diociaiuti, M.; Cametti, C. and Masci, G. Hyaluronic acid and alginate covalent nanogels by template cross-linking in polyion complex micelle nanoreactors. *Carbohydr. Polym.* **2014,** 101, 96–103.

[58] Nesamony, J.; Singh, P.R.; Nada, S.E.; Shah, Z.A. and Kolling, W.M. Calcium alginate nanoparticles synthesized through a novel interfacial cross-linking method as a potential protein drug delivery system. *J. Pharm. Sci.* **2012,** 101, 2177–2184.

[59] Nisisako T.; Torii, T.; Takahashi, T. and Takizawa, Y. Synthesis of monodisperse bicolored Janus particles with electrical anisotropy using a microfluidic co-flow system. *Adv. Mater*. **2006**, 18, 1152–1156.

[60] Christopher, G.F. and Anna, S.L. Microfluidic methods for generating continuous droplet streams. *J. Phys. D: Appl. Phys.* **2007,** 40, 319–336.

[61] Elvesys Microfluidics Innovation Center. Digital microfluidics: microfluidic droplets & emulsion science. https://www.elveflow.com/microfluidic-reviews/droplet-digital-microfluidics/digital-microfluidics-microfluidic-droplet-emulsion-science/ (accessed Oct 7, 2021).

[62] Utada, A.S.; Fernandez-Nieves, A.; Stone, H.A. and Weitz, D.A. Dripping to jetting transitions in coflowing liquid streams. *Phys. Rev. Lett.* **2007,** 99, 094502.

[63] Guillot, P.; Colin, A.; Utada, A.S. and Ajdari, A. Stability of a jet in confined pressure-driven biphasic flows at low Renolds numbers in various geometries. *Phys. Rev. E.* **2008,** 78, 1.

[64] Guillot, P.; Colin, A.; Utada, A.S. and Ajdari, A. Stability of a jet in confined pressure-driven biphasic flows at low Renolds numbers. *Phys. Rev. Lett.* **2007,** 99, 104502.

[65] Menech, M.D.; Garstecki, P.; Jousse, F. and Stone, H.A. Transition from squeezing to dripping in a microfluidic T-shaped junction. *J. Fluid Mech.* **2008,** 595, 141–161.

[66] Graaf, S.; Nisisako, T.; Schroen, C.G.P.H.; Sman, R.G.M. and Boom, R.M. Lattice Boltzmann simulations of droplet formation in a T-shaped microchannel. *Langmuir* **2006,** 22, 4144–4152.

[67] Baroud, C.N.; Gallaire, F. and Dangla, R. Dynamics of microfluidic droplets. *Lab Chip* **2010,** 10, 2032–2045.

[68] Xu, J.H.; Li, S.W.; Tan, J. and Luo, G.S. Controllable preparation of monodispersed calcium alginate microbeads in a novel microfluidic system. *Chem. Eng. Technol.* **2008,**

31, 1223–1226.

[69] Liu, Y. and Nisisako, T. Microfluidic encapsulation of hydrophobic antifouling biocides in calcium alginate hydrogels for controllable release. *ACS Omega* **2020**, *5*, 25695–25703.

[70] Ekanem, E.; Nabavi, S.A.; Vladisavljevic, G.T. and Gu, S. Structured biodegradable polymeric microparticles for durg delivery produced using flow focusing glass microfluidic devices. *ACS Appl. Mater. Interfaces* **2015,** 7, 23132–23143.

[71] Tan, S.H.; Semin, B. and Baret, J.C. Microfluidic flow-focusing in ac electric fields. *Lab Chip* **2014,** 14, 1009–1106.

Chapter 2

Microfluidic emulsion-based synthesis of calcium-alginate hydrogel particles

2.1 Introduction

2.1.1 Microfluidic processes for synthesizing hydrogel particles

The size and morphology of hydrogel particles are important in applications such as medication delivery and cell encapsulation. Since of their generally nanoporous nature, alginate-based hydrogel microbeads may be used to manage the kinetics of medication release because molecules can spread through the hydrogels at a predictable rate. Furthermore, the size and surface area of hydrogel microspheres are critical for controlling drug release kinetics since they determine drug release speed. As a consequence of their random surface area and inequable volume, polydisperse hydrogel particles with non-uniform morphologies may have limited control over the kinetics of drug release. Monodisperse hydrogel particles with spherical morphologies and tiny sizes, on the other hand, may give precise control of drug dose and release quantity with great repeatability [1–3]. The optimal hydrogel microcapsules for cell encapsulation should have a homogenous network structure with a regulated microenvironment that allows for the stable entrapment of the cells. Furthermore, the hydrogel microcapsules should be tiny enough (< 200 μm) to allow for efficient transport of oxygen and nutrients to the cells inside them [4]. As a consequence, precise control over the form, size, and size distribution of hydrogel particles is critical. The development of monodisperse hydrogel microparticles with very homogeneous morphologies is critical.

Several droplet-based microfluidic techniques for the synthesis of alginate-based hydrogel microparticles have been described so far. The alginate droplets were generated in the microfluidic devices prior to gelation in this procedure. Because microfluidic devices allow for more precise control of the multiphase flow pattern, so monodisperse alginate droplets with a coefficient of variation (CV) in diameter of less than 10% could be created, which is critical for

the production of the following hydrogel particles. The droplet-based microfluidic approaches may be subdivided into a number of distinct categories. (i) coalescence of a Na-alginate droplet with a droplet containing gelation ions, (ii) off-chip reaction of Na-alginate droplets in a gelation agent-containing bath, (iii) a gelation agent is added to the oil phase to trigger the reaction, (iv) internal gelation is achieved by utilizing a gelation chemical that is poorly soluble in water, (v) phase separation of double emulsion, and (vi) simultaneously reaction inside the single droplets (**Fig. 2.1**)

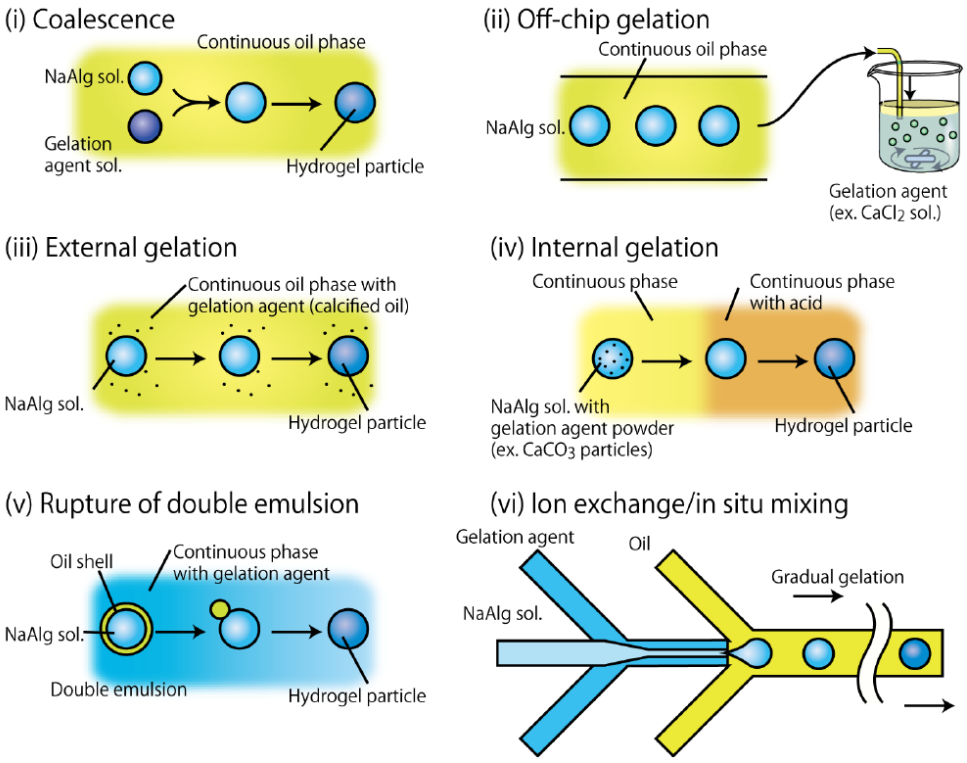

Fig.2.1 Schemes for making Na-alginate microspheres from droplets [5].

The following section provides an overview of prior research on the microfluidic manufacture of alginate particles using a variety of different approaches.

2.1.1.1 Continuous process

(1) Coalescence of a Na-alginate droplet with a droplet containing gelation ions

The Na-alginate droplets and droplets containing Ca^{2+} were generated at separate locations of a microchannel array device for this approach, which flowed downstream and consolidated

to create alginate hydrogel particles. Three examples based on this approach were listed. Firstly, as shown in **Fig. 2.2**, As a continuous microfluidic reactor, the microfluidic device consists of two independent infusing channels and a chemical reaction channel to manufacture hydrogel particles with size and shape control. They were successful in creating hydrogel microparticles with a variety of morphologies.

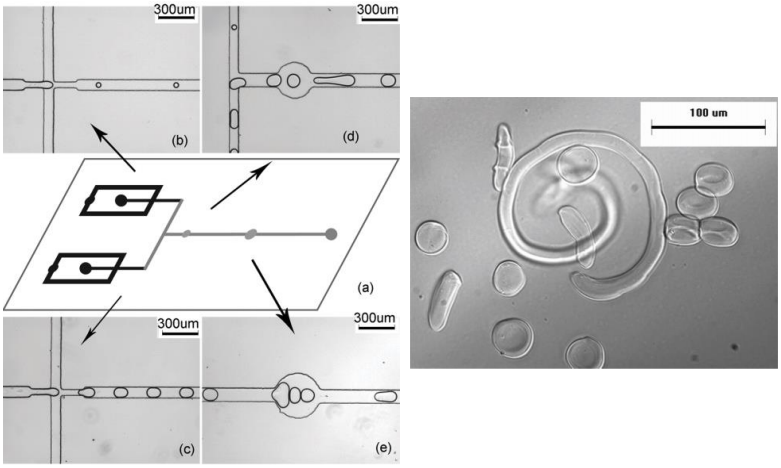

Fig. 2.2 Coalescence of a Na-alginate droplet with a $CaCl_2$ droplet to form Ca-alginate hydrogels particles. Reproduced with permission [6]. Copyright 2006 ACS.

Secondly, as shown in **Fig. 2.3**, the nozzle placed upstream of the microchannel produces a Na-alginate droplet. The generated alginate droplet then moves downstream of the main channel due to the continuous liquid phase flow and is merged with the droplets containing Ca^{2+} created from the nozzle positioned downstream, generating hydrogel particles. The Ca-alginate hydrogel particles formed in this study had a nonspherical and non-uniform shape.

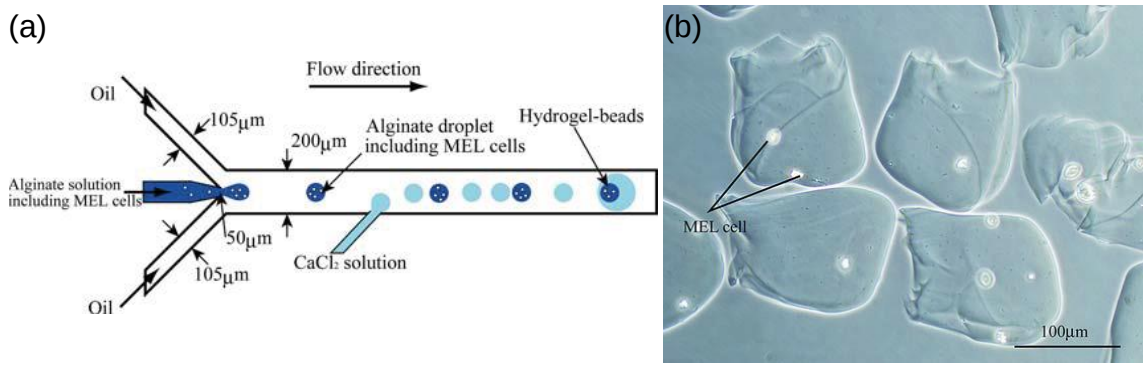

Fig. 2.3 Coalescence of a Na-alginate droplet with a $CaCl_2$ droplet. (a) Schematic graph and (b) obtained hydrogel particles. Reproduced with permission [7]. Copyright 2007 Springer.

Finally, as shown in **Fig. 2.4**, Alginate microgels were created using a microfluidic device with a co-flow structure. Using a glass capillary device with two parallel channels, the coupled cores preferentially coalesce after regulated delay under a strong capillary force imposed by a nonspherical exterior of the oil shell, resulting in the creation of single-core double-emulsion droplets. When the two segments contain alginate and Ca^{2+}, the fusion results in the creation of alginate microgels.

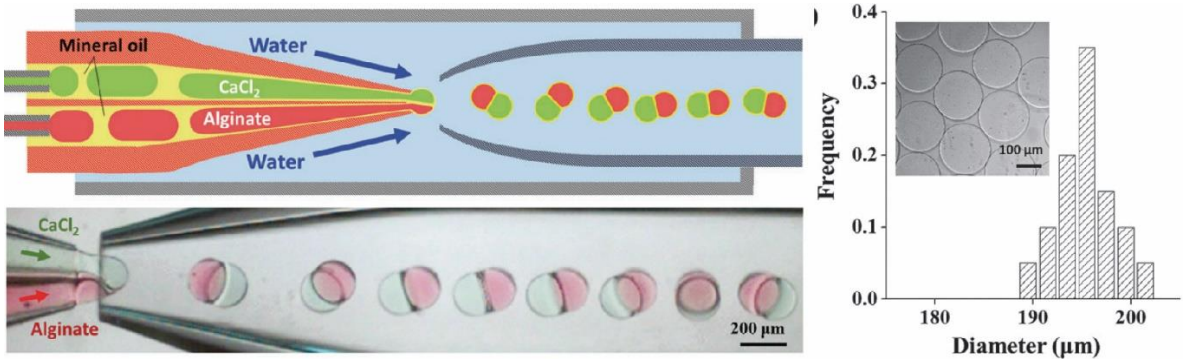

Fig. 2.4 Schematic graph of coalescence of Na-alginate droplet with $CaCl_2$ droplet. Reproduced with permission [8]. Copyright 2016 RSC.

(2) Off-chip reaction of Na-alginate droplets in a gelation agent-containing bath

The Na-alginate droplets were initially produced within the microchannels for this approach. They were then transferred to an outer reservoir containing a cross-linking reaction triggered agent (e.g., $CaCl_2$ solution) forming hydrogel particles [9]. An example is shown in **Fig. 2.5**.

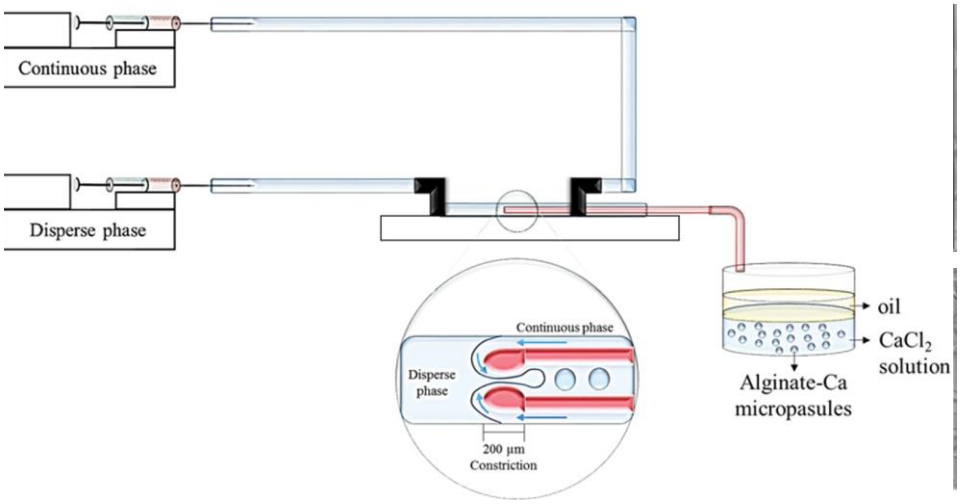

Fig. 2.5 Example of off-chip external gelation. Reproduced with permission [9]. Copyright 2017 Elsevier.

(3) A gelation agent is added to the oil phase to trigger the reaction

For this method, the gelation agent was delivered by the continuous oil phase. An example is shown in **Figs. 2.6 and 2.7**.

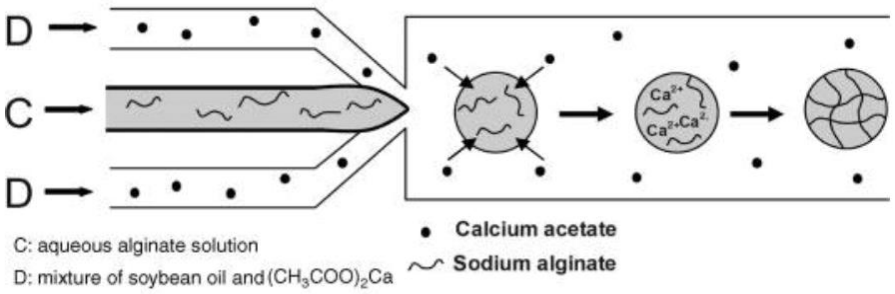

Fig. 2.6 External gelation utilizing an oil phase containing cross-linking chemicals. Reproduced with permission [10]. Copyright 2007 Wiley-VCH.

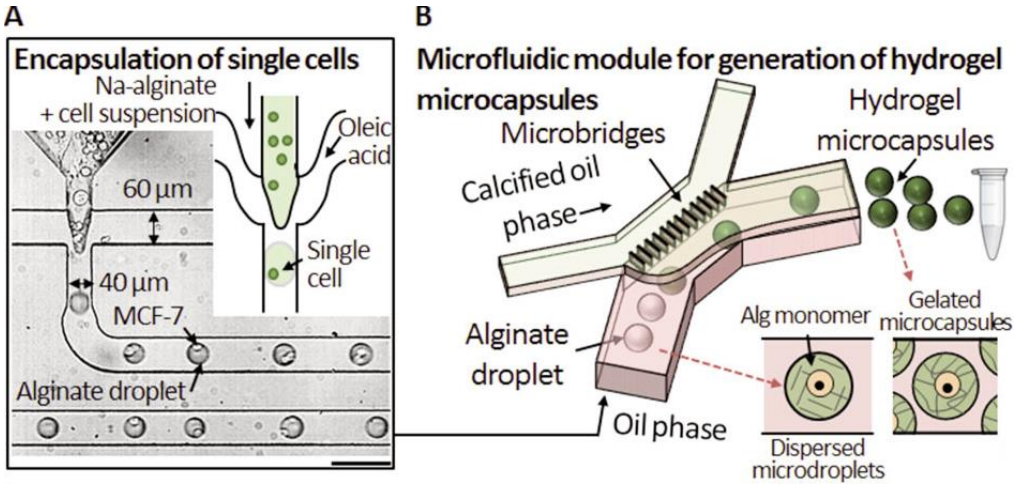

Fig. 2.7 Optical microscopy images of different alginate beads synthesized through gelation utilizing an oil phase containing cross-linking chemicals. Reproduced with permission [11]. Copyright 2014 Wiley-VCH.

(4) Phase separation of double emulsion

This approach makes use of the dissolution of a less soluble salt of divalent ions embedded in the droplets, which occurs in reaction to changes in the properties of the environment around the droplets, to produce the desired results. Three examples were listed here. Firstly, as shown in **Fig. 2.8**, in a continuous phase of corn oil, the Na-alginate droplets containing $CaCO_3$

nanoparticles were generated. The acetic acid in corn oil was injected farther downstream, and mixed with the oil flowing in the mainstream. When the acetic acid diffused into the Na-alginate droplets, Ca^{2+} was liberated from the insoluble calcium complex, triggering the gelation.

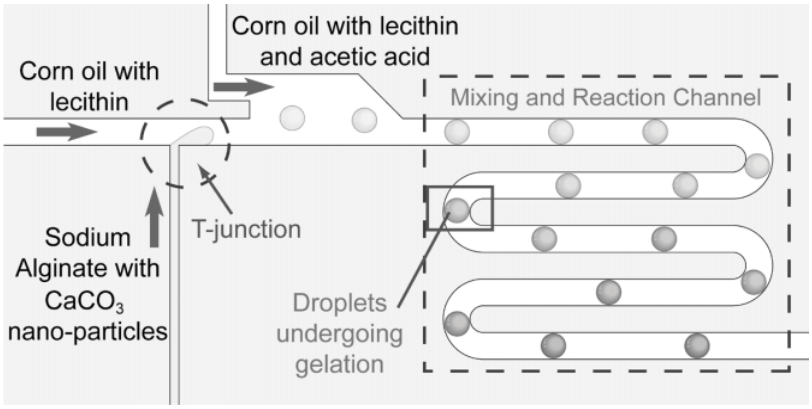

Fig. 2.8 Internal gelation that transfers the gelation agent inside the microchannel. Reproduced with permission [12]. Copyright 2007 Wiley-VCH.

Secondly, the aqueous Na-alginate droplets containing $CaCO_3$ nano-particles can form hydrogel particles by subsequently being transported into the outer bath containing gelation agent (**Fig. 2.9**) [13].

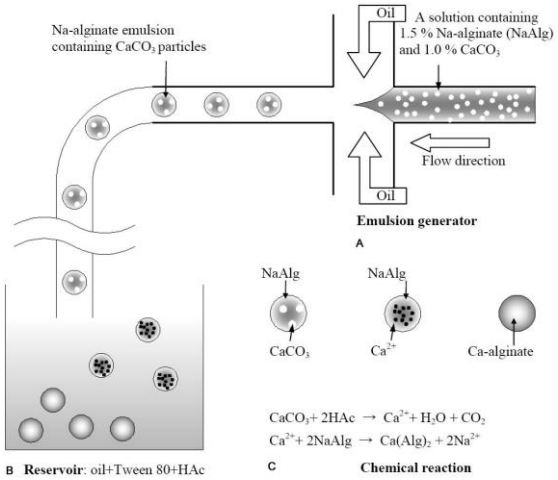

Fig. 2.9 internal gelation that transfers the gelation agent outside the microchannel. Reproduced with permission [13]. Copyright 2007 IMR.

Finally, the group of S. Utech et al. reported a technique that Ca^{2+} is delivered using a water-soluble calcium–ethylenediaminetetraacetic acid (EDTA) combination. Due to the use of the anti-chelating agent EDTA, calcium ions may stay in solution while being inaccessible to the alginate chains. With the addition of acetic acid to the continuous phase, they may cause the dissociation of the complex and the release of calcium ions after the creation of drops. A highly regulated interaction between free ions and alginate chains results in the formation of alginate hydrogel particles that have very outstanding structural uniformity. (**Fig. 2.10**).

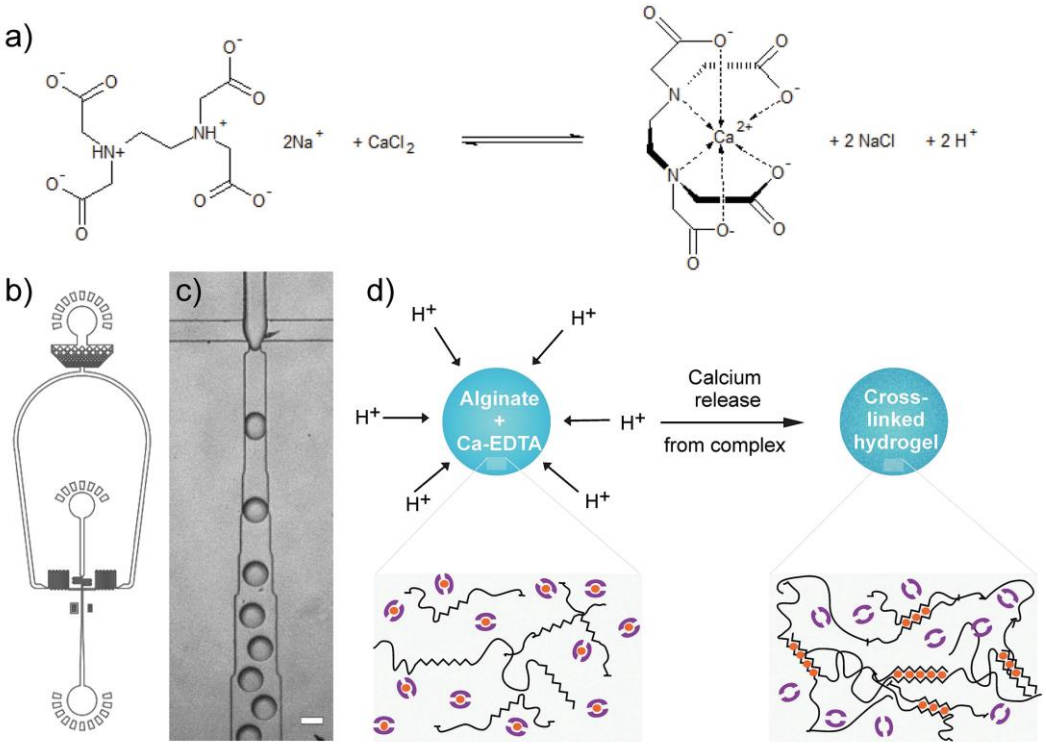

Fig. 2.10 Schematic of internal gelation using water-soluble Ca-EDTA. Reproduced with permission [4]. Copyright 2015 Wiley-VCH.

(5) Phase separation of double emulsion

Saeki et al. devised the double emulsion rupture approach. W/O/W emulsion droplets with a thin oil shell were created using microfluidic devices (**Fig. 2.11**). The center was a Na-alginate aqueous solution, while the outside aqueous phase included a gelation agent. When the thickness of the oil shell was tiny enough, the double emulsion droplets were readily ruptured, and the inner droplets quickly gelled.

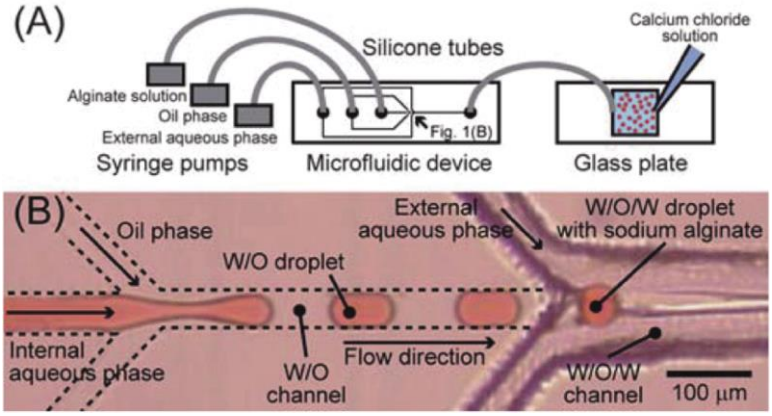

Fig. 2.11 Formation of Ca-alginate particles through double emulsion. Reproduced with permission [14]. Copyright 2010 RSC.

(6) Simultaneously reaction inside the single droplets

For this method, several kinds of aqueous solution flows were linked in a microchannel just before the creation of droplets, and the crosslinking process occurred in the droplets (**Fig. 2.12**) [15].

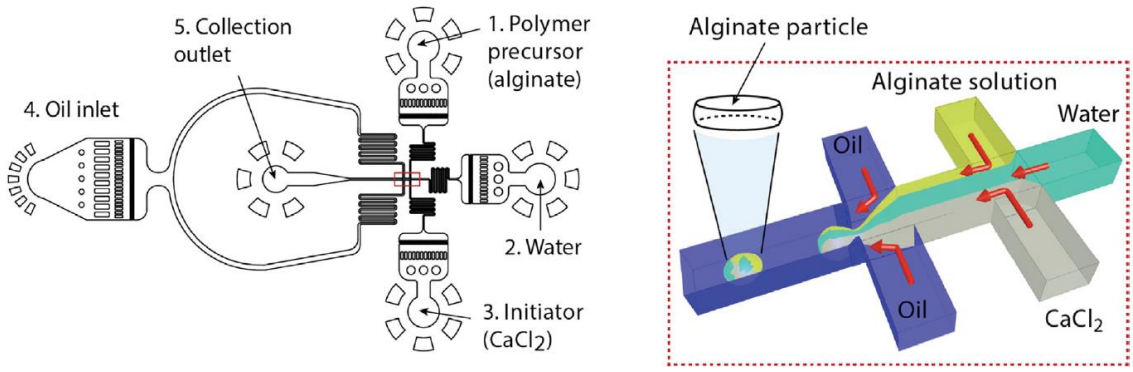

Fig. 2.12 In-situ mixing of alginate solution and $CaCl_2$ solution inside the droplets to form Ca-alginate microparticles. Reproduced with permission [15]. Copyright 2015 Wiley-VCH.

2.1.1.2 Batch process

The batch process for synthesizing hydrogel particles based on external gelation has also been reported recently. Droplets are generated in the air and then delivered into the aqueous phase to trigger the gelation (**Fig. 2.13**) [16].

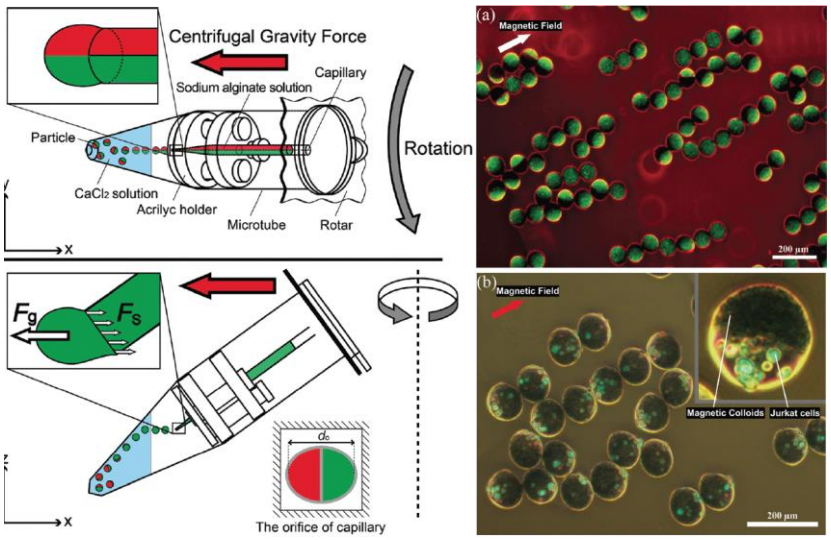

Fig. 2.13 Air-jet-based process to produce alginate microparticles. Reproduced with permission [16]. Copyright 2012 Wiley-VCH.

2.1.2 Comparison of different methods

As described above, the comparison of different methods to generate Ca-alginate hydrogel particles is shown in **Table 2.1**.

Table 2.1 Sizes and size distribution of alginate hydrogel beads prepared by a continuous and batch process in literature

Process	Method for supplying Ca^{2+} (or Ba^{2+})	Average diameter [μm]	Coefficient of variation [%]	Reference
Continuous Process (Internal gelation)	On-chip poorly soluble salt	94-150	< 2.9	12
		N.A.	N.A.	13
	On-chip water-soluble salt	10-50	N.A.	4
	On-chip coalescence of microfluidic water-in-oil droplets	ca. 20–50	< 3.6	6
		104–167	6.4	7
		195	1.5	8
		77.4–216	11.1–14.4	17
		34–53	< 5	18
	Off-chip gelation bath	100–250	N.A.	9
		226–244	11.4–36.7	19
		N.A.	N.A.	20
		6.2	< 10	21
Continuous Process	On-chip continuous flow of calcified oil	50–70	< 2	10
		16.7–39.7	2.7–6.6	11

(External gelation)		14.6–27.6	2.5–7.8	22
		~130	0.44	23
		69.6	N.A.	24
		N.A.	N.A.	25
	On-chip outer gelation phase of Water-in-oil-in-water emulsion	41.8	5.0	14
	On-chip gelation inside a multiphase droplet	N.A.	N.A.	15
		112	3.9	26
		N.A.	N.A.	27
Batch Process	Gelation bath under a jet nozzle (oil-free)	99	2.0	16
		20–60	N.A.	28
		120–300	< 7.5	29
		68.8	10.9	30

In conclusion, for the continuous process of manufacturing alginate hydrogel particles, internal gelation of Na-alginate droplets is commonly accomplished by the use of weakly soluble salts of divalent cations (e.g., $CaCO_3$ particles) [4,12,13,31–35]. Although the internal gelation process has response control, gelation necessitates alterations in the surrounding environment, such as a decrease in the pH of the droplets, which may cause harm to the enclosed cargos, such as live cells. Furthermore, the presence of weakly soluble salt particles restricts the size of the microchannels and, as a result, the dimensions of the hydrogel particles that are formed.

Continuous processes for generating alginate hydrogel particles based on external gelation of Na-alginate droplets have also been reported. For external gelation, the reactant divalent cations can be in the $CaCl_2$ solution droplets [6–8,17,18], off-chip bulk solution [9,19–21], or supplied directly through the oil phase [10,11,22–25,36]. The external gelation methods reported before all have some difficulties. For instance, in the method of coalescence of a Na-alginate droplet with a droplet containing cross-linking agent, a 1:1 pair of two types of droplets is necessary; instead, the distribution of particles diameter becomes broader, making it difficult to achieve high controllability of particle size. Furthermore, the procedure is simple for the approach that employs the off-chip bulk solution, but the contact of the Na-alginate droplets with the water-oil interface often causes the deformation of droplets, resulting in the creation of non-spherical particles. In addition, for the method that directly supplies the divalent cations through the oil phase, the incorporation of divalent cations and oil phase is a demanding task, because the reactant (e.g., calcium chloride) is usually insoluble in an oil phase. As a result, the reactant oil phase is typically made from the emulsion of an aqueous solution containing divalent cations

and oil through the evaporation of the water phase. But this method often creates extra solid residues that need filtration and low reactant concentration in the oil phase [22–25].

Moreover, as previously noted, the continuous process using external gelation often results in clogging problems and the development of non-uniform hydrogel particles as a result of the fast reaction speed and heterogeneous distribution of divalent cations inside devices.

Alternatively, batch techniques based on external gelation for the generation of hydrogel particles by droplets shooting in the air have also been described [16,28–30]. The comparatively limited throughput of droplet generation, on the other hand, restricts the scope of its applicability.

Therefore, although the microfluidic external gelation may be potentially suitable for the production of monodisperse hydrogel microspheres, to our knowledge, there has not yet been reported a continuous process for the production of highly spherical alginate-based hydrogel particles using external gelation.

2.1.3 Objectives

In this chapter, a microfluidic in-situ external gelation method utilizing $CaCl_2$ emulsion as a reactant that is used to produce extremely spherical Ca-alginate hydrogel particles was presented. Specifically, the microfluidic channel is comprised of two cross-junctions that are linked serially: the upstream cross-junction, which is used for the production of Na-alginate droplets in a sheath flow of corn oil, and the downstream cross-junction, which is used for the external gelation of a fine W/O emulsion containing $CaCl_2$ in a symmetrical co-flow of corn oil. The essential parameters to obtain the highly spherical hydrogel particles were also investigated.

The main objectives of this chapter are as follows:

(1) To design and fabricate a microfluidic device for synthesizing highly spherical hydrogel particles.

(2) To investigate the influence factors on the shapes and sizes of obtained hydrogel particles.

2.1.4 Outline of chapter

Section 2.1 Introduction

Introduces the background of previous researches about the alginate-based hydrogel particles.

Section 2.2 Materials and methods

Describes the peripheral equipment, our microfluidic device, and the materials that used in this experiment.

Section 2.3 Results and discussion

Demonstrates the experiments about synthesizing the highly spherical Ca-alginate hydrogel particles using our novel device. The influence factors of the roundness and sizes of obtained hydrogel beads are also reported.

Section 2.4 Conclusion

Describes the conclusion of this chapter.

2.2 Materials and methods

2.2.1 Microfluidic emulsion-based external gelation

The development of a microfluidic external gelation method using an on-chip water-in-oil (W/O) emulsion reactant for the production of highly spherical Ca-alginate hydrogel particles is described. The generated Na-alginate droplet in the microchannel contacted with the much smaller $CaCl_2$ droplets in the $CaCl_2$ aqueous/corn oil emulsion. The Ca^{2+} that goes inside the Na-alginate droplet can react with the alginate molecular forming a Ca-alginate polymer network (**Fig. 2.14**).

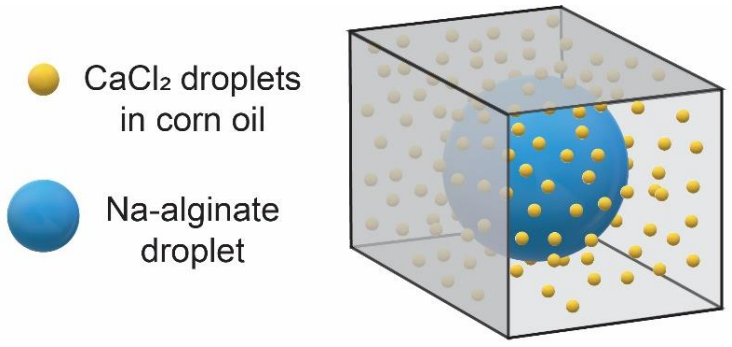

Fig. 2.14 Schematic graph of the emulsion-based external gelation

2.2.2 Microfluidic device

2.2.2.1 Design of the microfluidic channel

A microfluidic channel with two cross-junctions coupled serially: the upstream cross-junction for creating Na-alginate droplets in the corn oil flow and the downstream cross-junction for symmetrically co-flowing fine W/O emulsion carrying Ca^{2+} for external gelation was designed (**Fig. 2.15**). The four channels of the upstream cross-junction are 200 μm wide and 200 μm deep. The two input channels for reactant emulsion have a width of 200 μm at the downstream cross-junction, while the drain channel has a width of 400 μm, with a depth of 400 μm. This broader and deeper drainage channel was intended to produce spherical hydrogel particles even when the diameter of the precursor Na-droplets is greater than the cross-sectional dimension of the upstream channel (i.e., 200 m).

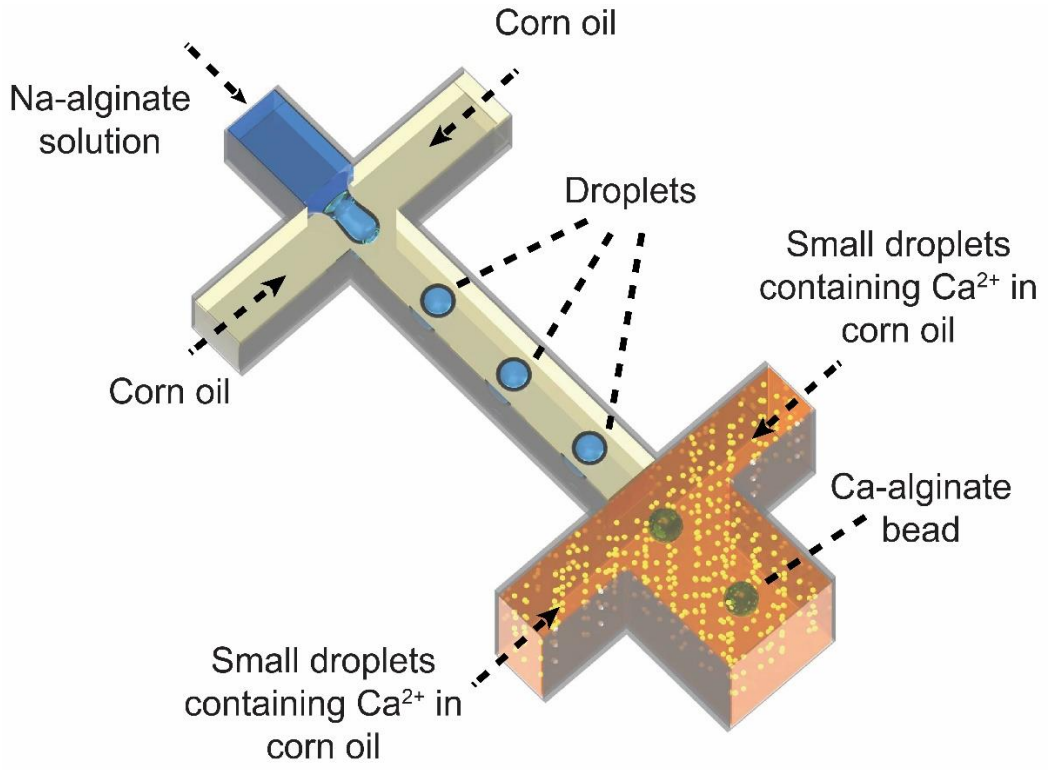

Fig. 2.15 Schematic graph of the microfluidic channel design.

2.2.2.2 Microfabrication

To create microgrooves and through-holes, mounted wheels were used with computer numerical control (CNC) machining on a quartz glass chip (15 mm x 15 mm, 2 mm thick)

(LB2000 EXII, OKUMA, Japan). Fused bonding was used to secure the microgrooves to a planer quartz glass piece of the same size (**Fig. 2.16**). The cross-section of the microgrooves is rectangular (**Fig. 2.17**). The details are shown in **Appendix (A.1.1)**.

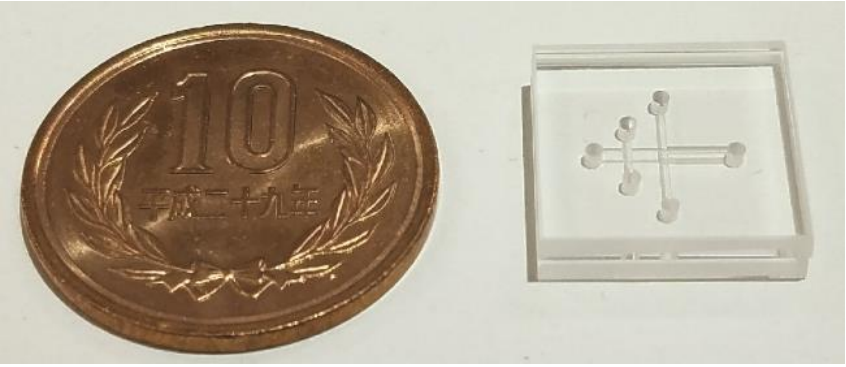

Fig. 2.16 Image of a fabricated microfluidic glass chip.

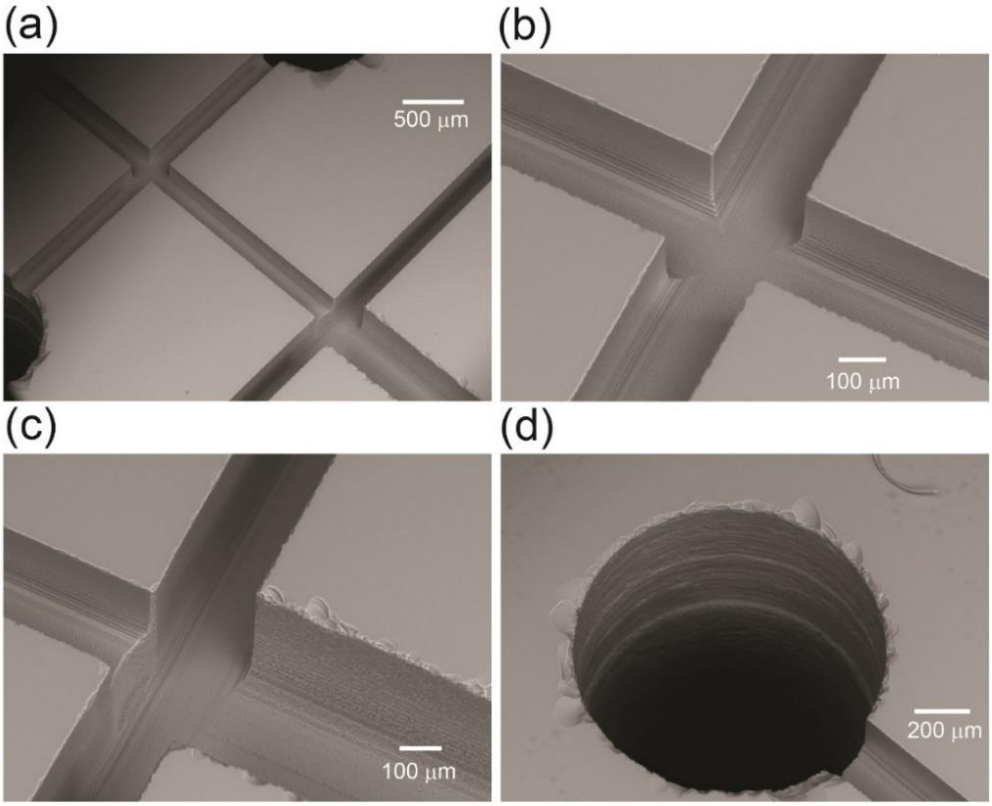

Fig. 2.17 The SEM images of (a) the fabricated rectangular microgrooves, (b) the upstream cross-junction, (c) the downstream cross-junction, and (d) the through-hole.

2.2.2.3 The preparation of microfluidic system

Syringe pumps were used to fill gastight glass syringes (1000 series, Hamilton Company, NV, USA) with the various liquids (KDS 200 and KDS LEGATO 200, KD Scientific Inc., PA, USA). An assembled glass microfluidic chip was mounted in a stainless steel supporting holder (36 mm x 36 mm x 10 mm) and connected to syringes via polytetrafluoroethylene (PTFE) tubes (0.5 mm inner diameter for input tubes and 0.8 mm inner diameter for output tubes) and connectors (0.5 mm inner diameter for input tubes and 0.8 mm inner diameter for output tubes). The details are shown in **Appendix (A.3)**.

2.2.2.4 Modification of the surface

The glass surface of the microfluidic chip was modified to hydrophobic to generate W/O droplets. As a surface-modifying agent, 1 wt percent octadecyltrichlorosilane (ODS, Shin-Etsu Chemical, Japan) in toluene was utilized.

2.2.3 Materials

Unless specific noted, all of the reagents were obtained from Wako Pure Chemical Industries, Japan. A 3 wt% aqueous solution of sodium alginate with a viscosity of about 1500 mPa·s served as the dispersion phase, and corn oil with a viscosity of approximately 60 mPa·s served as the continuous phase, resulting in the formation of sodium alginate droplets A 30 wt % aqueous solution of $CaCl_2$ was mixed with corn oil, which included a surfactant (SY-Glyster CRS-75, Sakamoto Yakuhin Kogyo, Osaka, Japan), by 0.1 wt% to produce the reactant W/O emulsion. To wash out the reactant emulsion and collect the hydrogel particles, pure water and hexane were utilized.

2.2.4 Preparation and characterization of reactant emulsion

The reactant W/O emulsion containing Ca^{2+} was created by homogenizing it for 3 minutes at 30,000 rpm in a mixer (T10 basic ULTRA-TURRAX, IKA, Germany). The diameters of reactant W/O emulsion droplets were determined using a laser scattering particle size distribution analyzer (Partica LA-960, HORIBA, Japan).

2.2.5 Preparation of Ca-alginate hydrogel particles

To collect the microcapsules, the mixture that exited the output tube (inner diameter, 0.8 mm; outer diameter, 1.58 mm) was placed over a nylon mesh (mesh size: 100 μm × 100 μm, Tokyo Screen, Tokyo, Japan). To remove the CaCl2 emulsion, deionized water was poured over the capsules. The leftover corn oil was then flushed away using hexane. Finally, distilled water was used to wash the hexane away.

2.3 Results and discussion

2.3.1 Formation of Na-alginate droplets

2.3.1.1 Droplet formation region

The generation procedure of Na-alginate droplets at the first junction was firstly investigated. It is well known that, in low Reynolds condition, there exists a specific mountain-shaped region in the diagram of continuous (Q_c) and disperse phases (Q_d). When the flow conditions fall within this region, monodisperse droplets can be formed [37]. As a consequence, this phase diagram (**Fig. 2.18**) was created to better comprehend the relationship between flow patterns and the hydrodynamic domains that follow them.

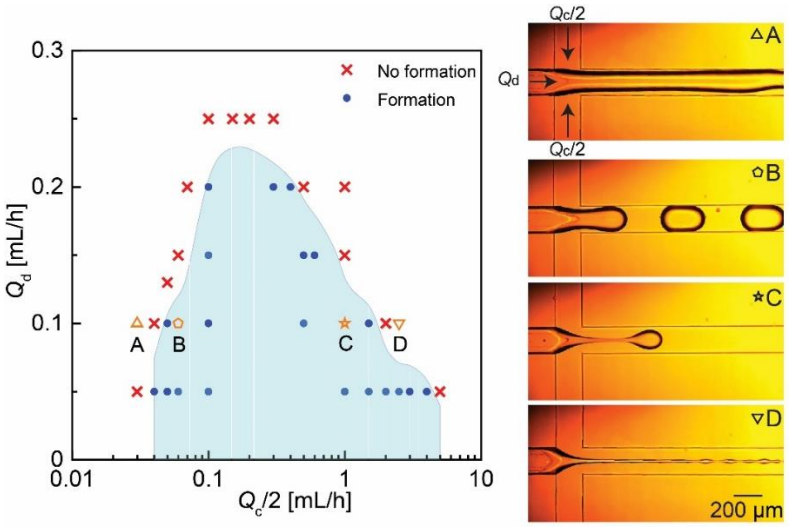

Fig. 2.18 A phase diagram depicting the circumstances in which Na-alginate droplets may generate. The horizontal axis is the flow rate of the continuous phase (Q_c) and the vertical axis is the flow rate of the dispersed phase (Q_d). The crosses represent a flow condition where monodisperse droplets cannot be formed. The solid circles depict the flow conditions under which monodisperse droplets may generate. The open triangles show the circumstances of a stream that is elongated (inset A), the open pentagon and star represent the condition where stable droplets formed in squeezing and dropping types respectively (inset B and C), the open inverted triangles represent condition for irregular jetting (inset D).

The Q_d for creating monodisperse drops was 0.2 mL/h, with Q_c varying from 0.2 mL/h to 0.8 mL/h. When Q_d was less than 0.2 mL/h, the Na-alginate solution produced a steady laminar

flow if Q_c was too low, while a disorganized generation of droplets was seen in the jetting regime when Q_c was too high. Droplets of similar size might develop if Q_c and Q_d were suitably tuned under low Reynolds number circumstances (ca. 0.02).

2.3.1.2 Droplet generated inside the microchannel

Figure 2.19 depicts a typical process of the production of a Na-alginate droplet when Q_c and Q_d are set to 2.0 mL/h and 0.1 mL/h, respectively, as shown in the experiment. In a dripping mechanism, droplets of similar size were progressively created, with the break-up rate averaging around 8 droplets/s. Since of the high viscosity of the Na-alginate aqueous solution, two satellite droplets with average diameters of 39 μm and 16 μm were generated; nevertheless, they merged with the main droplet on occasion (from 72 ms to 75 ms) because pure corn oil without surfactant was employed as the continuous phase. The satellite merged with the main droplet before reaching the downstream, so it did not affect the shape and surface of obtained hydrogel particles. Later, the droplets flowed into the downstream cross-junction and interacted with the reactant W/O emulsion (**Fig. 2.20**, t = 90 milliseconds)

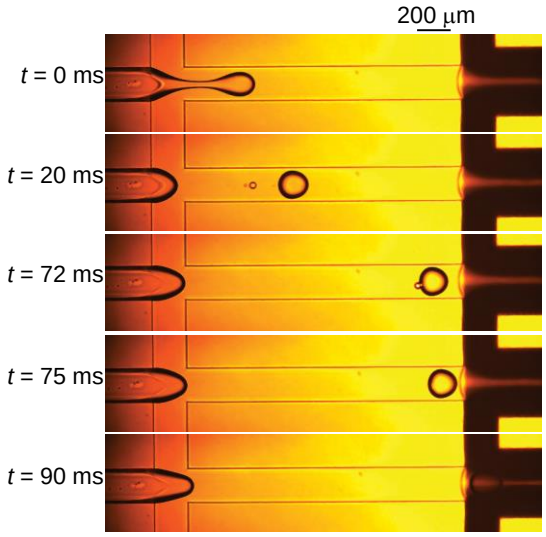

Fig. 2.19 Images of generation of a Na-alginate droplet. The Q_d and Q_c were 0.1 and 2.0 mL/h (= 1.0 mL/h × 2) respectively.

The symmetrical co-flow of reactant W/O emulsion at a downstream cross-junction caused the Na-alginate droplets to flow in the downstream channel's center. The downstream channel's greater cross-sectional area lowered flow velocities, reducing shear-induced significant droplet

deformation. Furthermore, the deeper and wider downstream channel allowed spherical droplets with diameters greater than the nozzle dimension of the upstream cross-junction to pass. If used routinely, the microfluidic chip may run indefinitely without gel blockage.

2.3.1.3 Produced droplets

(1) Experimental results

The sizes of Na-alginate droplets after collection outside the micro-channels were measured. Corn oil with a surfactant of 1 wt% was used rather than reactant W/O emulsion at the drain cross-junction to avoid the coalescence of Na-alginate droplets in the collecting reservoir. The flow rate of corn oil downstream was set as 20 mL/h.

The production of monodisperse Na-alginate droplets of various sizes was achieved by varying Q_c while maintaining a constant Q_d of 0.1 mL/h. In a Q_c of 2.0 mL/h, the produced Na-alginate droplets had an average diameter of 191 μm and a CV of 2.2%, indicating that the process was successful (**Fig. 2.20a**). When the flow rate was reduced to 1.2 mL/h, the Na-alginate droplets generated had an average diameter of 201 μm and a CV of 2.4%, respectively (**Fig. 2.20b**). When the flow rate was raised to 3.0 mL/h, the resulting Na-alginate droplets had an average diameter of 176 μm and a CV of 1.9%, respectively (**Fig. 2.20c**). These CV values indicate that the droplets were monodisperse and had a very limited size distribution, which is consistent with earlier work [23,38,39].

The influence of Q_c/Q_d on the size and CVs of generated droplets was also examined in more detail (**Fig. 2.20d**). It is showing that Changing the Q_c/Q_d ratio in the range of 6.0 to 30.0 might result in droplets that were both larger and smaller (ranging from 176–225 μm) than the orifice size and with CV values less than 3%, the findings show.

(2) Analysis of droplet scaling law

The huge number of geometrical aspect ratios that characterize flow-focusing devices has made it difficult to develop simple scaling equations to forecast droplet size, distribution, and generation frequency as a function of the essential parameters.

However, the mechanisms governing gas/liquid flow conditions confined in a microfluidic flow-focusing droplet generator have been reported by Garstecki et al. [40] and Dollet et al [41], showing that the break-up of bubbles occurs at a rate proportional to the velocity of the co-

flowing continuous fluid (v): $f \propto v$, where f is the break-up rate. And then, it is easy to conclude that the droplet diameter (D_d) is proportional to the minus one-third power of the Capillary number (Ca): $D_d \propto Ca$.

Whereas, it is unclear if this model for gas threads works in the same manner as the fluid flows (e.g. 1500 mPa·s in this case) reported by Cubaud et al. [42] or Lee et al. [43]. As a consequence, there are no perfect scaling equations available for transitions between distinct regimes, let alone for droplet size and production frequency [44].

Based on the published literatures on the mechanism of generation of droplets using the flow-focusing method, the diameter of a droplet (D_d) is determined by the flow rate ratio Q_c/Q_d for a given microchannel geometry [38]. Here, the following scaling law of the generated droplet sizes in the dripping mechanism is assumed:

$$D_d \,/\, D_h = \gamma \left(\frac{Q_c}{Q_d}\right)^a \tag{2-1}$$

D_h is the hydraulic diameter of the orifice, given by $D_h = 4A/P^{-1}$, where A is the cross-section area of the orifice and P is the perimeter of the orifice, γ and a are the parameters dependent on the microchannel geometry, fluid viscosity, and interfacial tensions. Through the linear fitting, the predicted relationship of the generated droplet diameter and flow rate ratios is:

$$D_d \,/\, D_h = 1.48 \left(\frac{Q_c}{Q_d}\right)^{-0.15} \tag{2-2}$$

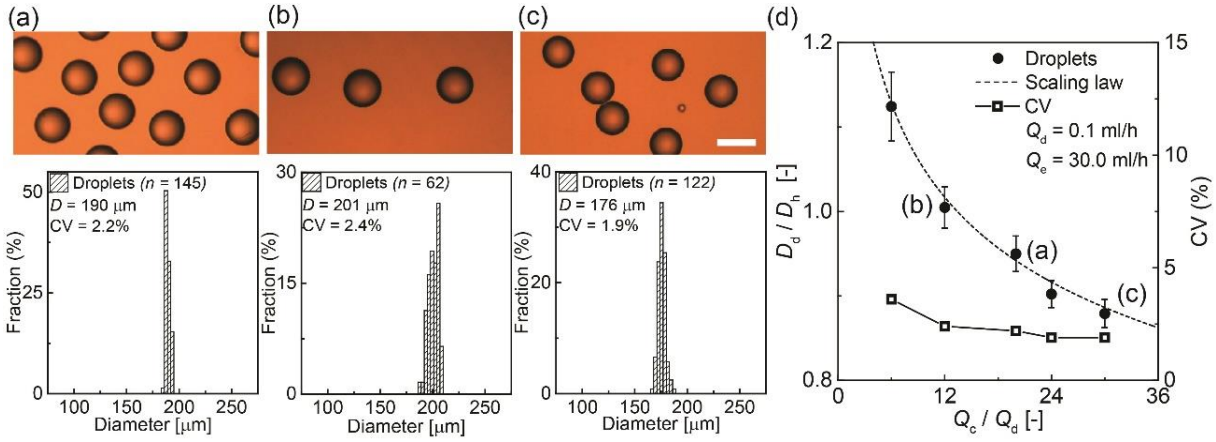

Fig. 2.20 Influence of Q_c on the diameter of the droplet. (a-c) Images of droplets and the size distribution at (a) Q_c/Q_d = 20.0, (b) Q_c/Q_d = 12.0, (c) Q_c/Q_d = 30.0. Q_d = 0.1 mL/h. (d) The flow rate ratio Q_c/Q_d vs. the sizes and CVs of Na-alginate droplets. The dashed line represents the scaling law. Scale bar is 200 μm.

2.3.2 Calcium chloride emulsion reactant

The reactant W/O emulsion was composed of a 30 wt% aqueous $CaCl_2$ solution combined with corn oil having a surfactant (SY-Glyster) which was fabricated through a mechanical homogenizer at the maximum rotation speed which is 30000 rpm. Before mixing, the corn oil phase and $CaCl_2$ aqueous solution phase have a clear interface boundary (**Fig. 2.21a**), because they are immiscible. After 3 minutes of homogenizing process, the mixture has a milk-white color (**Fig. 2.21b**).

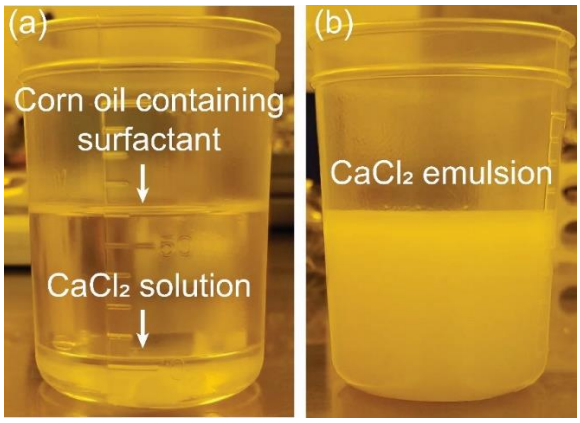

Fig. 2.21 Corn oil and $CaCl_2$ aqueous solution (a) before and (b) after mixing.

2.3.3 Highly spherical Ca-alginate hydrogel particles

In this section, the formation method of synthesizing highly spherical Ca-alginate hydrogel particles was demonstrated. Parameters including the property of reactant W/O emulsion and the flow rate of continuous and emulsion phase that can influence the shapes and sizes of produced hydrogel particles were fully investigated.

Averaged values of roundness (*R*, **Fig. 2.22**) was used to evaluate the shape of obtained gel particles, which is defined as:

$$R = \frac{4\pi S}{L^2} \tag{2-3}$$

where *L* is the hydrogel particle's perimeter and *S* is the projected area from the microscopic picture as determined by the program ImageJ.

The roundness of a body is determined by the shape's basic characteristics instead of the sharpness of its edges and corners, or the roughness of the surface of a manufactured item, which are both important factors. When the eccentricity of a smooth ellipse is considerable, it

might have a low roundness. Regular polygons get more rounded as the number of sides increases, despite the fact that they retain their sharp edges on the edges. The Q_d, Q_c, and flow rate of the emulsion phase Q_e were set at 0.1, 2.0 (= 1.0 mL/h × 2), and 20.0 mL/h (= 10.0 mL/h × 2) respectively throughout the experiments.

When the influence of the property of reactant W/O emulsion was investigated, the effects of concentration of surfactant and the faction of aqueous solution (W) in reactant emulsion were demonstrated, because the obtained microparticles had different sizes and morphologies when the reactant W/O emulsions were produced at varying conditions. The definition of W is according to the following equation:

$$W = W_1 \div W_2 \tag{2-4}$$

where W_1 is the weight of the aqueous solution and W_2 is the total weight of $CaCl_2$ emulsion.

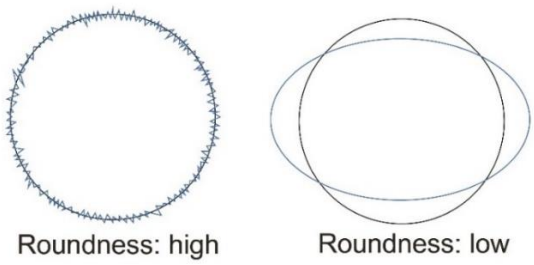

Fig. 2.22 Schematic illustration of roundness calculation.

2.3.3.1 The effect of surfactant concentration

Four kinds of reactant W/O emulsions containing surfactants at 0 wt%, 0.01 wt%, 0.1 wt%, and 0.3 wt% were prepared to test the influence of surfactant concentrations in the emulsion phase. The value of W was set to 0.33. The morphologies of the prepared hydrogel microbeads were examined (**Fig. 2.23**). When the concentration of surfactant was 0 and 0.01 wt%, hydrogel particles with significantly deformed shapes were produced and their roundness was 0.74 and 0.75 respectively (**Fig. 2.23-A and B**). When the surfactant concentration was increased to 0.1 wt%, more spherical hydrogel particles were produced and their roundness increased to 0.89 (**Fig. 2.23-C**). However, when the concentration of surfactant increased further to 0.3 wt%, bigger hydrogel particles with lower roundness of 0.78 were formed (**Fig. 2.23-D**). The relationship between surfactant concentration and roundness of obtained hydrogel particles is shown in **Fig. 2.24**.

The variance in roundness values of hydrogel particles formed at various surfactant concentrations may be linked to the durability of the reactant W/O emulsion. When the surfactant concentration was insufficient, the reactant W/O emulsion might be unstable, allowing aqueous droplets to readily combine and create larger aqueous droplets over time. These larger droplets were most likely responsible for the production of distorted hydrogel particles. However, if the surfactant concentration was too excessive, the reactant W/O emulsion may be too stable to merge with Na-alginate droplets, perhaps triggering mutual coalescence of several Na-alginate droplets prior to gelation, resulting in larger gel particles with reduced homogeneity. As a consequence, in the experiments, the ideal surfactant concentration was set at 0.1 wt%.

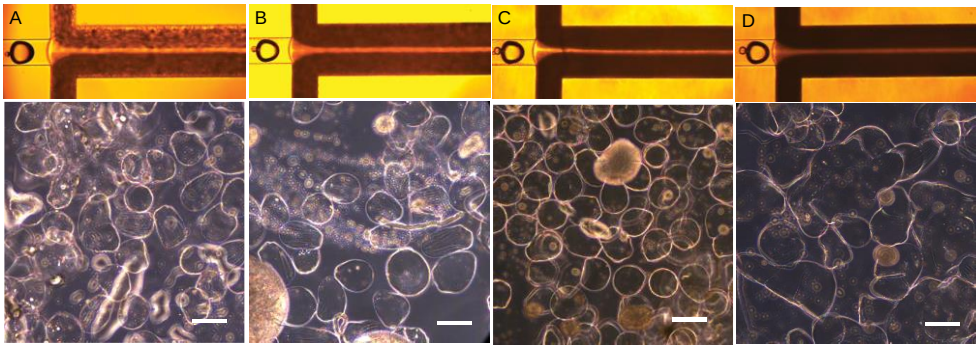

Fig. 2.23 Effect of surfactant concentration on the roundness of hydrogel particles. High-speed micrograph of hydrogel formation in the microchannel and micrograph of hydrogel particles produced by reactant emulsion with different concentrations of surfactant after filtered in pure water. (A) No-surfactant (roundness 0.735). (B) 0.01 wt% (roundness 0.746). (C) 0.1 wt% (roundness 0.889). (D) 0.3 wt% (roundness 0.784). The scale bar is 200 μm.

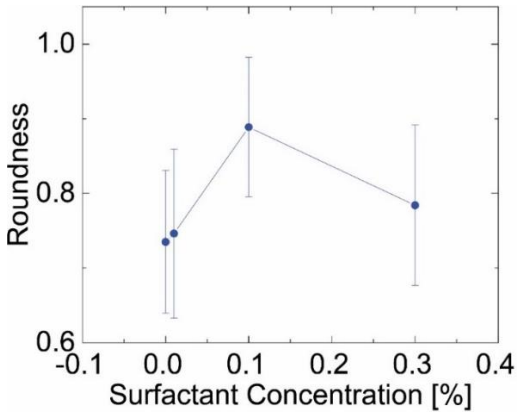

Fig. 2.24 Relationship between surfactant concentration and roundness of hydrogel particles. the weight fraction of 30 wt% $CaCl_2$ aqueous solutions in $CaCl_2$ emulsion (W) was set as 0.33.

2.3.3.2 The effect of the fraction of aqueous solution (*W*)

(1) Sizes of $CaCl_2$ emulsion at different *W*

The influences of *W* values on the morphology and size of hydrogel microparticles were investigated. The reactant W/O emulsions with surfactant at 0.1 wt% at *W* values in the range from 0.20 to 0.33 were prepared. The prepared reactant emulsion was first observed through the optical microscope which is shown in **Fig. 2.25**. Because the sizes of emulsion droplets are below 5 μm and their densities are too high, the reactant emulsion in corn oil with surfactant (SY-Glyster) of 1 % was diluted 50 times before observation.

Next, the sizes of reactant emulsions at three *W* values 0.20, 0.26, and 0.33 were measured by the laser scattering particles size distribution analyzer which is shown in **Fig. 2.26**.

Using the values of *W* as 0.20 and 0.26, the average diameter of aqueous droplets in reactant emulsion was 2.3 μm with a CV of 41.3% and 2.2 μm with a CV of 38.4%, respectively. In contrast, when *W* was raised to 0.33, the average diameter of aqueous droplets in reactant emulsion grew to 4.1 μm, which was almost twice as big as when *W* was 0.20 and 0.26. The CV of diameter grew as well, reaching 44.5%.

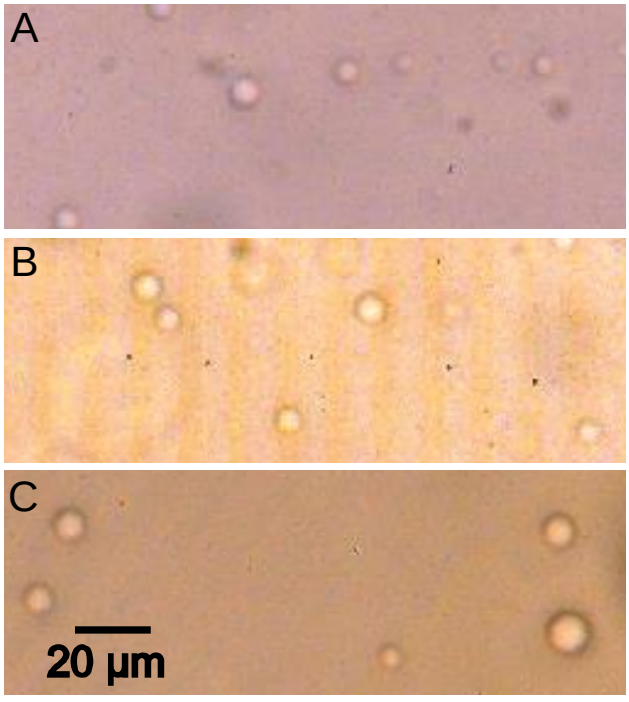

Fig. 2.25 $CaCl_2$ emulsion prepared at varying *W* values: (A)0.20, (B)0.26, and (C)0.33 after dilution in corn oil with a surfactant of 1 wt%.

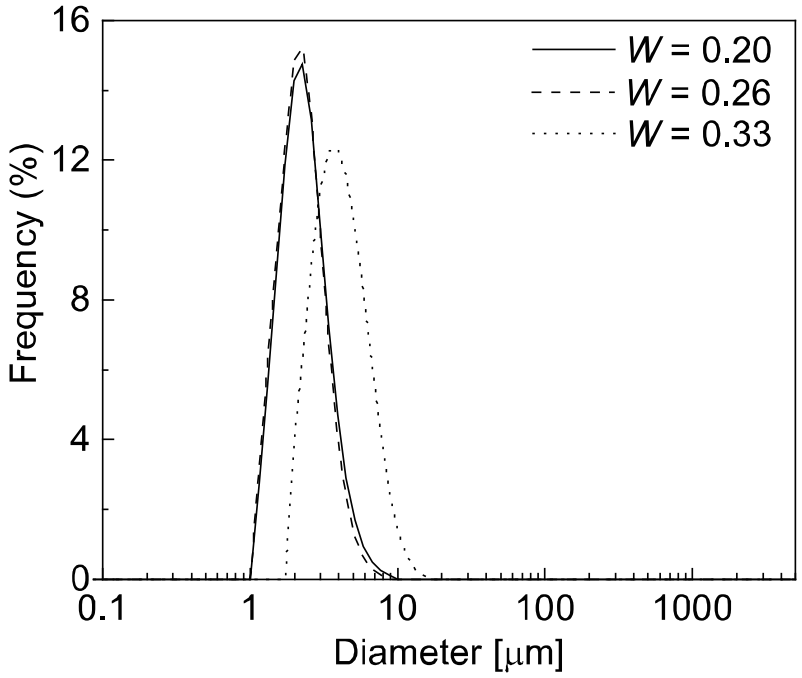

Fig. 2.26 Size distributions of aqueous droplets in reactant emulsion at *W*.

(2) Obtained Ca-alginate hydrogel particles at different *W*

The Q_d, Q_c, and Q_e were set at 0.1, 2.0, and 20.0 mL/h respectively for the following experiments. Obtained hydrogel microparticles using reactant W/O emulsions at three *W* values 0.20, 0.26, and 0.33 were shown in **Fig. 2.27.**

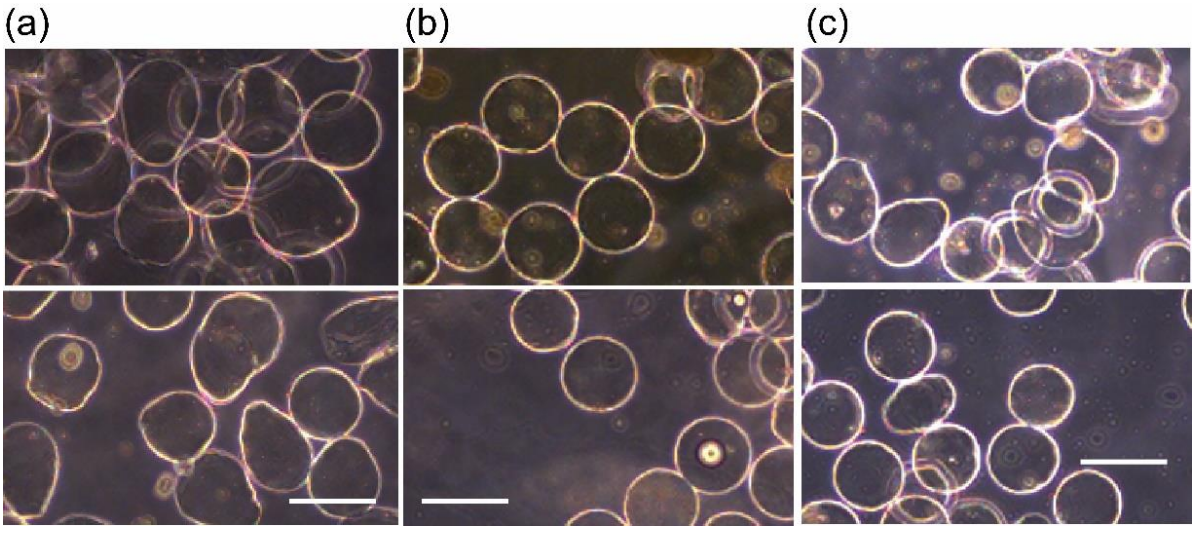

Fig. 2.27 Hydrogel microbeads generated at different *W* values: (a) 0.20, (b) 0.26, (c) 0.33. All scale bars are 200 μm.

Three repeated tests were also conducted to explore the influence of *W* on the roundness of hydrogel microparticles (**Fig. 2.28**). When *W* was 0.26, highly spherical hydrogel microspheres with a roundness of more than 0.96 were able to be synthesized; the average ± s.d. was 0.965±0.002 (n = 3). When *W* was more than 0.26, however, the calculated roundness of the hydrogel particles decreased as *W* grew. When *W* was less than 0.26, however, the roundness of the hydrogel particles reduced as *W* declined.

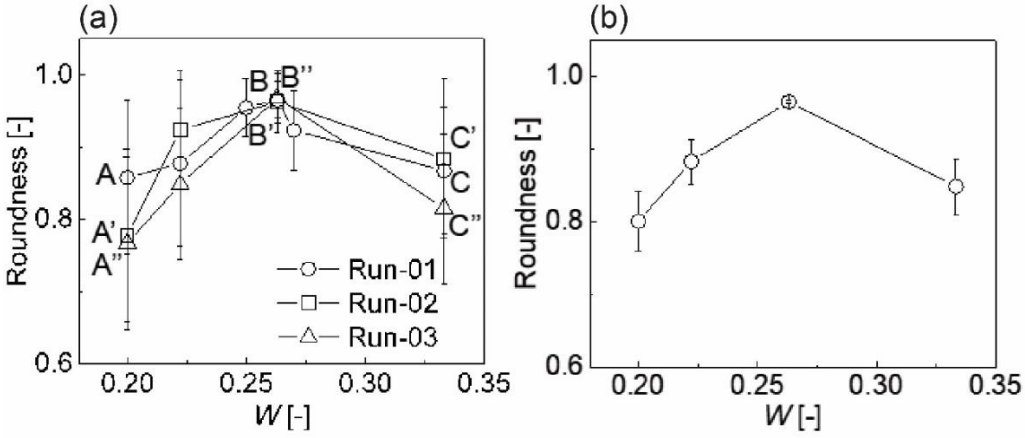

Fig. 2.28 The weight fraction of the aqueous phase in $CaCl_2$ emulsion *W*. (a) The influences of *W* on the roundness of hydrogel particles. (b) *W* vs. the average values of roundness (n = 3).

The three repeated studies studied the influence of *W* on the size and CVs of hydrogel particles in the same way (**Figs. 2.29, 30, and 31**). The produced gel particles had average diameters of 167 μm and a CV of 5.8% with a highly spherical form when *W* was 0.26 in the first run (**Fig. 2.27-B**); the average ± s.d. of the diameter and CV in the three tests were 162±4 μm and 4.3±1.1%. When *W* was more than 0.26, the diameters and CVs of the gel particles remained low. For instance, when *W* was 0.33 in the first run, the produced gel beads had average diameters of 154 μm and a CV of 6.4% with roundness about 0.87; in the three tests, the diameter, CV, and roundness were 159±9 μm, 6.1±1.1%, and 0.848±0.039. The gel particles that had been created had distorted into deformed morphologies (**Fig. 2.27-C**). When *W* was less than 0.26, the diameters and CV values of the beads increased. For example, when *W* was 0.20 in the first run, the generated hydrogel particles had a roundness of 0.86, a diameter of 166 μm, and a CV of 10.4%, implying that the generated hydrogel microbeads were larger and had

deformed structures (**Fig. 2.27-A**); the diameter, CV, and roundness in the three experiments were 170±5 μm, 12.1±1.2%, and 0.800±0.041, respectively.

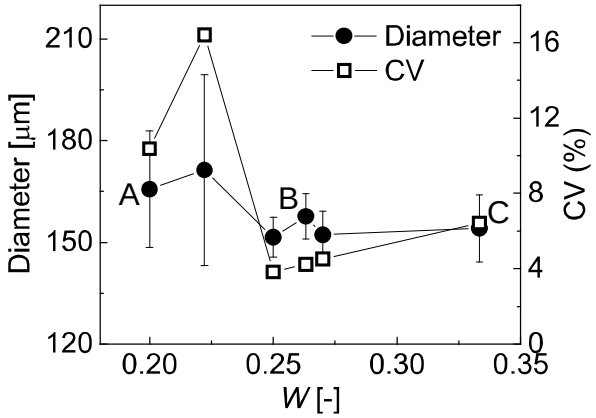

Fig. 2.29 The effect of *W* on diameter and its CV of the gels in the first run.

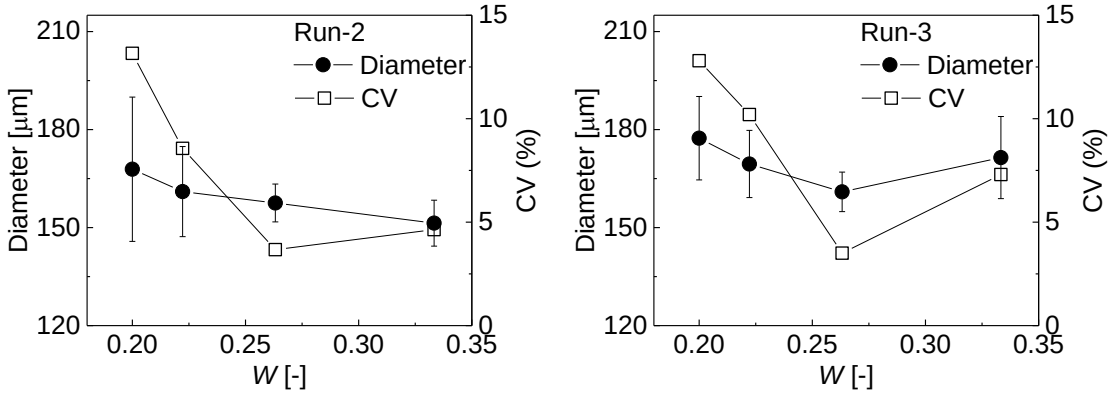

Fig. 2.30 Results of the second (left) and third (right) runs to measure the diameter and its CV values of the gels at four different *W* (= 0.20, 0.22, 0.26, 0.33).

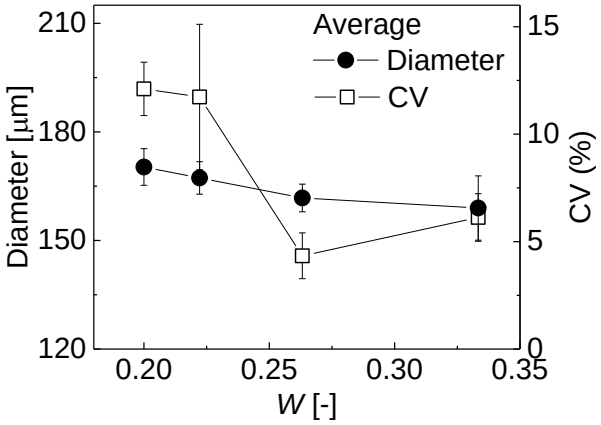

Fig. 2.31 The weight fraction of the aqueous phase in reactant emulsion *W* vs. the average values of diameter and CV (*n* = 3).

In conclusion, when the weight fraction of the aqueous phase in reactant W/O emulsion *W* was set as 0.26, monodispersed Ca-alginate hydrogel particles of highly spherical shape with an average roundness over 0.95 could be obtained (**Fig. 2.32**).

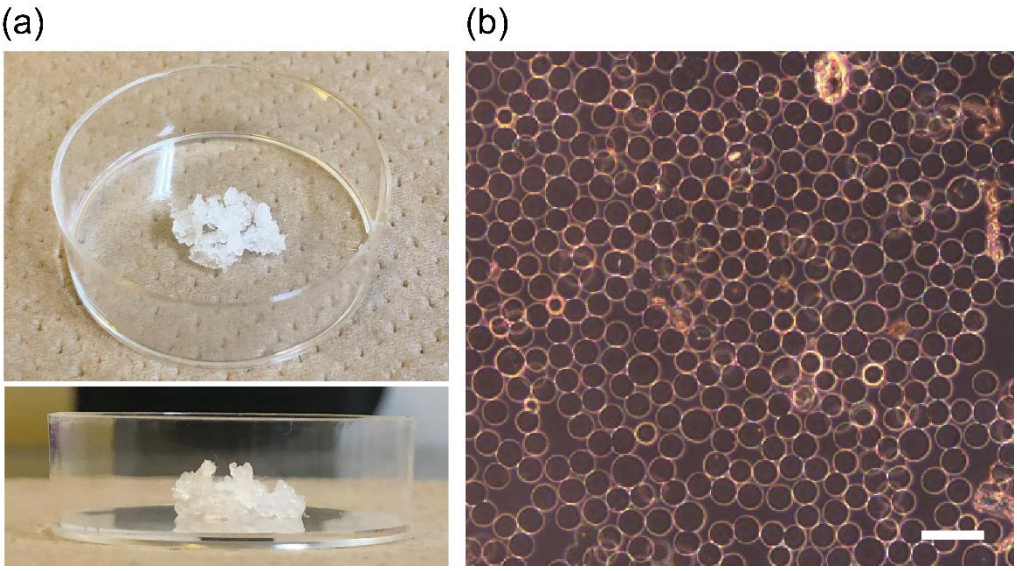

Fig. 2.32 Monodispersed Ca-alginate hydrogel particles obtained when *W* was set as 0.26. (a) Hydrogel particles were collected in 4 hours. (b) Microphotograph of prepared gel beads in pure water. The scale bar is 400 μm.

(3) Discussion

According to the experimental findings shown above, the *W* values, that is, the proportions of aqueous solution in the reactant W/O emulsion affected the aqueous droplet sizes of the reactant emulsion, which in turn influenced the morphologies of the hydrogel particles that were formed (**Fig. 2.33**). **Figure 2.26** shows that when *W* values were 0.20 and 0.26, the average diameters of aqueous droplets in reactant emulsion were quite near (2.3 and 2.2 μm, respectively), as revealed in the experiment. Therefore, a decrease in *W* could result in a lower density of aqueous droplets containing Ca^{2+} in the channel, which may have resulted in inadequate gelation of Na-alginate droplets in the channel, resulting in off-chip coalescence between the Na-alginate droplets and the formation of larger hydrogel particles with poor roundness (**Fig. 2.33a**). When *W* was increased to 0.33, the average diameter of aqueous droplets containing Ca^{2+} was increased by more than twofold (4.1 μm), and the size distribution

of aqueous droplets was widened significantly. The high *W* value may result in more polydisperse aqueous droplets containing Ca^{2+} with big sizes. It is likely that the presence of large reactant aqueous droplets created a heterogeneous distribution of Ca^{2+} surrounding the Na-alginate droplets, which resulted in the deformation of the hydrogel particles that were formed (**Fig. 2.33c**).

Through the experiments, it can be concluded that the fraction of aqueous solution in reactant W/O emulsion influences the size of aqueous droplets containing Ca^{2+} in reactant emulsion that can control the morphologies of obtained hydrogel particles in advance. As a consequence, to synthesize spherical hydrogel particles, the reactant W/O emulsion should be prepared at optimal *W* which is 0.26 in the following experiments.

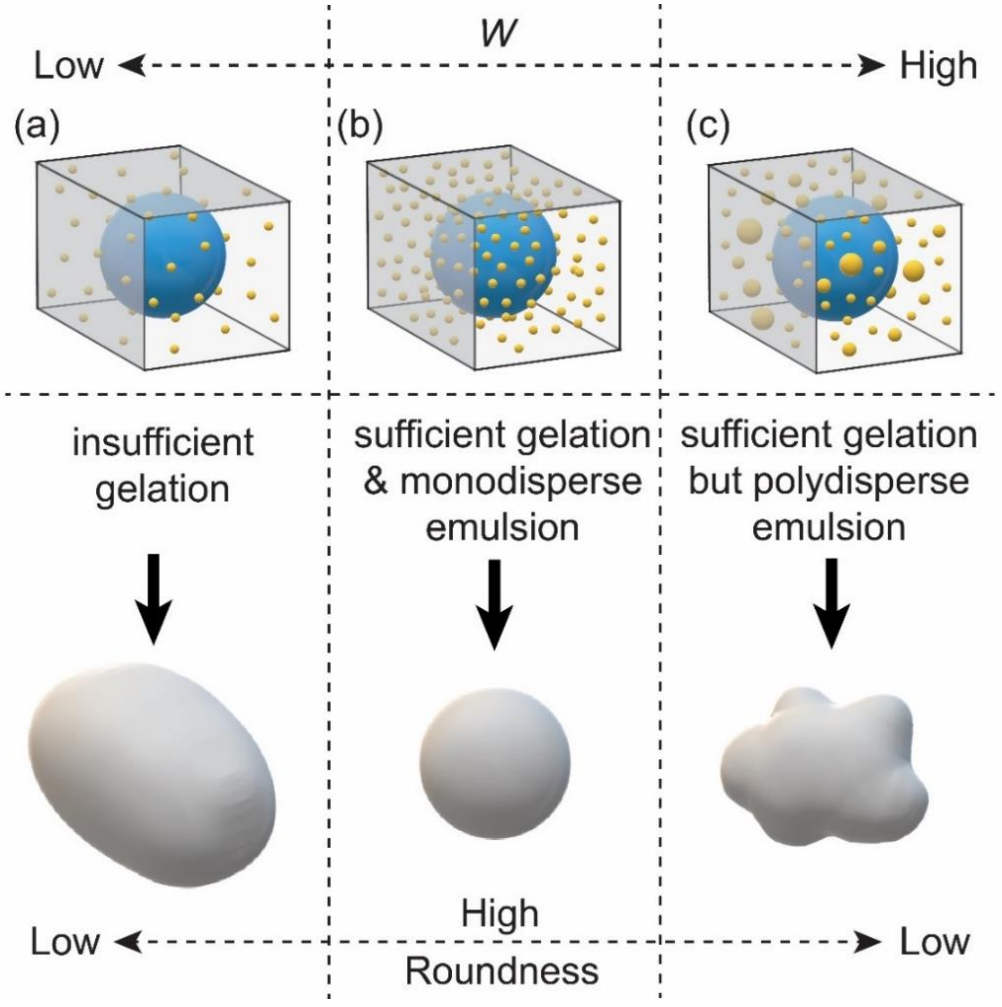

Fig. 2.33 Influences of *W* on the morphologies of the hydrogel particles. Formation of (a) bigger and non-spherical, (b) spherical, (c) deformed and non-spherical hydrogel particles.

2.3.3.3 Identification of obtained Ca-alginate hydrogels

To identify, analyze, and define the synthesized Ca-alginate hydrogel particles, the Fourier transform infrared (FTIR) spectra of used Na-alginate powder and obtained Ca-alginate beads were measured (**Fig. 2.34**).

The FTIR spectrum of Na-alginate has specific absorption peaks caused by the hydroxyl, either, and carboxylate functional groups. Stretching vibrations of O–H bonds of alginate appeared in the range of 3600 cm^{-1} to 3000 cm^{-1}. Observed peaks in 1598 cm^{-1} and 1406 cm^{-1} were attributed to asymmetric and symmetric stretching vibrations of carboxylate salt ion ($–COO^-$) (**Fig. 2.34a**). Ca-alginate microparticles showed significant differences in absorption peaks in comparison with the FTIR spectra of Na-alginate (**Fig. 2.34b**). It is clear that the asymmetric stretching peak of $–COO^-$ at 1598 cm^{-1} is gradually replaced by a new absorption peak at 1743 cm^{-1}, which is caused by the interaction of Ca^{2+} with the $–COO^-$ groups of Na-alginate.

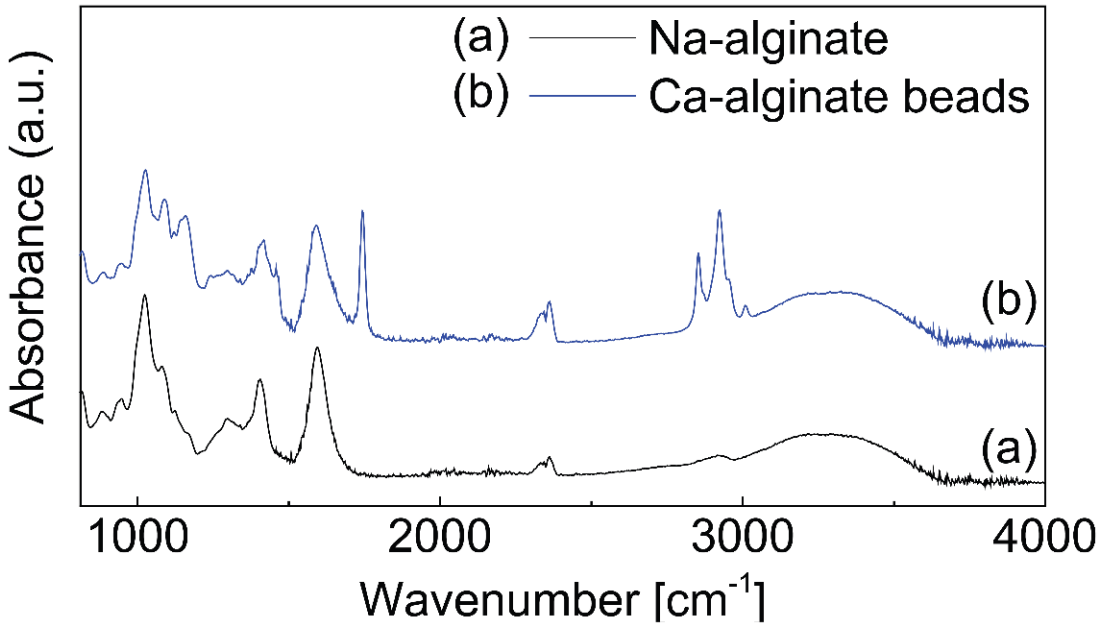

Fig. 2.34 FTIR spectra of Na-alginate powder and synthesized Ca-alginate particles.

2.3.3.3 Effects of a flow rate of continuous and emulsion phases

(1) Effects of a flow rate of emulsion phase

It was established that Q_e has an influence on the roundness of hydrogel particles. Reactant W/O emulsion with the optimum percentage of aqueous solution ($W = 0.26$) was utilized in this

experiment. During the experiment, Q_d was 0.1 mL/h. When Q_c was maintained at 1.2 or 2.0 mL/h while varying Q_e, the average roundness of the hydrogel beads steadily reduced as Q_e rose (**Fig. 2.35**). **Fig. 2.35-A** shows that when Q_e was 40.0 mL/h, the generated gel particles have homogeneous bullet morphologies with average roundness less than 0.80 at three different Q_c values: 1.2, 2.0, and 3.0 mL/h (**Fig. 2.34-II**).

The deformation of a Newtonian fluid droplet in continuous flow is positively correlated with the velocity of the fluid motion. Therefore, when Q_e was 40.0 mL/h, the high velocity of the emulsion phase applied high shearing force on the Na-alginate droplets and elongated the spherical droplets before gelation. As a result, the hydrogel particles of bullet shape were obtained. Thus, there is a limit for Q_e to produce hydrogel particles with spherical shapes.

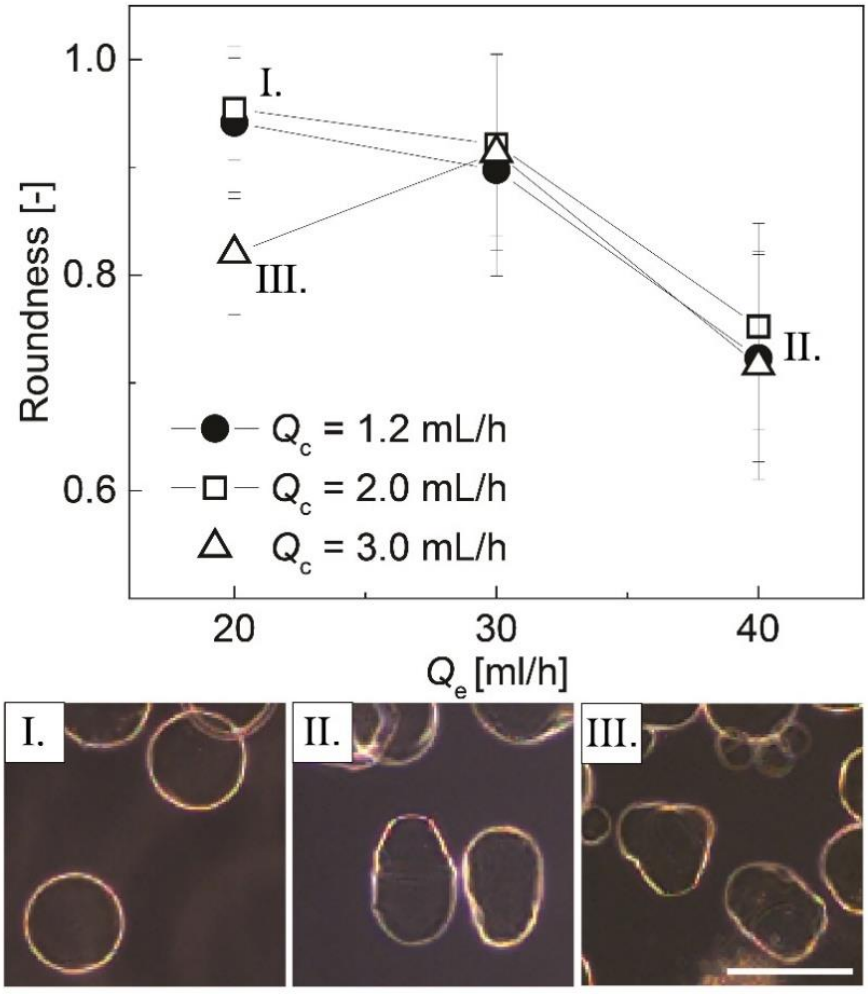

Fig. 2.35 Effect of the Q_e on the roundness of the hydrogel particles. Scale bars are 200 μm.

(2) Effects of a flow rate of the continuous phase

Furthermore, as shown in **Fig. 2.35**, when Q_e was 20.0 mL/h, on the one hand, highly spherical gel microspheres with roundness ~0.95 could be obtained as Q_c was 1.2 and 2.0 mL/h (**Fig. 2.35-I**). On the other hand, deformed and non-spherical gel microbeads with roundness ~0.82 were obtained as Q_c increased to 3.0 mL/h (**Fig. 2.35-III**).

The distribution of light intensity, which has a reciprocal connection with the distribution of emulsion density at the downstream cross-junction, was studied to determine the cause of this drop in roundness. When Q_c was as low as 1.2 and 2.0 mL/h, the middle region with low emulsion density was narrow and the obtained gel beads were highly spherical, that is probably because the generated droplets also spun at downstream channel. However, when seen in **Fig. 2.36**, as Q_c rose, the middle region with low emulsion density became larger. This indicates that when Q_c increased, the emulsion density at the core of the downstream cross-junction decreased, causing the distribution of aqueous droplets containing Ca^{2+} surrounding Na-alginate droplets to become heterogeneous, resulting in distorted and non-spherical hydrogel particles.

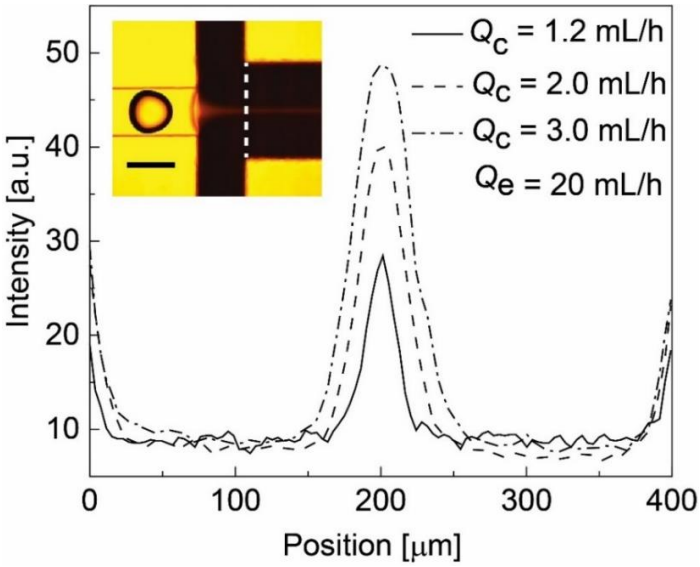

Fig. 2.36 Light-intensity distribution across the reaction channel. Scale bars are 200 μm.

(3) Conclusion

As a result, first of all, the Q_e should not be as high as 40 mL/h to prevent high shearing stress that probably causes the deformation of droplets. Next, there is an optimal range of Q_e for a given Q_c to produce highly spherical hydrogel particles.

2.3.4 Spherical Ca-alginate hydrogel particles of varied sizes

2.3.4.1 Experimental results

Based on the results above, when Q_e was adjusted at 30 mL/h, spherical hydrogel particles of various sizes and narrow size distribution could be produced by altering the Q_c/Q_d value. A reactant W/O emulsion with the appropriate aqueous solution fraction (W = 0.26). The Q_d was then set at 0.1 mL/h while the Q_c was changed; the produced hydrogel particles had roundness around 0.90 at all Q_c levels. The results are shown in **Fig. 2.37**.

The produced hydrogel particles had an average diameter of 176 μm and a CV of 5.3% when Q_c was 1.2 mL/h (**Fig. 2.37a**). The generated hydrogel particles had an average diameter of 160 μm and a CV of 4.2% when Q_c was 2.0 mL/h (**Fig. 2.37b**). The obtained hydrogel particles had an average diameter of 147 μm and a CV of 6.3% when Q_c was 3.0 mL/h (**Fig. 2.37c**). Their monodispersity is reflected in the narrow size distribution graphs, which have average CVs of roughly 5%. The influence of Q_c/Q_d on the size and CVs of hydrogel particles was also studied (**Fig. 2.37d**).

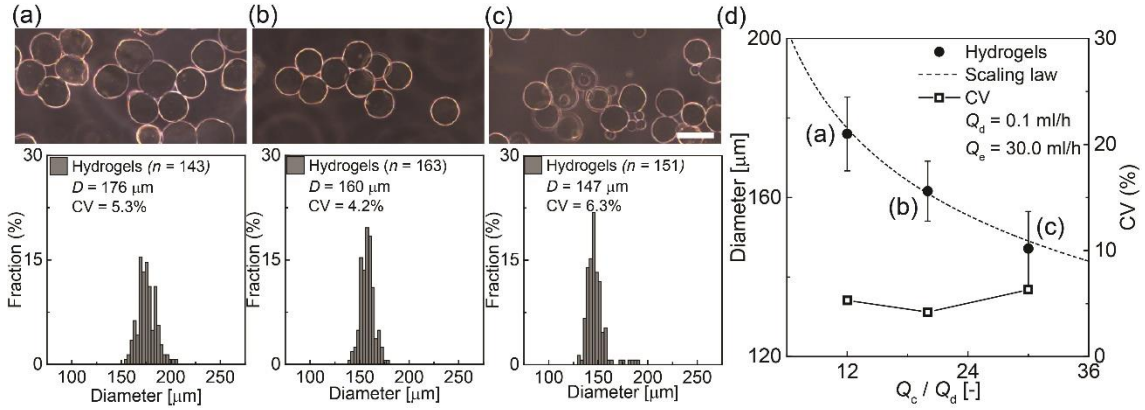

Fig. 2.37 Effect of Q_c on the diameter of hydrogel particles. (a-c) Images of hydrogel particles in deionized water and their size distribution at (a) Q_c/Q_d = 12.0, (b) Q_c/Q_d = 20.0, (c) Q_c/Q_d = 30.0. Q_d = 0.1 mL/h, Q_e = 30.0 mL/h. Scale bar is 200 μm. (d) The Q_c / Q_d vs. the sizes and CVs of hydrogels.

The results demonstrate that the size of hydrogel particles could be easily regulated by altering the Q_c/Q_d ratio between 12.0 and 30.0, and the average diameter of created hydrogel particles varied between 147 μm and 176 μm. At the same Q_c/Q_d ratio, the diameter of hydrogel

particles was smaller and their CV value was greater than that of Na-alginate droplets, as shown in **Fig. 2.20**. The diameter of hydrogel particles reduced because the Na-alginate droplets shrank (about 17% in diameter) following gelation because the cross-linking process limited the space between the alginate molecules [45]. The water desorption from the hydrogel particles during hexane cleaning was not the primary source of shrinkage since hexane's solubility in water is relatively low, and the hexane-washed hydrogel particles were flushed and re-dispersed in water before measurement. The somewhat greater CVs of the hydrogel particles were owing to the presence of a few larger and nonspherical hydrogel particles.

2.3.4.2 Flow simulation results

The sizes of generated droplets in the microchannel can be estimated through the flow simulation using commercial software (Fluent 19.0, ANSYS, USA). The details of the simulation are shown in **Appendix 4.3**. As shown in **Fig. 2.38**, similar to the experimental results, when Q_c was 1.2 mL/h, the Na-alginate droplets with sizes bigger than the channel width (200 μm) were generated. When Q_c was 2.0 mL/h, the droplets of sizes cross to the channel width were formed (similar to **Fig. 2.19**). Further, when Q_c increased to 3.0 mL/h, the sizes of generated droplets were clearly smaller than the width of the microchannel.

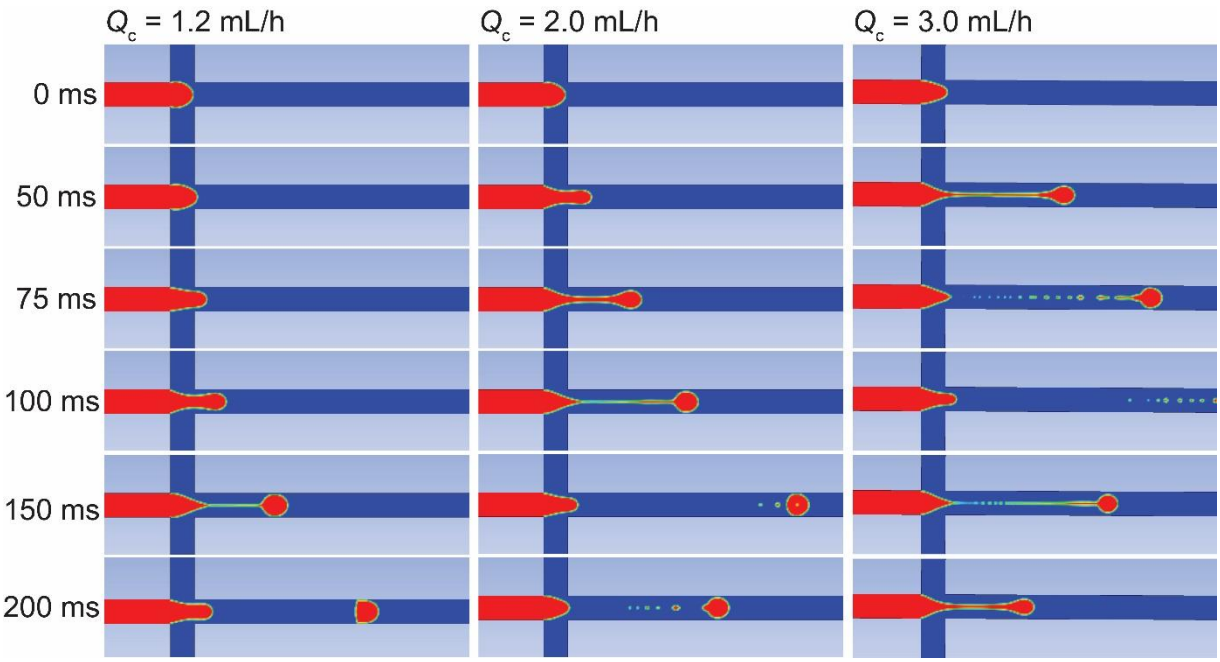

Fig. 2. 38 Flow simulation of droplet formation in the microchannel at different flow conditions.

The comparison of sizes of prepared droplets and hydrogel particles between the flow simulation and actual experiments is shown in **Fig. 2.39**. The sizes of simulated hydrogel particles were equal to the sizes of simulated droplets time the shrinkage ratio (ca. 83%). When Q_c was 1.2 mL/h, the estimated diameter of obtained Na-alginate droplets and hydrogel beads was 207 μm and 181 μm, respectively. When Q_c was 2.0 mL/h, the estimated diameter of obtained Na-alginate droplets and hydrogel beads was 197 μm and 165 μm, respectively. Finally, when Q_c was 3.0 mL/h, the estimated diameter of obtained Na-alginate droplets and hydrogel beads was 173 μm and 145 μm, respectively. The estimated sizes of droplets and hydrogel particles have a high similarity with the actual experimental results proving that the sizes of prepared hydrogel particles could be precisely evaluated through the simulation approach.

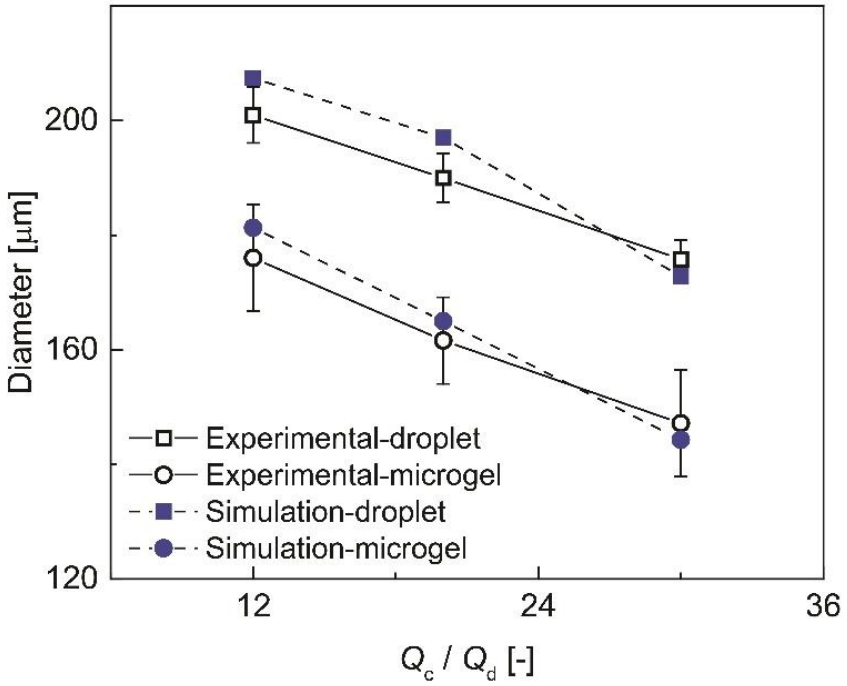

Fig. 2.39 Comparison between flow simulation results and experimental results on the sizes of generated droplets and hydrogel microparticles.

In addition, it seems from the experimental findings that, when the reactant W/O emulsion is at its optimum *W* (0.26), monodisperse spherical hydrogel particles that are larger or smaller in size than the orifice size could be prepared as long as the flow parameters are suitably

configured. This is because, on the one hand, the fine reactant emulsion can provide sufficient gelation of Na-alginate droplets. On the other hand, they have relatively small sizes (~2 μm) compare with the Na-alginate droplets (over 140 μm) that can provide a homogeneous distribution of calcium ions around the Na-alginate droplets, then further ensuring the sphericity of formed hydrogel particles. In another word, for synthesizing spherical hydrogel particles, the sizes of reactant emulsion should be small enough to match the sizes of Na-alginate droplets. So, if the reactant W/O emulsion with nano-sizes which can be obtained through conventional sonication was used[46], this design has the potential to produce spherical hydrogel particles with much smaller sizes (below 50 μm).

2.4 Conclusion

Section 2.1. Introduction

This section describes the background, previous researches, and the objectives of this chapter.

Section 2.2. Materials and methods

This section describes the peripheral equipment, our microfluidic device, and the materials that used in our experiments.

Section 2.3. Results and discussion

This section covers the microfluidic external gelation technique used to create spherical Ca-alginate hydrogel microparticles. The effects of the fraction of aqueous phase in the reactant W/O emulsion, as well as the flow rates of the continuous and emulsion phases, on the roundness of the obtained hydrogel microbeads, were investigated. A conclusion that homogeneous spatial distribution of Ca^{2+} around precursor Na-alginate droplets is required to obtain highly spherical hydrogel particles is presented. The effects of the property of reactant W/O emulsions and the flow rate of the continuous phase and emulsion phase were investigated. By adjusting the abovementioned factors, monodisperse hydrogel particles with a diameter of 147–176 μm and roundness of 0.90–0.96 could be prepared.

References

[1] Boontheekul, T.; Kong, H.J. and Mooney, D.J. Controlling alginate gel degradation utilizing partial oxidation and bimodal molecular weight distribution. *Biomaterials* **2005,** 26, 2455–2465.

[2] Maiti, S.; Singha, K.; Ray, S.; Dey, P. and Sa, B. Adipic acid dihydrazide treated partially oxidized alginate beads for sustained oral delivery of flurbiprofen. *Pharm. Dev. Technol.* **2009,** 14, 461–470.

[3] Bouhadir, K.H.; Alsberg, E. and Mooney, D.J. Hydrogels for combination delivery of antineoplastic agents. *Biomaterials* **2001**, 22, 2625–2633.

[4] Utech, S.; Prodanovic, R.; Mao, A.S.; Ostafe, R.; Mooney, D.J. and Weitz, D.A. Microfluidic generation of monodisperse, structurally homogeneous alginate microgels for cell encapsulation and 3D cell culture. *Adv. Healthc. Mater.* **2015,** 4, 1628–1633.

[5] Yamada, M. and Seki, M. Multiphase microfluidic processes to produce alginate-based microparticles and fibers. *J. Chem. Eng. Jpn*. **2018,** 51, 318–330.

[6] Liu, K.; Ding, H.J.; Liu, J.; Chen, Y. and Zhao, X.Z. Shape-controlled production of biodegradable calcium alginate gel microparticles using a novel microfluidic device. *Langmuir* **2006,** 22, 9453–9457.

[7] Shintaku, H.; Kuwabara, T.; Kawano, S.; Suzuki, T.; Kanno, I. and Kotera, H. Micro cell encapsulation and its hydrogel-beads production using microfluidic device. *Microsyst. Technol.* **2007,** 13, 951–958.

[8] Lee, T.Y.; Praveenkumar, R.; Oh, Y.K.; Lee, K. and Kim, S.H. Alginate microgels created by selective coalescence between core drops paired with an ultrathin shell. *J. Mater. Chem. B* **2016,** 4, 3232–3238.

[9] Boggione, D.M.G.; Batalha, L.S.; Gontijo, M.T.P.; Lopez. M.E.S.; Teixeira, A.V.N.C.; Santos, I.J.B. and Mendonca, R.C.S. Evaluation of microencapsulation of the UFV-AREG1 bacteriophage in alginate-Ca microcapsules using microfluidic devices. *Colloids. Surf. B*. **2017,** 158, 182–189.

[10] Zhang, H.; Tumarkin, E.; Sullan, R.M.A.; Walker, G.C. and Kumacheva, E. Exploring microfluidic routes to microgels of biological polymers. *Macromol. Rapid Commun*. **2007,** 28, 527–538.

[11] Lee, D.H.; Jang, M. and Park, J.K. Rapid one-step purification of single-cells encapsulated in alginate microcapsules from oil to aqueous phase using a hydrophobic filter paper: Implications for single-cell experiments. *Biotechnol. J*. **2014,** 9, 1233–1240.

[12] Tan, W.H. and Takeuchi, S. Monodisperse alginate hydrogel microbeads for cell encapsulation. *Adv. Mater.* **2007,** 19, 2696–2701.

[13] Huang, K.S.; Lai, T.H. and Lin, Y.C. Using a microfluidic chip and internal gelation reaction for monodisperse calcium alginate microparticles generation. *Front. Biosci.* **2007,** 12, 3061–3067.

[14] Saeki, D.; Sugiura, S.; Kanamori, T.; Sato, S. and Ichikawa, S. Formation of monodisperse calcium alginate microbeads by rupture of water-in-oil-in-water droplets with an ultra-thin oil phase. *Lab Chip* **2010,** 10, 2292–2295.

[15] Mazutis, L.; Vasiliauskas, R. and Weitz, D.A. Microfluidic production of alginate hydrogel particles for antibody encapsulation and release. *Macromol. Biosci.* **2015,** 15, 1641–1646.

[16] Maeda, K.; Onoe, H.; Takinoue, M. and Takeuchi, S. Controlled synthesis of 3D multi-compartmental particles with centrifuge-based microdroplet formation from a multi-barrelled capillary. *Adv. Mater.* **2012,** 24, 1340–1346.

[17] Sugiura, S.; Oda, T.; Izumida, Y.; Aoyagi, Y.; Satake, M.; Ochiai, A.; Ohkohchi, N. and Nakajima, M. Size control of calcium alginate beads containing living cells using micro-nozzle array. *Biomaterials* **2005,** 26, 3327–3331.

[18] Liu, K.; Deng, Y.; Zhang, N.; Li, S.; Ding, H.; Guo, F.; Liu, W.; Guo, S. and Zhao, X. Generation of disk-like hydrogel beads for cell encapsulation and manipulation using a droplet-based microfluidic device. *Microfluid. Nanofluid.* **2012,** 13, 761–767.

[19] Capretto, L.; Mazzitelli, S.; Balestra, C.; Tosi, A. and Nastruzzi, C. Effect of the gelation process on the production of alginate microbeads by microfluidic chip technology. *Lab Chip* **2008,** 8, 617–621.

[20] Hu, Y.; Wang, Q.; Wang, J.; Zhu, J. Wang, H. and Yang, Y. Shape controllable microgel particles prepared by microfluidic combining external ionic crosslinking. *Biomicrofluidics* **2012,** 6, 026502.

[21] Chuah, A.M.; Kuroiwa, T.; Kobayashi, I.; Zhang, X. and Nakajima, M. Preparation of uniformly sized alginate microspheres using the novel combined methods of microchannel

emulsification and external gelation. *Colloid Surf. A-Physicochem. Eng. Asp.* **2009,** 351, 9–17.

[22] Lian, M.; Collier, C.P.; Doktycz, M.J. and Retterer, S.T. Monodisperse alginate microgel formation in a three-dimensional microfluidic droplet generator. *Biomicrofluidics* **2012,** 6, 044108.

[23] Kim, C.; Park, J. and Kang, J.Y.A microfluidic manifold with a single pump system to generate highly mono-disperse alginate beads for cell encapsulation. *Biomicrofluidics* **2014,** 8, 066504.

[24] Lee, D.H.; Lee, W.; Um, E. and Park, J.K. Microbridge structures for uniform interval control of flowing droplets in microfluidic networks. *Biomicrofluidics* **2011,** 5, 034117.

[25] Agarwal, P.; Zhao, S.; Bielecki, P.; Rao, W.; Choi, J.K. Zhao, Y.; Yu, J.; Zhang, W. and He, X. One-step microfluidic generation of pre-hatching embryo-like core-shell microcapsules for miniaturized 3D culture of pluripotent stem cells. *Lab Chip* **2013,** 13, 4525–4533.

[26] 鶴岡朗, ″マイクロ流路内の微小対流を利用した単分散ゲル微粒子の調製″, 平成 20 年度修士論文, 東京工業大学.

[27] Xu, J.H.; Li, S.W.; Tan, J. and Luo, G.S. Controllable preparation of monodispersed calcium alginate microbeads in a novel microfluidic system. *Chem. Eng. Technol.* **2008,** 31, 1223–1226.

[28] Kojima, N.; Takeuchi, S. and Sakai, Y. Fabrication of microchannel networks in multicellular spheroids. *Sens. Actuator B-Chem.* **2014,** 198, 249–254.

[29] Sugiura, S.; Oda, T.; Aoyagi, Y.; Matsuo, R.; Enomoto, T.; Matsumoto, K.; Nakamura, T.; Satake, M.; Ochiai, A.; Ohkohchi, N. and Nakajima, M. Microfabricated airflow nozzle for microencapsulation of living cells into 150 micrometer microcapsules. *Biomed. Microdevices* **2007,** 9, 91–99.

[30] Onoe, H.; Inamori, K.; Takinoue, M. and Takeuchi, S. Centrifuge-based cell encapsulation in hydrogel microbeads using sub-microliter sample solution. *RSC Adv.* **2014,** 4, 30480.

[31] Reis, C.P.; Neufeld, R.J.; Vilela, S.; Ribeiro, A.J. and Veiga, F. Review and current status of emulsion/dispersion technology using an internal gelation process for the design of alginate particles. *J. Microencapsul*. **2006,** 23, 245–257.

[32] Zhang, H.; Tumarkin, E.; Sullan, R.M.A.; Walker, G.C. and Kumacheva, E. Exploring microfluidic routes to microgels of biological polymers. *Macromol. Rapid Commun.* **2007,** 28, 527–538.

[33] Morimoto, Y.; Tan, W.H. and Takeuchi, S. Three-dimensional axisymmetric flow-focusing device using stereolithography. *Biomed. Microdevices* **2009,** 11, 369–377.

[34] Marquis, M.; Renard, D. and Cathala, B. Microfluidic generation and selective degradation of biopolymer-based Janus microbeads. *Biomacromolecules* **2012,** 13, 1197–1203.

[35] Akbari, S.; Pirbodaghi, T.; Kamm, R.D. and Hammond, P.T.A. Versatile microfluidic device for high throughput production of microparticles and cell microencapsulation. *Lab Chip* **2017,** 17, 2067–2075.

[36] Zhang. H.; Tumarkin, E.; Peerani, R.; Nie, Z.; Sullan, R.M.A.; Walker, G.C. and Kumacheva, E. Microfluidic production of biopolymer microcapsules with controlled morphology. *J. Am. Chem. Soc.* **2006,** 128, 12205–12210.

[37] Nisisako, T.; Torii, T.; Takahashi, T. and Takizawa, Y. Synthesis of monodisperse bicolored janus particles with electrical anisotropy using a microfluidic co-flow system. *Adv. Mater.* **2006,** 18, 1152–1156.

[38] Xu, J.H.; Li, S.W.; Tan, J. and Luo, G.S. Controllable preparation of monodispersed calcium alginate microbeads in a novel microfluidic system. *Chem. Eng. Technol.* **2008,** 31, 1223–1226.

[39] Huang, K.S.; Lai, T.H. and Lin, Y.C. Manipulating the generation of Ca-alginate microspheres using microfluidic channels as a carrier of gold nanoparticles. *Lab Chip* **2006,** 6, 954–957.

[40] Garstecki, P.; Stone, H.A. and Whitesides, G.M. Mechanism for flow-rate controlled breakup in confined geometry: A route to monodisperse emulsions. *Phy. Rev. Lett*. **2005,** 94, 164501.

[41] Dollet, B.; Hoeve, W.V.; Raven, J.P.; Marmottant, P. and Versluis, M. Role of the channel geometry on the bubble pinch-off in flow-focusing devices. Phy. *Rev. Lett*. **2008,** 100, 034504.

[42] Cubaud, T. and Mason, T.G. Capillary threads and vicious droplets in square microchannels. *Phys. Fluids.* **2008,** 20, 053302.

[43] Lee, W.; Walker, L.M. and Anna, S.L. Role of geometry and fluid properties in droplet

and thread formation processes in planar flow focusing. *Phys. Fluids.* **2009,** 21, 032103.

[44] Baroud, C.N.; Gallaire, F. and Dangla, R. Dynamics of microfluidic droplets. *Lab chip* **2010,** 10, 2032–2045.

[45] Kuo, C.K. and Ma, P.X. Ionically crosslinked alginate hydrogels as scaffolds for tissue engineering: Part 1. Structure, gelation rate and mechanical properties. *Biomaterial* **2001,** 22, 511–521.

[46] Harada, T.; Kanda, T.; Suzumori, K.; Ono, T.; Iwabuchi, S.; Ito, K.; Ogawara, K. and Higaki, K. Emulsion generating microchannel device oscillated by 2 . 25 MHz ultrasonic vibrator. *Jpn. J. Appl. Phys.* **2010,** 49, 1–6.

Chapter 3

Functional Janus calcium-alginate hydrogel particles

Unpublished contents

Chapter 4

Surface coating on calcium-alginate hydrogel particles

4.1 Introduction

4.1.1 Overview

As described in **Chapter 3, Section 1**, hydrogel microparticles coupled with nanoparticles are of tremendous interest due to their versatility in a variety of applications. The indented nanoparticles could be incorporated in the hydrogel beads by two main approaches: encapsulation or coating (**Fig. 4.1**).

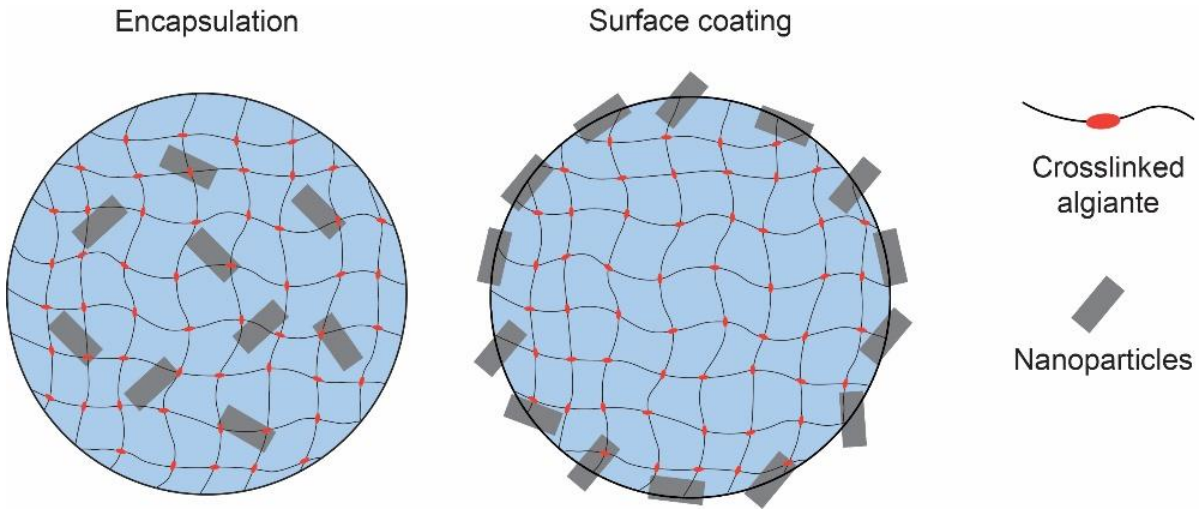

Fig. 4.1 Illustration graph of nanoparticles encapsulated and coated on the alginate hydrogel particles.

The most typical method to combine the functional nanoparticles with the hydrogel microbeads is to encapsulate them inside the hydrogel particles (**Fig. 4.2**) [1-5]. Whereas, when the hydrogel particles are used as a capsule and carry cargos inside, the presence of inorganic nanoparticles inside the hydrogel microcapsules would probably influence their effectiveness and efficiency.

In contrast, the nanoparticles could also be coated on the surface of the microparticles. However, few studies have been reported for preparing microparticles with functional nanoparticles coating. Mask templating is a common approach that can achieve a surface coating of hydrogel beads. For example, a succession of spin coatings and etchings on a photoresist resulted in the formation of a golden-faced JP on silica particles, according to Bao et al (**Fig. 4.3**) [6]. Nevertheless, the templating techniques could prepare microparticles with partial coatings and have difficulties achieving a whole surface coating.

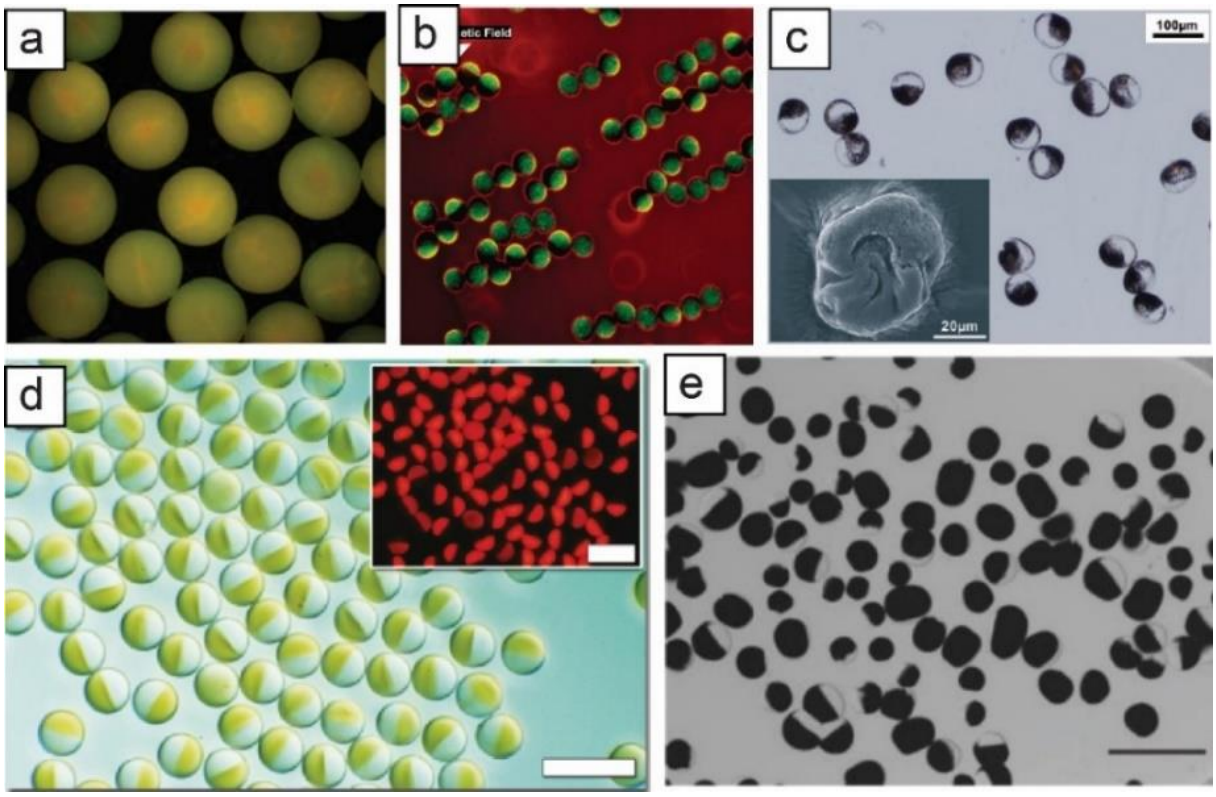

Fig. 4.2 Nanoparticles encapsulated inside the hydrogel particles. (a) Fluorescent nanoparticles encapsulated in PS-PMAA microspheres. Reproduced with permission [1]. Copyright 2015 ACS. (b) Magnetic nanoparticles and cells encapsulated in Ca-alginate microspheres by centrifugal process. Reproduced with permission [2]. Copyright 2012 Wiley-VCH. (c) Magnetic nanoparticles in Ca-alginate microspheres. Reproduced with permission [3]. Copyright 2009 RSC. (d) Magnetic nanoparticles encapsulated in PEG hydrogels. Reproduced with permission [4]. Copyright 2010 ACS. (e) Magnetic nanoparticles encapsulated in Ca-alginate microbeads. Reproduced with permission [5]. Copyright 2016 Elsevier.

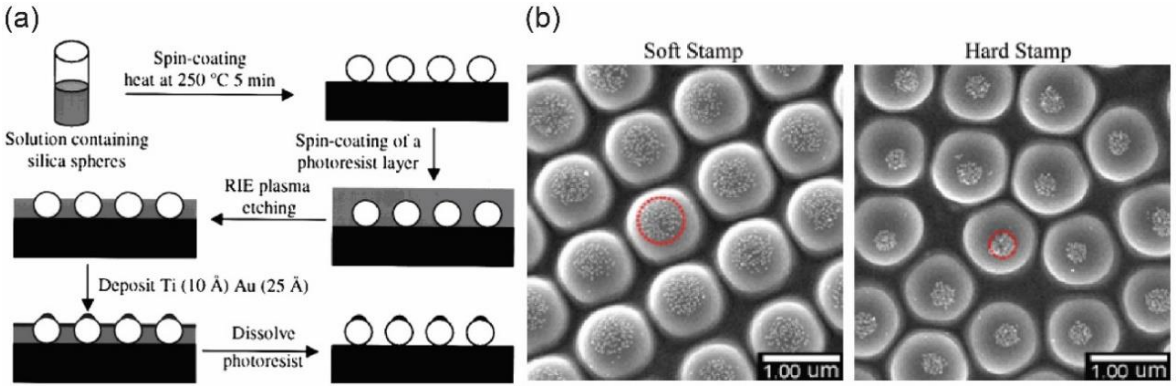

Fig. 4.3 Patterning of nanoparticles on particles surface. (a) An illustration graph of typical templating technique. Reproduced with permission [6]. Copyright 2002 ACS. (b) Silica particles with partial Au nanocrystal coating. Reproduced with permission [7]. Copyright 2009 ACS.

In addition, Karg et al. reported Au nanorod-coated pNIPAM microgels created by sonicating aqueous microgel dispersions with varying volumes of an aqueous solution of the gold (**Fig. 4.4**) [8].

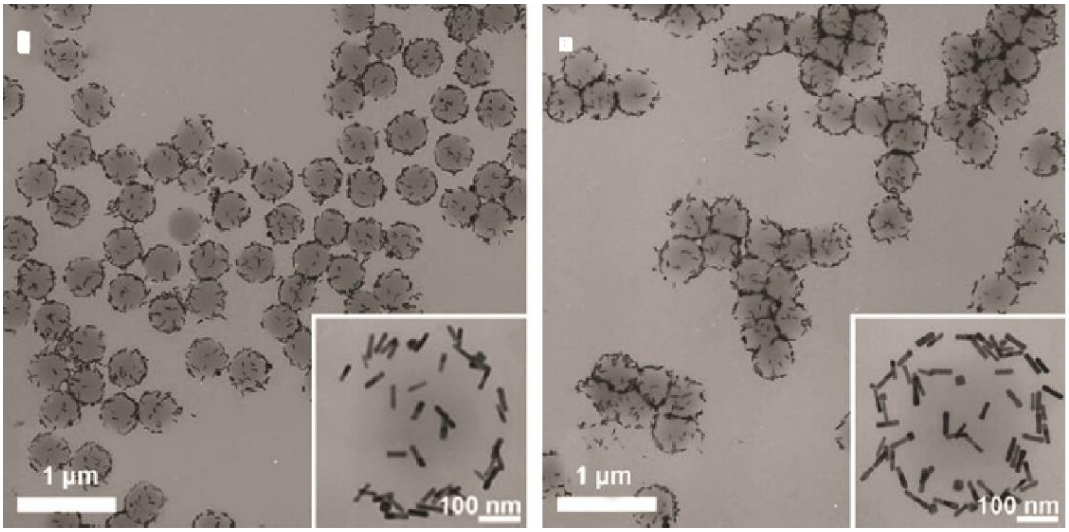

Fig. 4.4 Gold nanorods coated pNIPAM microgels. Reproduced with permission [8]. Copyright 2007 Wiley-VCH.

As a result, the surface coating of alginate hydrogel microparticles with functional nanobeads has not yet been reported that needs to be further researched.

4.1.2 Objectives

In this chapter, a microfluidic on-chip external gelation employing W/O emulsion containing Ca^{2+} and functional nanoparticles as a reactant was described for the creation of extremely spherical Ca-alginate hydrogel microparticles with appropriate surface coatings. The Fe_3O_4 nanoparticle or fluorescent nanoparticles was dispersed in the aqueous $CaCl_2$ solution for producing $CaCl_2$ emulsion-carrying nanoparticles. By infusing the different reactant emulsions from the downstream inlets, Ca-alginate hydrogel microparticles with whole magnetic or fluorescent surface coatings could be obtained and hydrogel microbeads with magnetic and fluorescent coatings, which might be beneficial in biological applications such as medication delivery and sustained release.

The main objectives of this chapter are as follows:

(1) To fabricate hydrogel particles with whole magnetic or fluorescent surface coatings.

(2) To fabricate hydrogel particles with both magnetic and fluorescent surface coatings.

4.1.3 Outline of chapter

Section 4.1 Overview

Introduces the background of the surface coating of hydrogel particles.

Section 4.2 Materials and methods

Describes the peripheral equipment, our microfluidic device, and the materials that used in this experiment.

Section 4.3 Results and discussion

Demonstrates the experiments about synthesizing the spherical hydrogel microspheres with magnetic and/or fluorescent surface coatings.

Section 4.4 Conclusion

Describes the conclusion of this chapter.

4.2 Materials and methods

4.2.1 Principle

In this study, a microfluidic emulsion-based external gelation was used for synthesizing Ca-alginate hydrogel particles with different surface coatings (**Fig. 4.5**). First, hydrophilic nanoparticles were manually dispersed in the $CaCl_2$ solution. Then, the prepared $CaCl_2$ solution was mixed with corn oil forming the reactant water-in-oil emulsion phase. Finally, the reactant emulsion was infused into the microfluidic channel where they reacted with the Na-alginate droplets on-chip. As shown in **Fig. 4.5**, once the aqueous droplets containing Ca^{2+} in the emulsion phase contacted the Na-alginate droplets, they tended to merge with each other to minimize the interfacial area and to decrease the oil-water interfacial energy. The calcium ions would diffuse into the droplets and immediately trigger the cross-linking reaction between the alginate molecular in the droplet forming a stable cross-linked network. Whereas, the nanoparticles could only embed on the particles' surface because the pore sizes of cross-linked alginate film are much smaller than the sizes of nanoparticles.

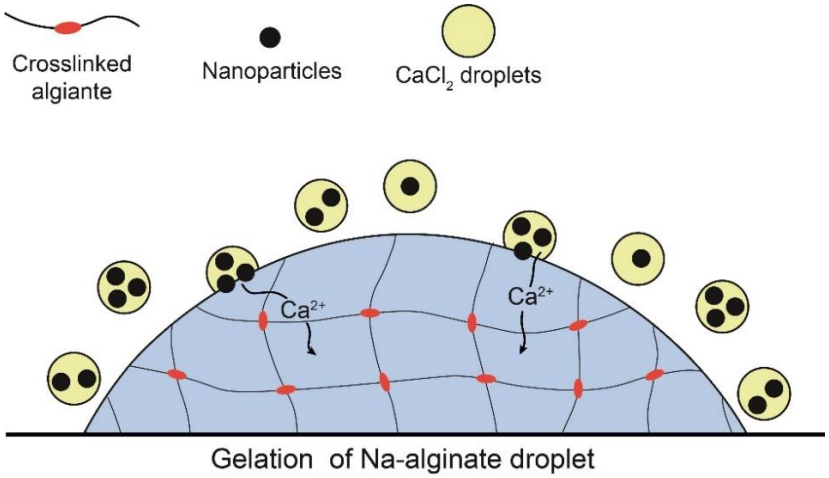

Fig. 4.5 Schematic illustration of the surface coating of Ca-alginate hydrogel particles using emulsion-based external gelation.

4.2.2 Microfluidic device

In this study, the microfluidic device has the same geometry as the one that used in **Chapter 2**. Here, the symmetric or asymmetric stream of W/O reactant emulsion containing Fe_3O_4 or

fluorescent nanoparticles resulted in magneto-responsive and/or fluorescent hydrogel particles with entire or quasi-hemispherical coverings. The schematic graph is shown in **Fig. 4.6**.

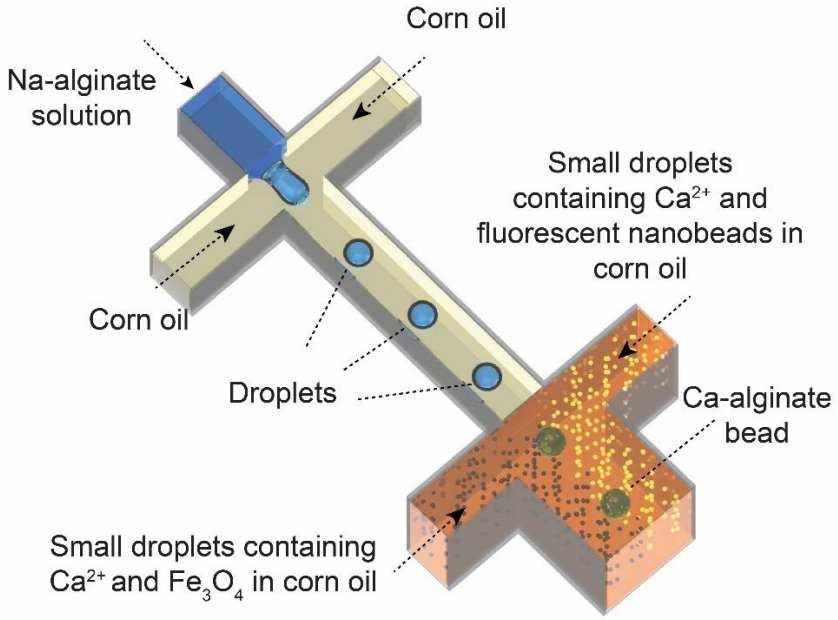

Fig. 4.6 A schematic depiction of how to make hydrogel microparticles with a magnetic and fluorescent nanoparticle-coated surface.

4.2.3 Materials

The Fe_3O_4 nanoparticles (< 500 nm, **Fig. 4.7**) were added in a 30.0 wt% aqueous solution containing $CaCl_2$ by 2.0 wt%, then combined with corn oil having surfactant (0.1 wt%, SY-Glyster, CRS-75) as the W/O emulsion reactant phase (**Fig. 4.8a**). Similarly, fluorescent carboxylate microspheres (#24051-10, 300 nm, Polysciences, U.S.) were put in a 30.0 wt% aqueous $CaCl_2$ solution by 2.5 wt% (**Fig. 4.8b**).

4.2.4 Generation and collection of Ca-alginate hydrogel particles

For hydrogel particles with whole magnetic-responsive coatings, the $CaCl_2$ emulsion phase containing Fe_3O_4 nanoparticles was infused into the inlet microchannel at downstream cross-junction from both sides. Further, for hydrogel particles with whole fluorescent coatings, the $CaCl_2$ emulsion phase containing fluorescent nanoparticles was infused into the inlet microchannel at downstream cross-junction from both sides. Last, for the hydrogel particles

with both fluorescent and magnetic coatings, the $CaCl_2$ emulsion phase that contained Fe_3O_4 nanoparticles was infused from one side and the $CaCl_2$ emulsion phase contained fluorescent nanoparticles from the other side.

Following collection, deionized water was used to remove the reactant phase from the mesh container. Hexane was then used to remove the remaining corn oil. The hexane was then washed away with fresh water. Finally, on a petri plate, the hydrogel particles were spread in water for observation.

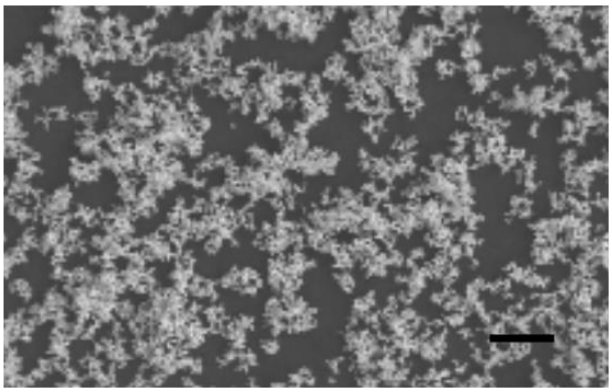

Fig. 4.7 An SEM image of Fe_3O_4 nanoparticles. The scale bar is 10 μm.

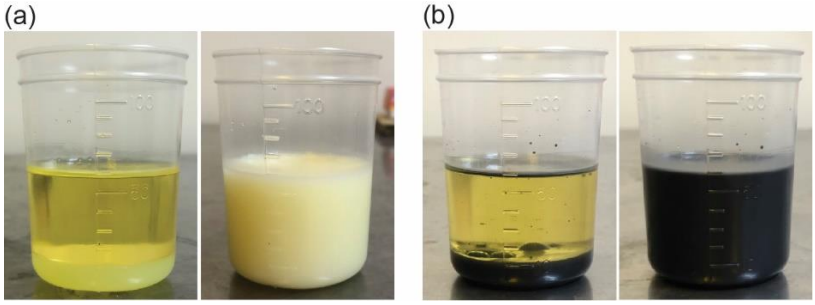

Fig. 4.8 Water-in-oil $CaCl_2$ emulsion containing (a) fluorescent polystyrene nanoparticles and (b) Fe_3O_4 nanoparticles before and after mixing.

4.3 Results and discussion

4.3.1 Hydrogel particles with whole Fe_3O_4 coatings

(1) Droplet formation in the microchannel

The flow rate of the continuous phase (Q_c), disperse phase (Q_d), and the emulsion phase (Q_e) at 1.0, 0.1, and 20.0 mL/h respectively which were the same as the flow rates used in **Chapter**

2. The droplet formation process in the microchannel was also similar to that described in **Chapter 2, Section 2.3.1.2** (**Fig. 4.9**). Because the $CaCl_2$ emulsion was originally opaque, the existence of Fe_3O_4 nanoparticles could not be observed under the optical microscope.

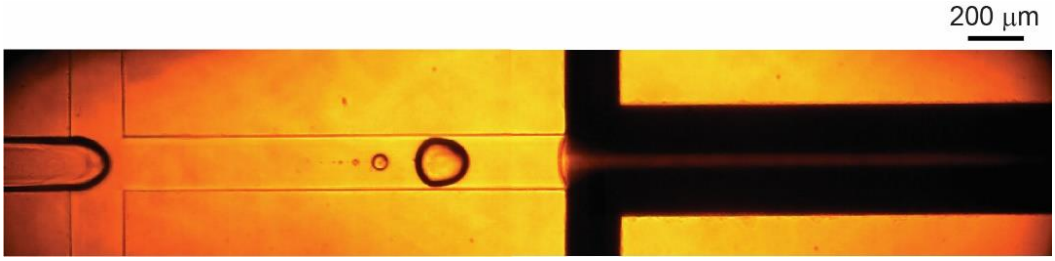

Fig. 4.9 Image of the generation process of a Na-alginate droplet.

(2) Obtained hydrogel particles with Fe_3O_4 coatings

The image of the generated hydrogel microparticles reveals that the Fe_3O_4 nanoparticles accumulated around the surface of the gel beads rather than being absorbed by the hydrogel balls (**Fig. 4.10**). The collected hydrogel microbeads had an average diameter of 160 μm with a CV value of 3.8% that is similar to the results reported in the previous chapter.

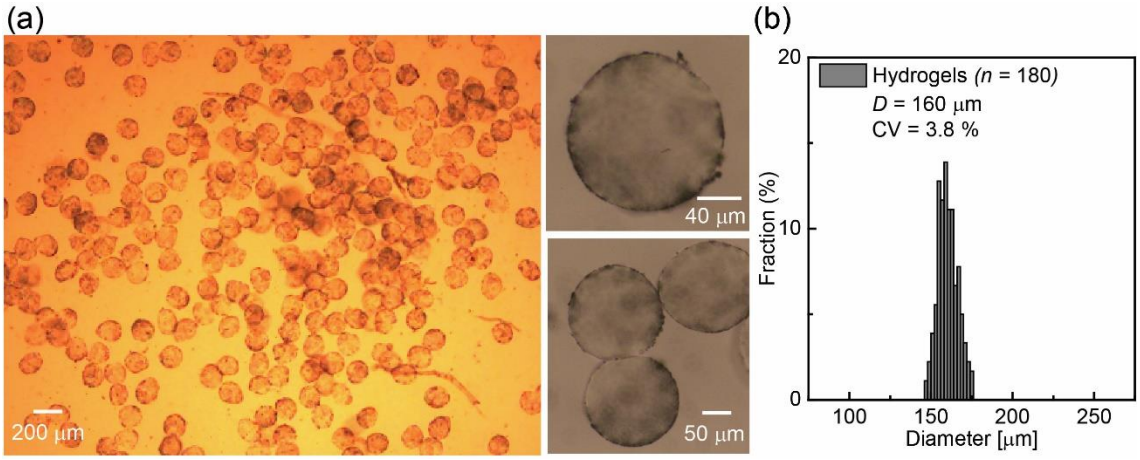

Fig. 4.10 Obtained hydrogel particles with Fe_3O_4 coatings. (a) Images of the hydrogel microparticles in water. (b) The size distribution of prepared hydrogel beads.

After the obtained hydrogel particles fully dried, the gel particles were observed through a SEM. The SEM images are shown in **Fig. 4.11**. The Fe_3O_4 nanoparticles coating of hydrogel microsphere can be demonstrated through the SEM images of dried aerogel beads (**Fig. 4.11a**),

and the Fe_3O_4 nanoparticles were partly embedded on the surface of alginate gel microspheres (**Fig. 4.11b**).

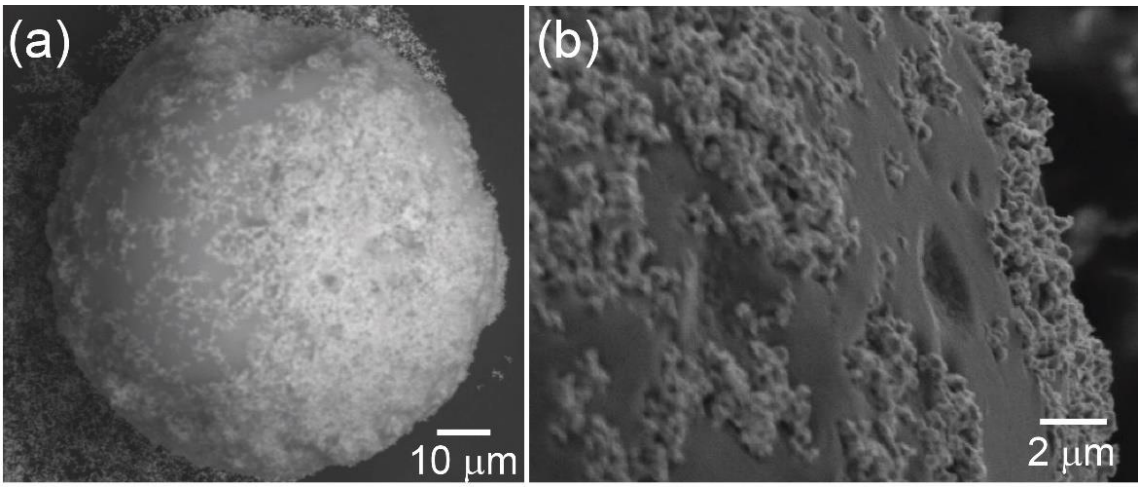

Fig. 4.11 (a) An SEM image of an aerogel bead. (b) An enlarged SEM image of the surface.

(3) Movement of magneto-responsive hydrogel particles

After the hydrogel particles were collected and filtered, they were dispersed in pure water. Using an external magnetic field, the manipulation of magneto-responsive hydrogel microparticles was shown (**Fig. 4.12**). The external magnetic field was manipulated by a neodymium magnet. The magneto-responsive Janus hydrogel particles could be easily controlled under the magnet field.

It was found that when Fe_3O_4 nanoparticles were added to the W/O reactant emulsion, the Ca^{2+} would enter the alginate droplets, forming cross-linked hydrogels with calcium ions, while the Fe_3O_4 nanoparticles remained on top of the alginate droplets, preventing impurities from entering the inside of the particles. Several researches suggest that cross-linked alginate film pores have mesh sizes lower than 30 nm [9–11]. The cross-linked hydrogel structure prevented nanoparticles smaller than 500 nm from entering.

The utilization of hydrogel microparticles with coated Fe_3O_4 nanoparticles in applications such as drug administration and release, sorting, and separation may hold tremendous promise since these hydrogel particles with coated Fe_3O_4 nanoparticles may be manipulated by an external driving force. Besides, coated Fe_3O_4 nanoparticles that exist on the surface of hydrogels have no damage for encapsulated cargos such as living cells.

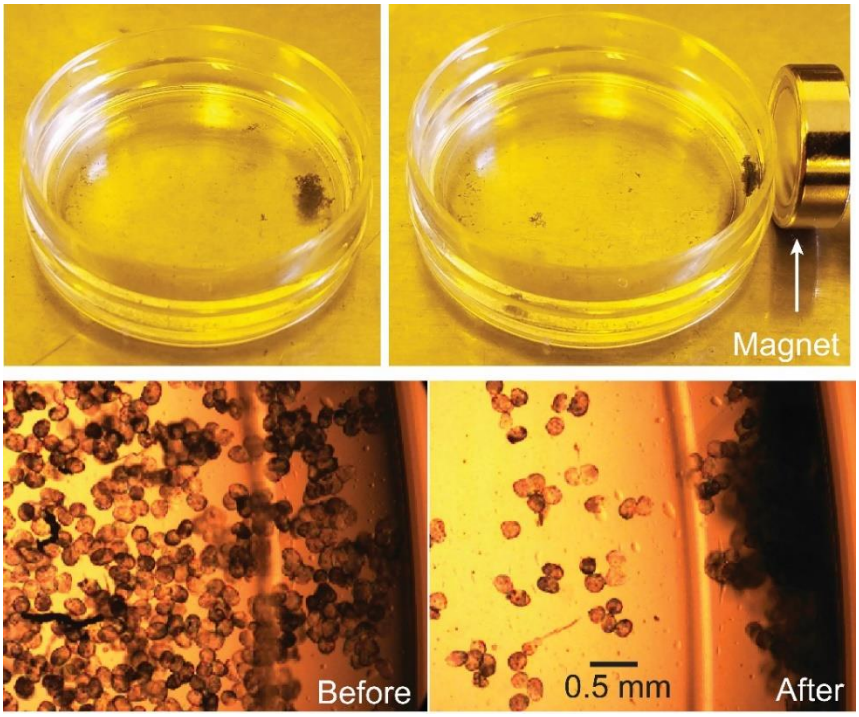

Fig. 4.12 Images of the Janus hydrogel particles in water that can be magnetically controlled.

4.3.2 Hydrogel particles with whole fluorescent coatings

(1) Droplet formation in the microchannel

For synthesizing the Ca-alginate hydrogel particles with fluorescent coatings, the $CaCl_2$ emulsion carrying fluorescent nanoparticles was infused from the two downstream inlet channels at the flow rate of 20 mL/h (10 mL/h × 2). The flow rates at the upstream cross-junction were set as Q_d = 0.1 mL/h and Q_c = 1.0 mL/h.

As shown in **Fig. 4.13**, when t = 0 ms, the formed Na-alginate droplet reached the downstream cross-junction. When t = 17.5 ms, the Na-alginate droplet moved to the deeper downstream channel. The droplet was sheltered by the black $CaCl_2$ emulsion in the bright filed microphotograph but had a clear boundary with the $CaCl_2$ emulsion in the fluorescent images suggesting that the fluorescent particles did not go inside the flowing Na-alginate droplet at the downstream channel.

(2) Obtained hydrogel particles with fluorescent coating

The collected Ca-alginate hydrogel particles with fluorescent coating were firstly observed by bright-field microscopy in pure water (**Fig. 4.14**). The generated hydrogel beads had an

average diameter of 165 μm with a CV value of 3.4% that is similar to the result in **Fig. 4.10**. The hydrogel particles had a highly spherical shape with an average roundness of around 0.95. Besides, because the fluorescent polystyrene microspheres are transparent under the bright-field microscopy, the embedded fluorescent nanoparticles could not be easily defined under small magnification such as the images in **Fig. 4.14a**.

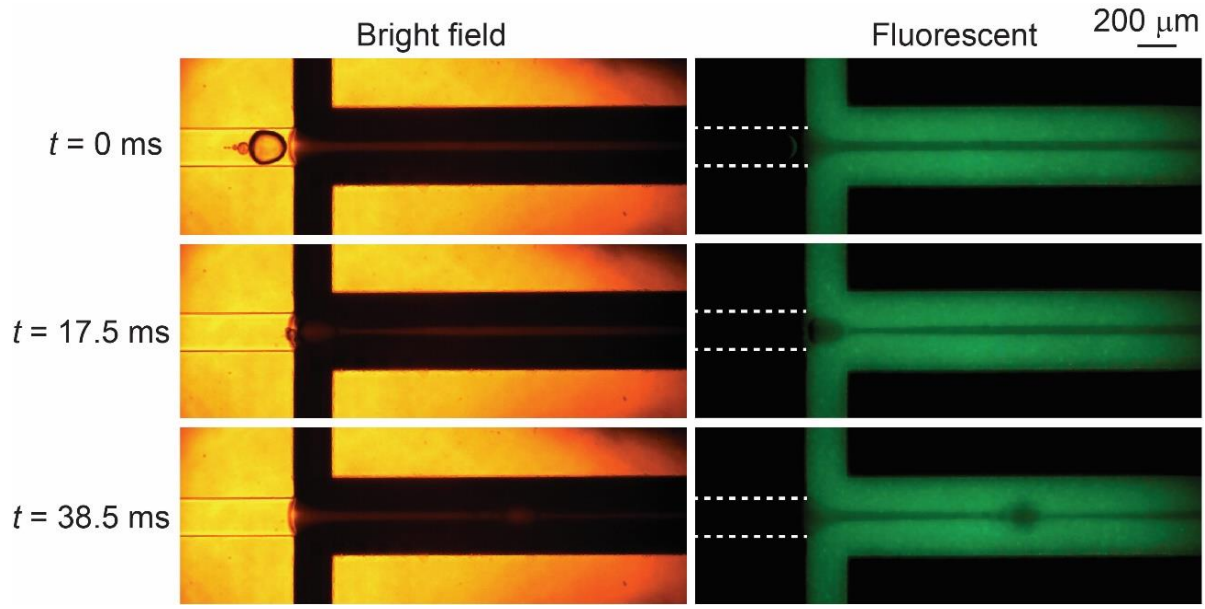

Fig. 4.13 Images of generation of a Ca-alginate hydrogel particle with a fluorescent coating.

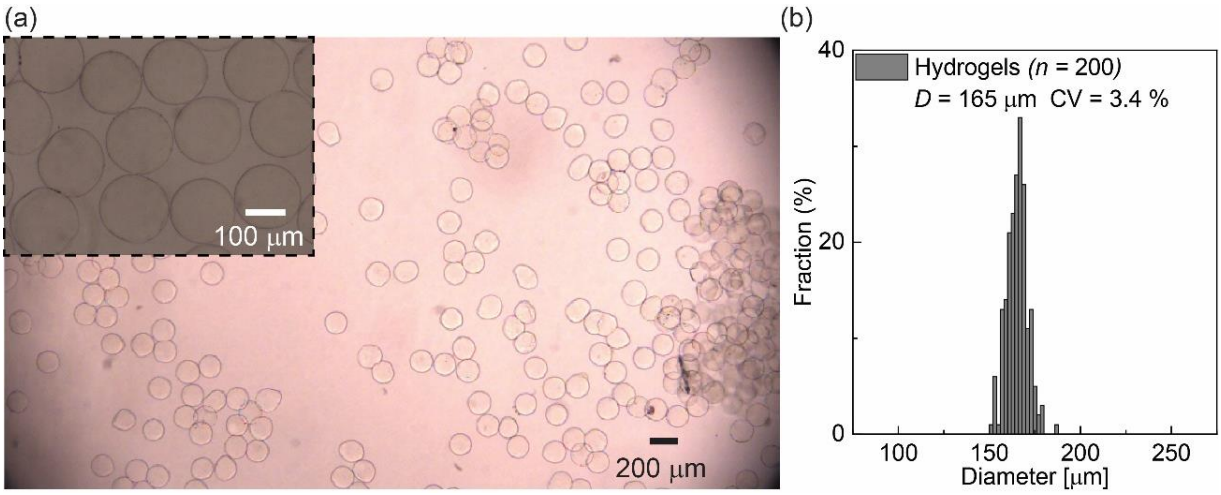

Fig. 4.14 Obtained hydrogel particles with fluorescent coatings. (a) An image of the hydrogel microbeads in water. (b) The size distribution of prepared hydrogel beads.

To demonstrate the fluorescent coatings of obtained hydrogel particles, the microgels were further observed by the bright-field and fluorescent microscopy. As shown in **Fig. 4.15**, the fluorescent feature of the surface of the hydrogel particles could be confirmed. Under the fluorescent background, it is shown that the fluorescent particles only existed on the surfaces of the prepared Ca-alginate particles instead of going inside the hydrogel beads.

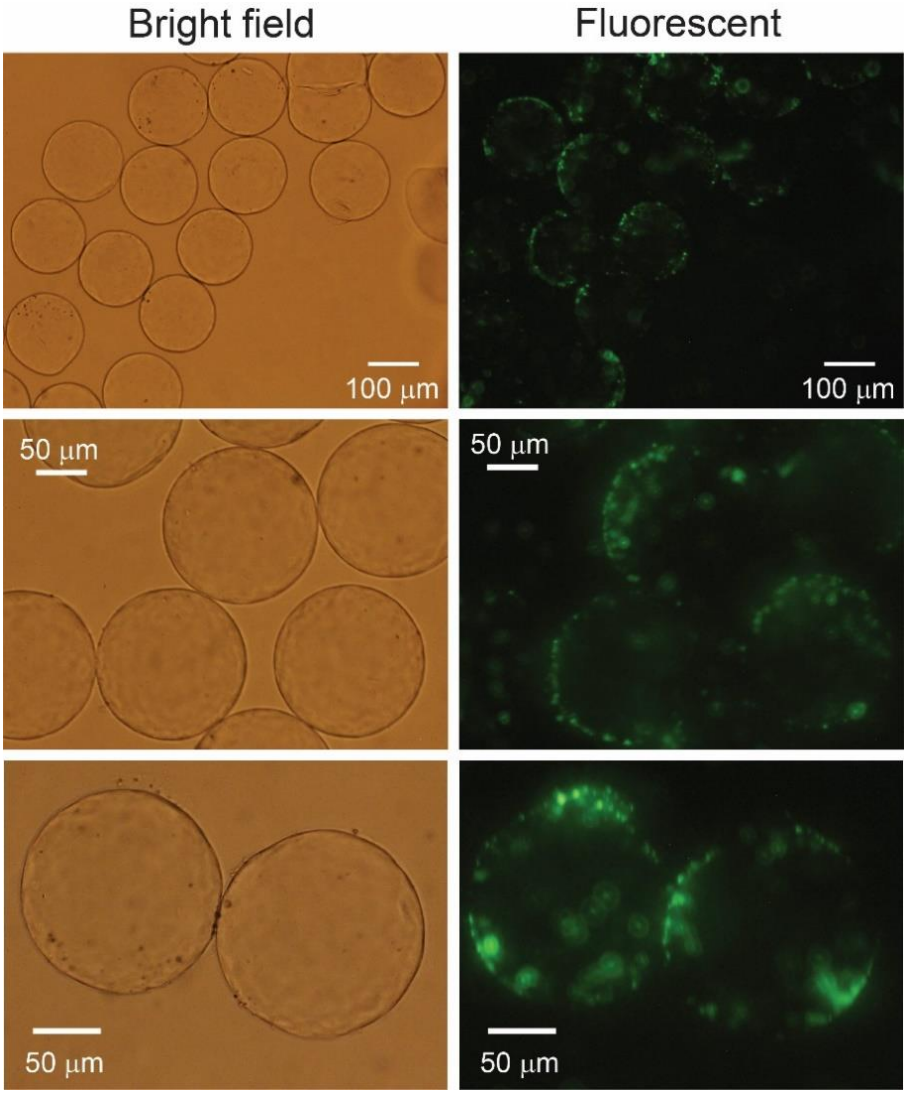

Fig. 4.15 Hydrogel particles with fluorescent coating observed by bright-field and fluorescent microscopy in pure water.

The dried particles were also observed through the SEM. An SEM image is shown in **Fig. 4.16**. Through the SEM image, the fluorescent polystyrene nanoparticles were demonstrated,

the white small dots in **Fig. 4.16**, were successfully embedded on the surface of the Ca-alginate hydrogel particles. However, the number of embedded polystyrene nanoparticles was small. That is might due to the low volume proportion of the nanoparticles in the W/O reactant emulsion phase (ca. 6×10^{-5} %).

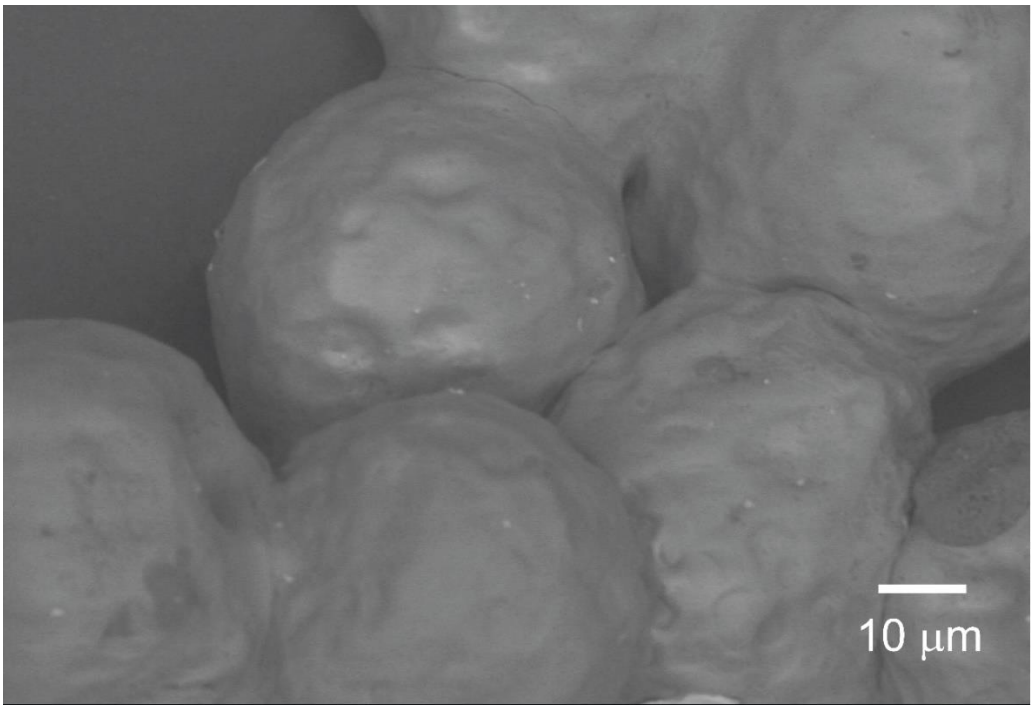

Fig. 4.16 An SEM image of dried gel particles with fluorescent nanoparticles embedded on the surfaces.

4.3.3 Gel particles with both magnetic and fluorescent coatings

(1) Droplet formation in the microchannel

For synthesizing the Ca-alginate hydrogel particles with both magnetic and fluorescent coatings, the $CaCl_2$ emulsion reactant containing Fe_3O_4 nanoparticles or fluorescent polystyrene microspheres was used. Considering that the dispersion of both Fe_3O_4 nanoparticles and fluorescent polystyrene microspheres into the $CaCl_2$ emulsions might decrease the concentration of calcium ions inside the $CaCl_2$ aqueous droplets of the emulsion and further influence their crosslinking reaction with the Na-alginate droplets. The $CaCl_2$ emulsion phase containing Fe_3O_4 nanoparticles or fluorescent microspheres was infused from separate inlets into the downstream channels at the flow rate of 20 mL/h (10 mL/h × 2). The flow rates at the

upstream cross-junction were set as Q_d = 0.1 mL/h and Q_c = 1.0 mL/h.

As shown in **Fig. 4.17**, only one side of the downstream had fluorescence under the fluorescent microscopy, and the fluorescent side had a clear boundary with the non-fluorescent side. Then when t = 0 ms, the formed Na-alginate droplet reached the downstream cross-junction. When t = 14 ms, the Na-alginate droplet moved to the deeper downstream channel. Similar to **Fig. 4.13**, The droplet flowing at the downstream channel had a clear boundary with the fluorescent $CaCl_2$ emulsion reactant phase (**Fig. 4.17**, t = 37 ms)

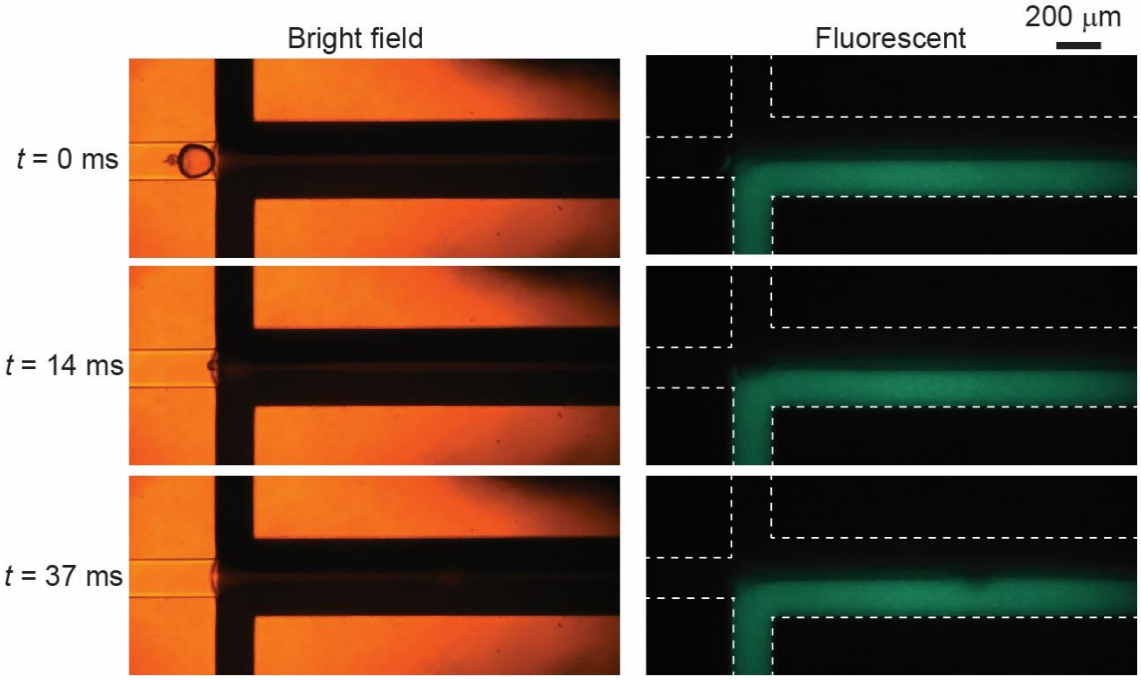

Fig. 4.17 Images of generation of a Ca-alginate hydrogel particle with both magnetic and fluorescent coating at the downstream cross-junction.

(2) Obtained hydrogel particles with both magnetic and fluorescent coating

The collected Ca-alginate hydrogel particles with both magnetic and fluorescent coating were firstly observed by bright-field microscopy in pure water (**Fig. 4.18**). The generated hydrogel beads had an average diameter of 156 μm with a CV value of 2.5%. The hydrogel particles had a highly spherical shape with an average roundness of around 0.97. Compared with the hydrogel particles that only have the fluorescent coating in **Fig. 4.14**, the embedded black Fe_3O_4 magnetic on the surface of obtained hydrogel particles could be observed under the bright-field microscopy. Besides the embedded fluorescent polystyrene microspheres could be confirmed by the bright-field microscopy under a large magnification (**Fig. 4.19**). As shown in

Fig. 4.19-D, both the Fe_3O_4 nanoparticles and fluorescent polystyrene microspheres existed on the surface of prepared Ca-alginate hydrogel microparticles.

Further, the fluorescence of obtained Ca-alginate hydrogel particles was observed under ultra-violet light and the image shows that the prepared microbeads had a clear fluorescent coating on their surfaces (**Fig. 4.20**).

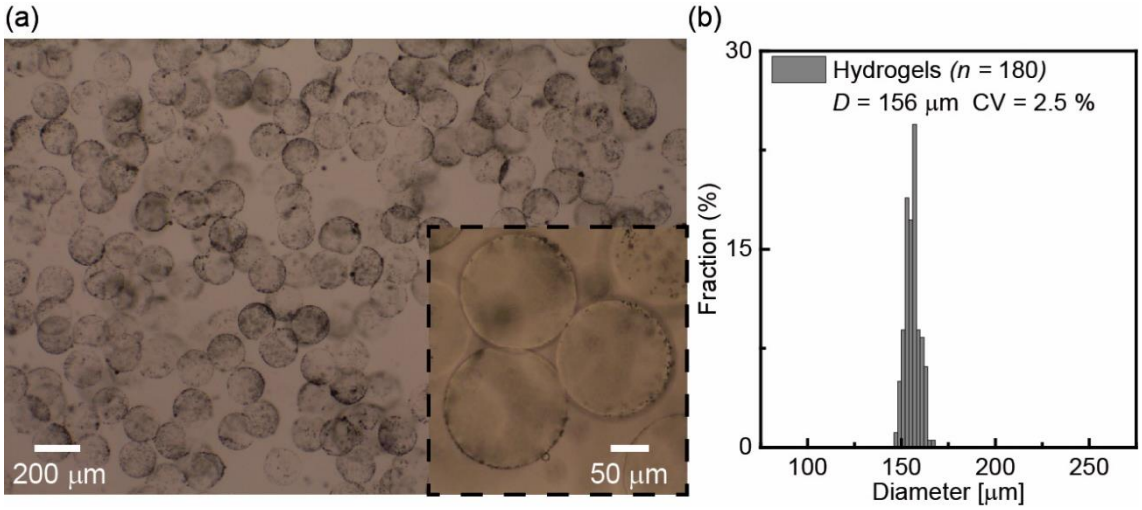

Fig. 4.18 Obtained hydrogel particles with both magnetic and fluorescent coatings. (a) A bright-field image of the hydrogel particles in water. (b) The size distribution of prepared hydrogel beads.

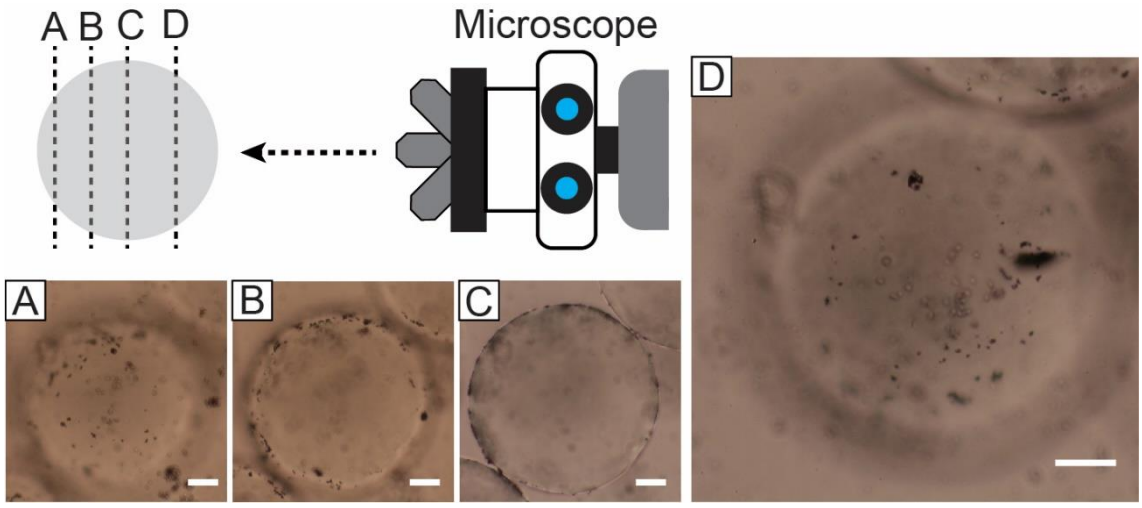

Fig. 4.19 A hydrogel microparticle with magnetic and fluorescent coating was observed at different focuses in pure water. The scale bars are 25 μm.

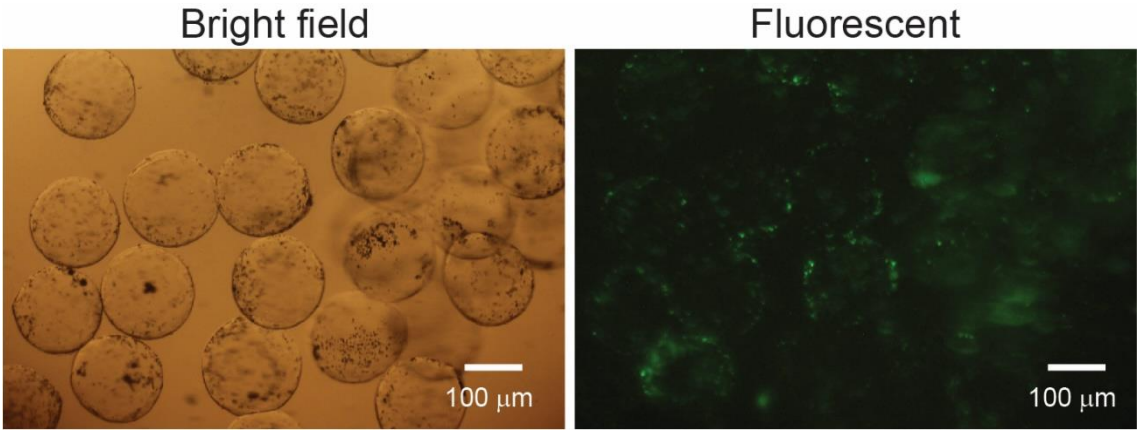

Fig. 4.20 Hydrogel particles with magnetic and fluorescent coating observed by bright-field and fluorescent microscopy in pure water.

4.4 Conclusion

Section 4.1. Introduction

This section describes the background, previous researches, and the objectives of this chapter.

Section 4.2. Materials and methods

This section describes the peripheral equipment, our microfluidic device, and the materials that used in our experiments.

Section 4.3. Results and discussion

This section explains how to use microfluidic external gelation to create highly spherical Ca-alginate hydrogel microparticles with magnetic and/or fluorescent coatings.

1) Highly spherical Ca-alginate hydrogel particles that had whole Fe_3O_4 nanoparticles coating with an average diameter of 160 μm, a CV value of 3.8%, and roundness around 0.90 were prepared. The manipulation of obtained particles under the exterior magnetic field was also demonstrated.

2) The Ca-alginate hydrogel beads that had whole fluorescent polystyrene microspheres coating with an average diameter of 165 μm, a CV value of 3.4%, and roundness around 0.95 were generated. The obtained hydrogel particles had a clear fluorescence under the fluorescent microscopy.

3) The Ca-alginate microgels that had both fluorescent and magnetic coating with an average diameter of 156 μm, a CV value of 2.5%, and roundness around 0.97 were synthesized. The produced hydrogel particles with various coatings have the potential to be highly useful in applications such as drug administration and release, high-resolution imaging, sorting, and separation.

References

[1] Wang, H.; Yang, S.; Yin, S.N.; Chen, L. and Chen, S. Janus suprabead displays derived from the modified photonic crystals toward temperature magnetism and optics multiple responses. *ACS Appl. Mater. Interfaces* **2015**, 7, 8827–8833.

[2] Maeda, K.; Onoe, H.; Takinoue, M. and Takeuchi, S. Controlled synthesis of 3D multi-compartmental particles with centrifuge-based microdroplet formation from a multi-barrelled capillary. *Adv. Mater*. **2012**, 24, 1340–1346.

[3] Zhao, L.B.; Pan, L.; Zhang, K.; Guo, S.S.; Liu, W.; Wang, Y.; Chen, Y.; Zhao, X.Z. and Chen, H.L.W. Generation of Janus alginate hydrogel particles with magnetic anisotropy for cell encapsulation. *Lab Chip* **2009**, 9, 2981–2986.

[4] Yuet, K.P.; Hwang, D.K.; Haghgooie, R. and Doyle, P.S. Multifunctional superparamagnetic Janus particles. *Langmuir* **2010**, 26, 4281–4287.

[5] Lan, J.; Chen, J.; Li, N.; Ji, X.; Yu, M. and He, Z. Microfluidic generation of magnetic-fluorescent Janus microparticles for biomolecular detection. *Talanta* **2016**, 151, 126–131.

[6] Bao, Z.; Chen, L.; Weldon, M.; Chandross, E.; Cherniavskaya, O.; Dai, Y. and Tok, J.B.H. Toward controllable self-assembly of microstructures: selective functionalization and fabrication of patterned spheres. *Chem. Mater.* **2002**, 14, 24–26.

[7] Jiang, S. and Granick, S. A simple method to produce trivalent colloidal particles. *Langmuir* **2009**, 25, 8915–8918.

[8] Karg, M.; Pastoriza-Santos, I.; Perez-Juste, J.; Hellweg, T. and Liz-Marzan, L.M. Nanorod-coated PNIPAM microgels: thermoresponsive optical properties. *Small* **2007**, 3, 1222–1229.

[9] Chan, A.W. and Neufeld, R.J. Tunable semi-synthetic network alginate for absorptive encapsulation and controlled release of protein therapeutics. *Biomaterials* **2010**, 31, 9040–9047.

[10] Li, R.H.; Altreuter, D.H. and Gentile, F.T. Transport characterization of cell encapsulation. *Biotechnol. Bioeng.* **2003**, 50, 365–373.

[11] Jejurikar, A.; Lawrie, G.; Martin, D. and Grøndahl, L.A novel strategy for preparing

mechanically robust ionically cross-linked alginate hydrogels. *Biomed. Mater.* **2011**, 6, 025010.

Chapter 5

Mass production of calcium-alginate hydrogel particles

Unpublished contents

Chapter 6

Microencapsulation of hydrophobic antifouling biocide

6.1 Introduction

6.1.1 Antifouling biocide

Biofouling on ship hulls and exterior walls are the most prominent examples of surface fouling [1-4]. Antifouling coatings containing antifoulants are the most often used methods for preventing fouling of surfaces in numerous manufacturing fields and the general public. Antifouling paint formulations can be split into three kinds. The schematic illustration of three primary methods to introduce the antifoulants into the paint formulation is shown in **Fig. 6.1**. First, antifoulants are easily and molecularly disseminated in wet paints [5-7]. This method is simple to manage, but it often results in the prematurely releasing or deterioration of biologically active substances [8,9]. As a result, it is difficult to meet the intended lifetime due to the fast release speed (e.g. 10 years for facade coatings). Extravagant drug amounts were often employed in paints to increase their functional duration, although this generally causes environmental contamination 10 and may result in macro phase separation in the coatings [8]. Second, the immobilization of items such as binder and pigments may be used to limit the rate of biocide release [9,11,12]. Nonetheless, this technique is confined to a small number of biocides that must meet certain practical conditions or include appropriate ligands. Because the majority of fouling issues are caused by a variety of fouling organisms with varied sensitivity to biocides [13,14], incompatibility hinders the combining of multiple types of biocide in a single paint composition with effective antifouling performance.

When compared to traditional biocide formulations, microencapsulation offers several benefits in the creation of coating paints to prevent fouling issues, including [8,15-18]: (i) the delayed release of actives from the microcapsules to the exterior paint matrix can be used to regulate the release rate of encapsulated actives; (ii) the degradation of biocides can be prevented through encapsulation; (iii) selected biocides can be combined for usage without

possible macro phase separation; (iv) after encapsulation, biocides will be considerably simpler to handle and apply, because some biocides (e.g. Irgarol or SEA-NINE 211) may cause eye irritation and skin sensitization.

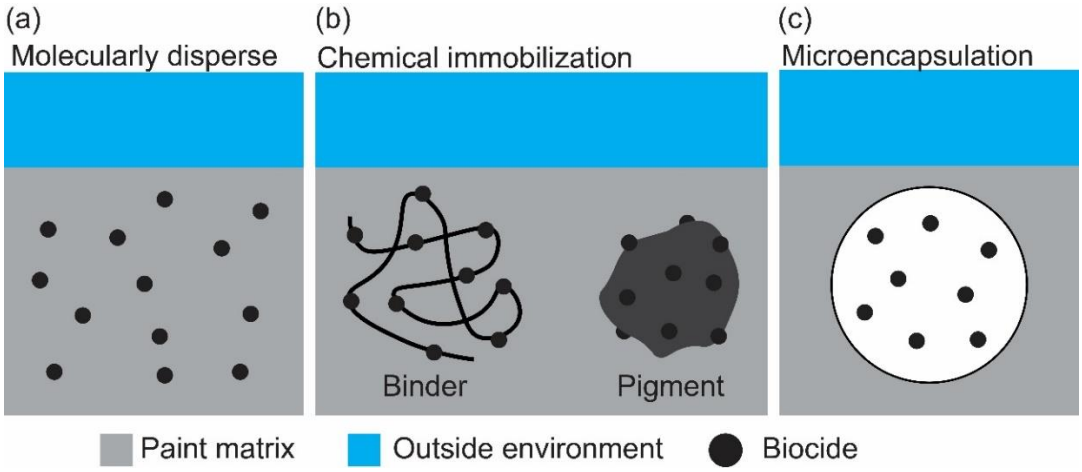

Fig. 6.1 Antifouling biocides can be added into the formulation of coating paints by (a) molecular dispersion, (b) immobilization to a large component, and (c) encapsulation.

6.1.2 Microencapsulation of antifouling biocide

(1) Polymeric urushiol (PUL)

Zheng et al. reported a facile one-pot synthesis of polymeric urushiol microcapsules for encapsulating silver nanoparticles for the marine antifouling (**Fig. 6.2**) [17].

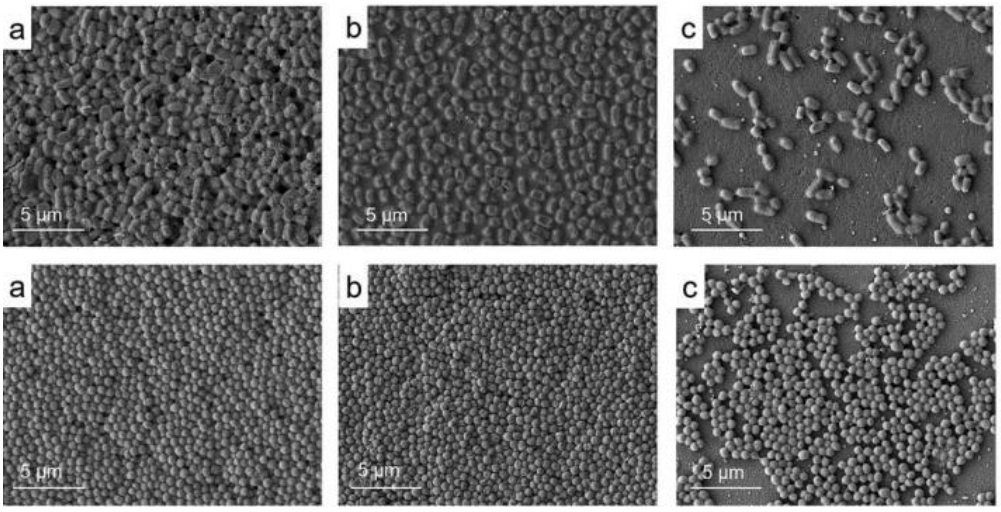

Fig. 6.2 Microencapsulation of silver nanoparticles in PUL microparticles. Reproduced with permission [17]. Copyright 2020 RSC.

(2) Poly(l-lactide)

Fay et al. presented work in which polymers were employed to design delivery devices with a long lifespan. To produce biodegradable antifouling paints based on non-toxic chemicals and bioactive surfaces, chlorhexidine was encapsulated in poly(l-lactide) microcapsules and integrated into antifouling compositions (**Fig. 6.3**) [19].

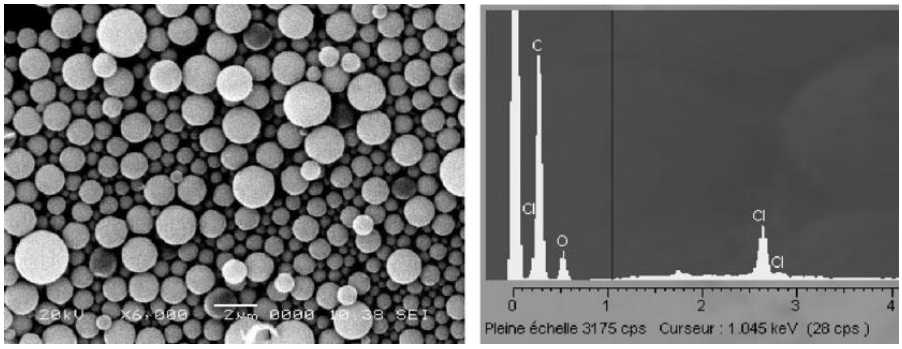

Fig. 6.3 Microencapsulation of chlorhexidine in poly(L-lactide) microparticles. Reproduced with permission [19]. Copyright 2008 Wiley-VCH.

(3) Poly(lactide-co-glycolide)

Further, perfluorooctyl bromide was encapsulated in the poly(lactide-co-glycolide) (PLGA) microcapsules through a solvent-evaporation technique (**Fig. 6.4**) [20].

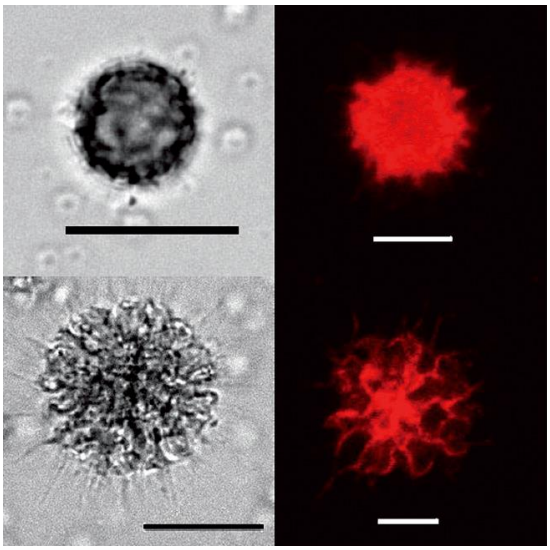

Fig. 6.4 Microencapsulation of perfluorooctyl bromide in PLGA microparticles. Reproduced with permission [20]. Copyright 2009 RSC.

(4) Melamine formaldehyde

Long et al. presented a new double-shell microcapsule containing a melamine-formaldehyde (MF) polymer and ripened $CaCO_3$ nanoparticle for the encapsulation of aldehydes, alcohols, and esters, that could be used for antifouling applications (**Fig. 6.5**) [21].

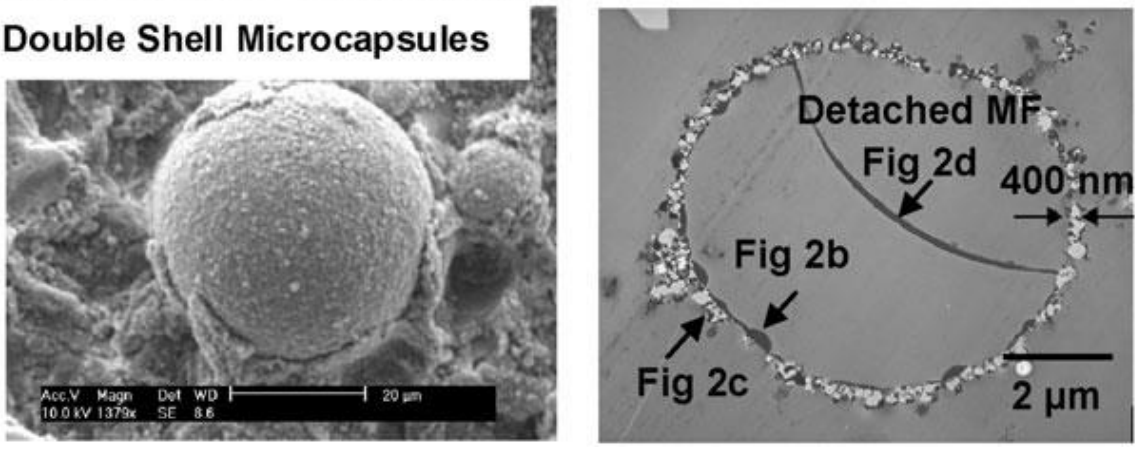

Fig. 6.5 Microencapsulation of perfluorooctyl bromide in PLGA microparticles. Reproduced with permission [20]. Copyright 2010 RSC.

(5) Poly(methyl methacrylate)

The antifoulant including medetomidine (**Fig. 6.6**) [8], dodecane [22], Iodopropynyl butylcarbamate (IPBC) [23], and aurantiol [24] have been encapsulated in poly(methyl methacrylate) (PMMA) microparticles as a useful tool for the creation of coatings that provide extended protection against bio-contamination.

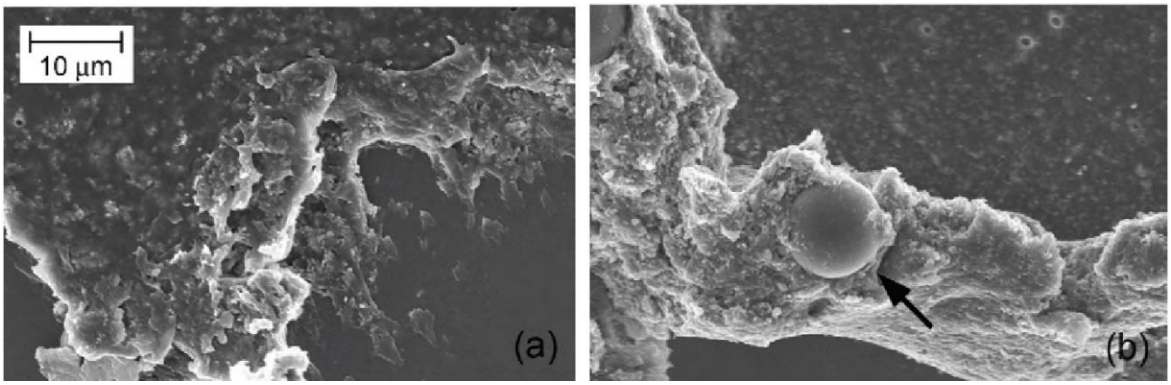

Fig. 6.6 Dispersion of PMMA microparticles containing medetomidine in paint coating. Reproduced with permission [8]. Copyright 2017 MDPI.

The summary of the shapes and size distribution of microparticles used for the antifouling biocide encapsulation is shown in **Table 6.1**. It is obvious that the shape and distribution of diameter of these kinds of microcapsules are often inadequately regulated, which might make producing a predictable dose and highly repeatable slow release of the encapsulated chemicals.

Furthermore, the materials of microcapsule have to be suitable with the wet paint in order to prevent inhomogeneous dispersion, aggregation of microparticles, and other undesired effects. 25. Encapsulating biocides in a hydrophilic substance, for example, would be excellent for use with aqueous paints and varnishes, which offer advantages such as non-combustibility and low viscosity [26].

Last but not least, to minimize contamination, the microcapsule components should be biodegradable and environment-friend.

Table 6.1 Sizes and size distributions of microcapsules for biocides encapsulation in literature.

Materials	Biocides	Average diameter	Coefficient variation	Ref.
PLA (Poly(L-lactide))	Chlorhexidine	1 μm	N.A.	[19]
PLGA and PLGA-PEG	Perfluorooctyl bromide	12–26 μm	N.A.	[20]
Melamine formaldehyde	Aldehydes, alcohols, esters	15 μm	13%	[21]
PMMA	Medetomidine	12 μm	41.6%	[8]
PMMA	Dodecane	2.4 μm	19%	[22]
PMMA	IPBC	N.A.	N.A.	[23]
PMMA	Aurantiol	20–200 μm	N.A.	[24]

6.1.3 Objectives

In this chapter, a novel microfluidic external gelation method using reactant W/O emulsion, as described in **Chapter 2**, was used to show the biocompatible hydrophilic encapsulation of a hydrophobic antifouling biocide in Ca-alginate hydrogel microcapsules. The antifouling biocide Irgarol was effectively encapsulated in the hydrogel particles in this chapter. The rates of release of encapsulated and non-encapsulated biocides were studied. The hydrogel capsules were then reinforced with cellulose fiber to increase the mechanical property. Finally, utilizing water grass, the antifouling activity of the encapsulated chemicals was examined (*Bacopa monnieri*).

The main objectives of this chapter are as follows:

(1) To design highly spherical hydrogel particles for encapsulating antifouling biocide Irgarol.

(2) To investigate the release speeds of the encapsulated and non-encapsulated drug Irgarol.

(3) To incorporate the cellulose fiber with the gel microspheres to increase their mechanical feature.

(4) To evaluate the antifouling functions of the loaded chemicals by using water grass (*Bacopa monnieri*).

6.1.4 Outline of chapter

Section 6.1 Introduction

Introduces the background of previous researches about the antifouling biocide capsules.

Section 6.2 Materials and methods

Describes the peripheral equipment, our microfluidic device, and the materials that used in this experiment.

Section 6.3 Results and discussion

Demonstrates the experiments about synthesizing the Ca-alginate hydrogels carrying the drug Irgarol. The release speeds of the encapsulated and non-encapsulated antifouling drugs are reported. The effects of cellulose fibers inside the hydrogel capsules are investigated and the antifouling effects of our microcapsules are presented.

Section 6.4 Conclusion

Describes the conclusion of this chapter.

6.2 Materials and methods

6.2.1 Microfluidic chip

6.2.1.1 Design of the microfluidic chip

The structure of the microfluidic chip used in this chapter is the same as **Chapter 2**. The difference is that the Na-alginate solution carrying drugs was used as the disperse phase.

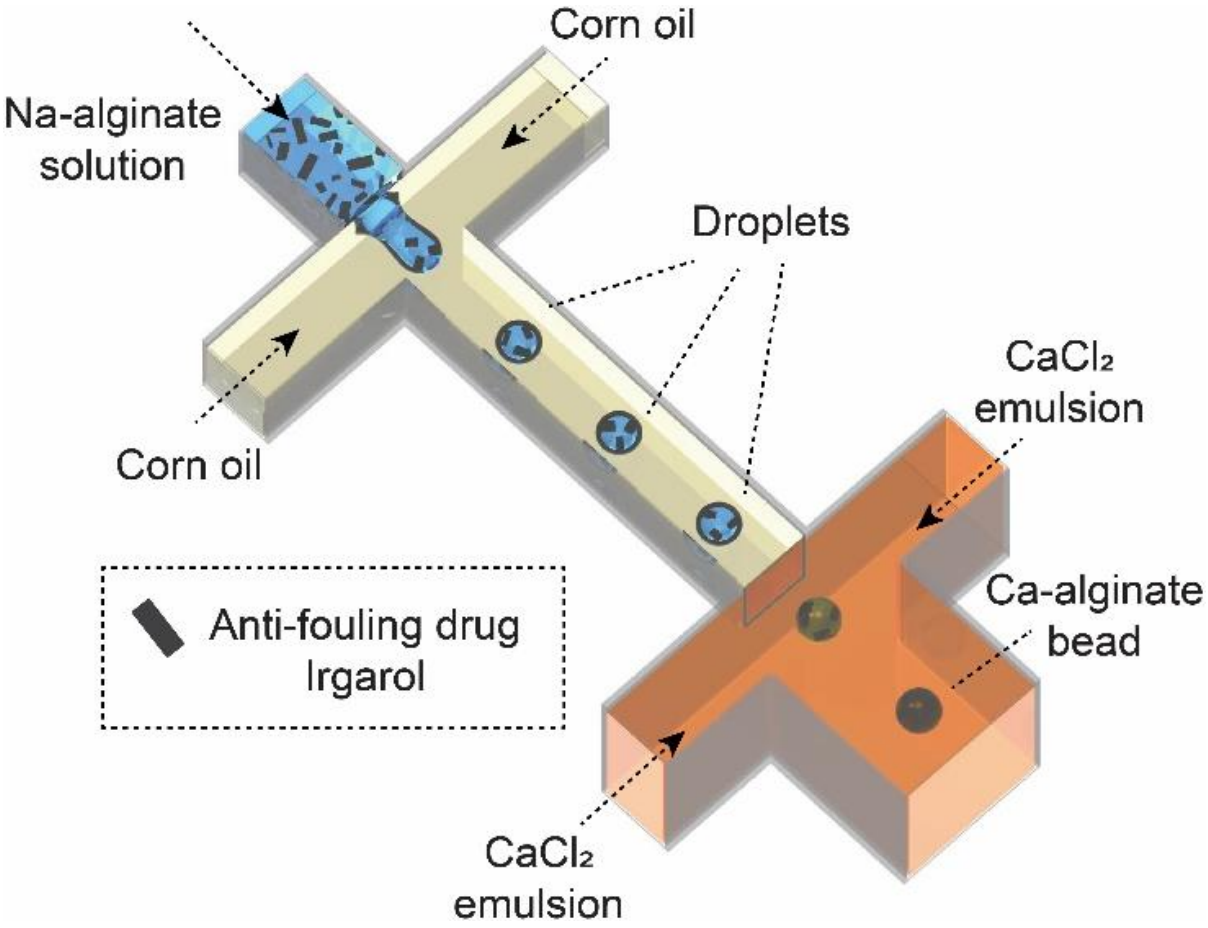

Fig. 6.7 Microfluidic procedure to generate Ca-alginate microcapsules containing the antifouling drug Irgarol® [27].

6.2.1.2 The preparation of microfluidic system

The setup of the microfluidic device is the same as **Chapter 2**. The details are shown in **Appendix**.

6.2.2 Materials

6.2.2.1 Antifouling drug Irgarol®

Antifouling chemical compound Irgarol® 1071 (N-cyclopropyl-N'-(1,1-dimethylethyl)-6-(methylthio)-1,3,5-triazine-2,4-diamine) (Ciba, USA.) (**Fig. 6.8**) was used for the experiments of drug encapsulation and sustained release. The drug Irgarol is a kind of hydrophobic and particularly phytotoxic algaecide that has lately been widely employed in long-term antifouling coatings for aquatic utilization and construction constituents due to its ability to disrupt photosystem II in water plant species and impede their development (**Fig. 6.9**) [28,29].

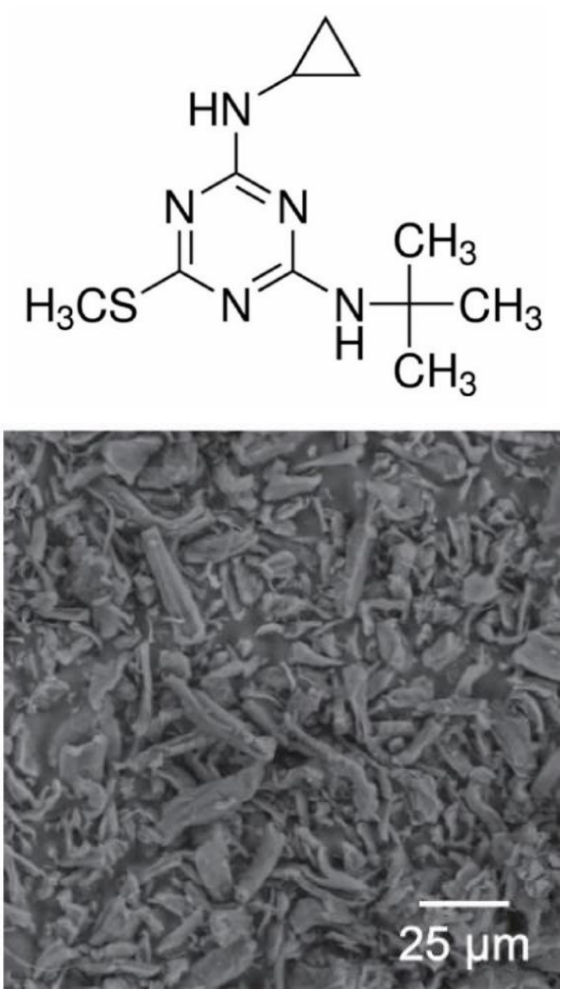

Fig. 6.8 Chemical structure and a scanning electron microscopy (SEM) photograph of antifouling drug Irgarol® 1071.

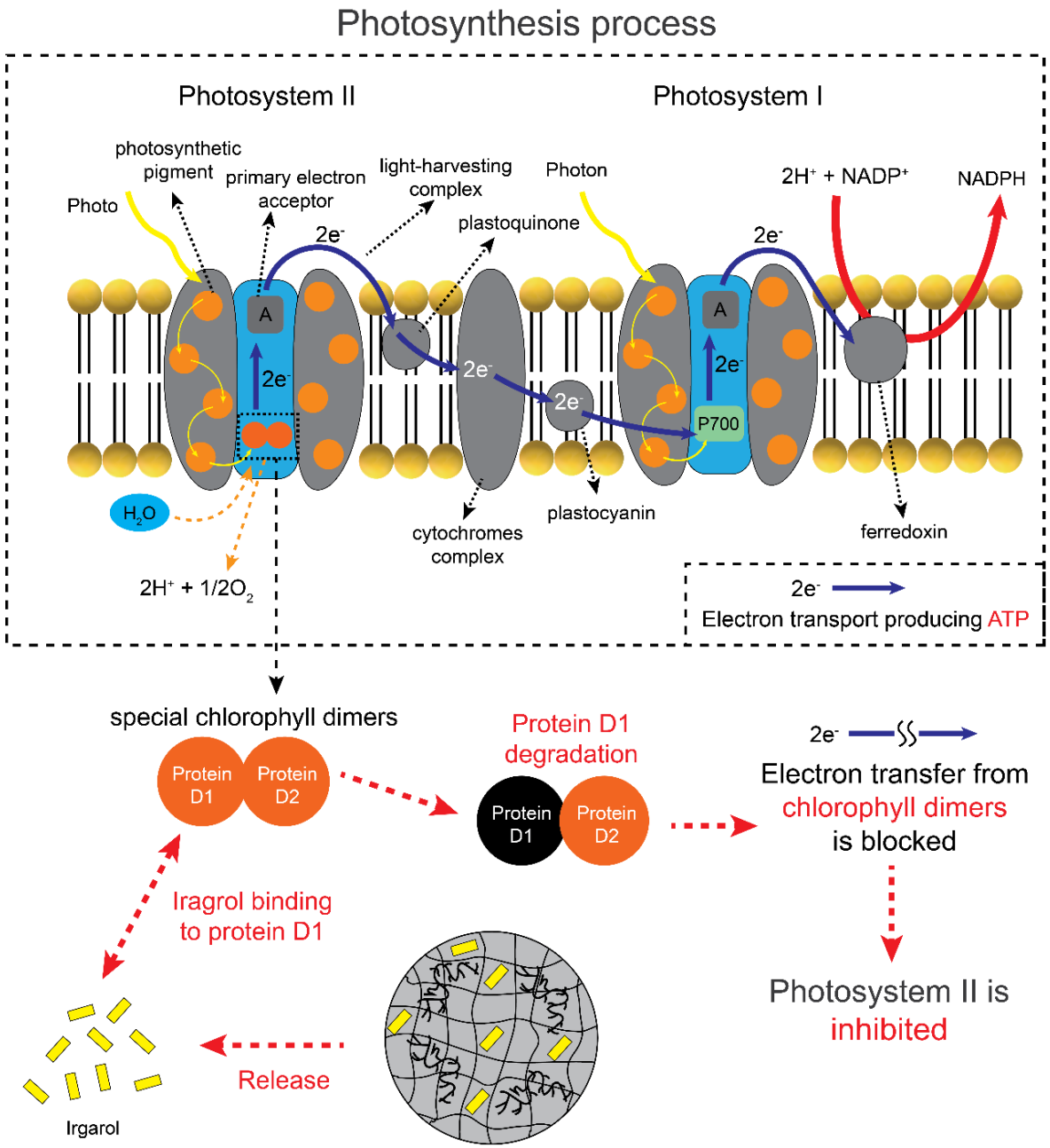

Fig. 6.9 Antifouling mechanism of Irgarol ® on aquatic plant species.

6.2.2.2 Cellulose fiber

Cellulose fibers (Arbocel® UFC 100, JRS, MI, USA) (**Fig. 6.10**) were added to the hydrogel microparticles to enhance their mechanical strength.

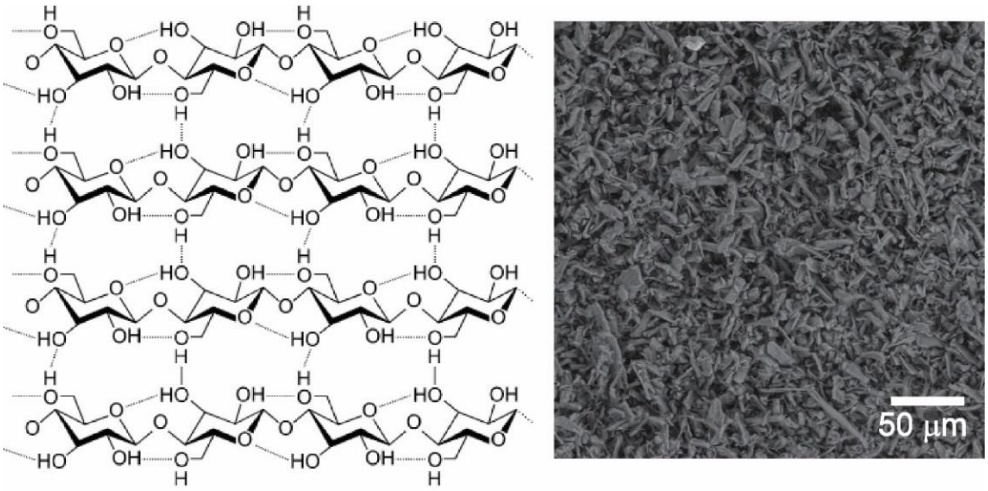

Fig. 6.10 Cellulose chains linked by hydrogen bonds and a SEM photograph of the cellulose fiber (Arbocel® UFC 100) [30].

6.2.2.3 Preparation of Ca-alginate microcapsules

A disperser was used to create the disperse phase by mixing a 3 wt% aqueous Na-alginate solution containing Irgarol® 1071 or with both the medication and cellulose fibers (Arbocel® UFC 100, JRS, MI, USA). **Table 6.2** shows the components of the dispersion phase utilized in the experiments. The other materials and preparation procedures of synthesized microcapsules are the same as **Chapter 2**.

Table 6.2 The disperse phase used in the experiment.

	3 wt% Na-alginate solution	Irgarol® 1071	Cellulose fiber	Mixing time (30000 rpm)
Disperse #1	20.0 g	0.1 g	-	3 min
Disperse #2	20.0 g	0.05 g	-	3 min
Disperse #3	20.0 g	0.1 g	1.0 g	5 min

6.2.2.4 Water grass (*Bacopa monnieri*)

Using a collection reservoir with 80 g of specialized soil (Sunsun, Zhoushan, Zhejiang, China) and 20 mL of deionized water, 0.5 g of grass seed (*B. monnieri*, Balai, Japan) was cultivated. After 7 days of culture, the hydrogel microbeads were collected, dried on nylon mesh,

and flushed with 30 mL of deionized water into a collection reservoir containing tested grass. The glass beakers were placed in a typical outdoor place with plenty of sunshine.

6.2.3 Ultraviolet-visible (UV-Vis) spectroscopy

Light in the visible and neighboring wavelengths is used in ultraviolet-visible spectroscopy. The absorption or reflectance of a substance in the visible spectrum has a direct impact on its apparent color. Atoms and molecules experience electronic transitions in this area of the electromagnetic spectrum. Anti-bonding molecular orbitals may be raised by absorbing light energy in ultraviolet or visible light that contains bonded or nonbonding electrons. The greater the wavelength of light that electrons can absorb, the more quickly they can be activated. UV/Vis spectrophotometry is often employed in diagnostic chemistry to quantify various analytes such as metal ion transitions, highly conjugated chemical substances, and biological macromolecules. The device could also be used to combine with HPLC. When an analyte is present, the response is expected to be proportionate to the solubility level. The response factor is the response for a certain concentration. **Figure 6.11** depicts a typical UV-Vis spectroscopy setup.

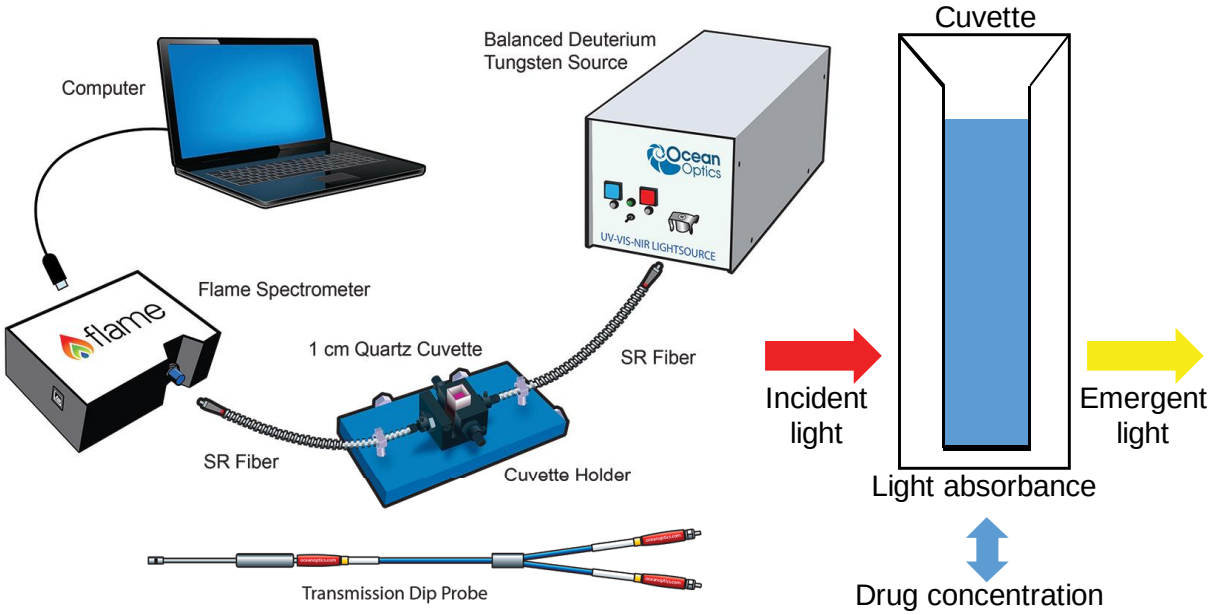

Fig. 6.11 A typical UV-Vis spectroscopy setup [31].

In these experiments, a spectrometer, a light source, a glass cuvette, and a cuvette holder were used (**Appendix**).

6.2.3.1 *Beer-lambert* law

The wavelengths of absorption peaks may be associated with the kinds of bonds present in a specific molecule, and this information is useful in detecting the functional groups included inside a molecule. With the use of *Beer-Lambert* law, the approach is most often used to quantitatively measure the concentrations of an absorbing species present in a liquid solution. In terms of mathematical formulas, the transmittance of a material sample is proportional to its optical depth τ and its absorbance A as:

$$T = \Phi_e^t/\Phi_e^i = e^{-\tau} = 10^{-A} \quad (6\text{-}1)$$

where Φ_e^i is the radiant flux that the material sample received and Φ_e^t is the radiant flux that the material sample transmitted. So the equation can be written as:

$$A = log_{10}(I_0/I) \quad (6\text{-}2)$$

where A is the measured absorbance, I_0 is the transmitted intensity of UV-Vis light after passing through the pure water, I is the transmitted intensity of light pass through the test solution.

6.2.3.2 Measurement procedure of UV-Vis device

The gel microparticles were gathered on the nylon mesh in preparation for the UV-Vis measurement. Then particles on the mesh were scraped off and put into a glass reservoir containing 50 mL of deionized water, which completed the experiment. After that, 1.5 mL of the tested solution was transported to a glass cuvette for measuring purposes. The tested liquids were poured back to the reservoir containing microcapsules to finish the experiment (**Fig. 6.12**).

6.2.3.3 UV-Vis absorbance *vs.* drug concentration

The relation between the observed UV-Vis light absorbance and the concentration of the drug of the tested solution was demonstrated. Five samples were produced with a drug concentration of about 7.5 mg/L. **Table 6.3** describes the five samples in detail.

Table 6.3 The details of the five samples.

	Water (mL)	Drug weight (mg)	Concentration (mg/L)
Sample 1	399.6	3.0	7.5
Sample 2	399.4	2.9	7.3
Sample 3	399.5	3.0	7.5
Sample 4	399.4	3.0	7.5
Sample 5	399.6	3.0	7.5

Each sample was diluted by 1/6, 1/4, 1/3, 1/2, 2/3, and 5/6. Irgarol® showed just one absorbance peak (~ 224 nm) at wavelengths spanning from 195 nm to 527 nm (**Fig. 6.13**). A chart showing the connection between the concentration of Iragrol in the tested sample liquids and the maximum absorbance amount (224 nm) was created (**Fig. 6.14a**), and scattering points were linearly fitted (**Fig. 6.14b**). The equation below was used to calculate the connection between peak absorption intensity and medication concentration.

$$C_a = 8.93A \tag{6-3}$$

where C_a is the drug concentration of the tested solution and A is the maximum light absorbance value. **Table 6.4** shows the details of this linear fitting.

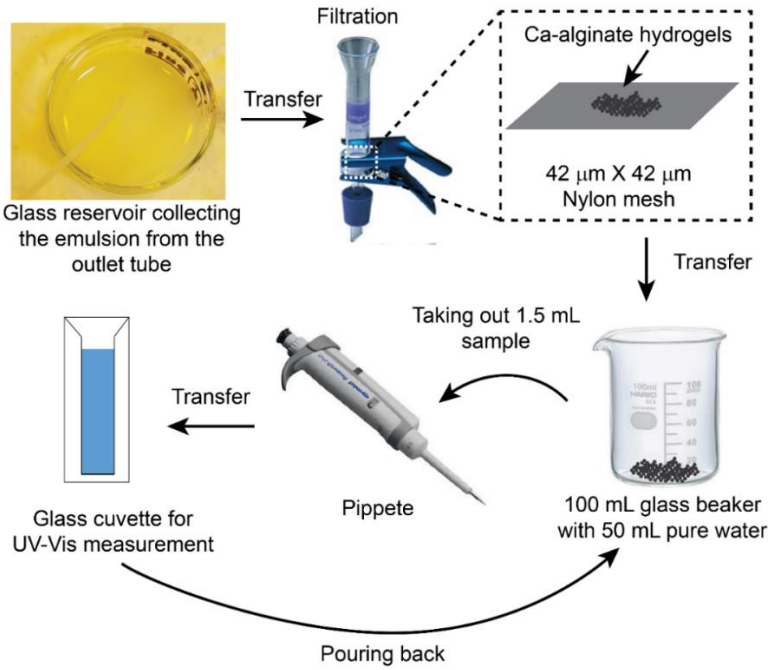

Fig. 6.12 Schematic illustration of the UV-Vis measurement process.

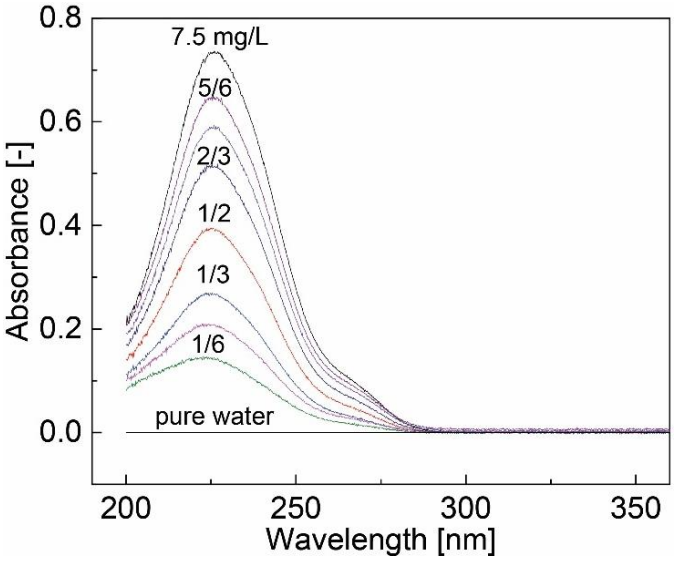

Fig. 6.13 Measurement of UV-Vis absorbance spectra of Irgarol® 1071 (Sample 1) at different dilution ratios. The inset is an SEM image of Irgarol® 1071.

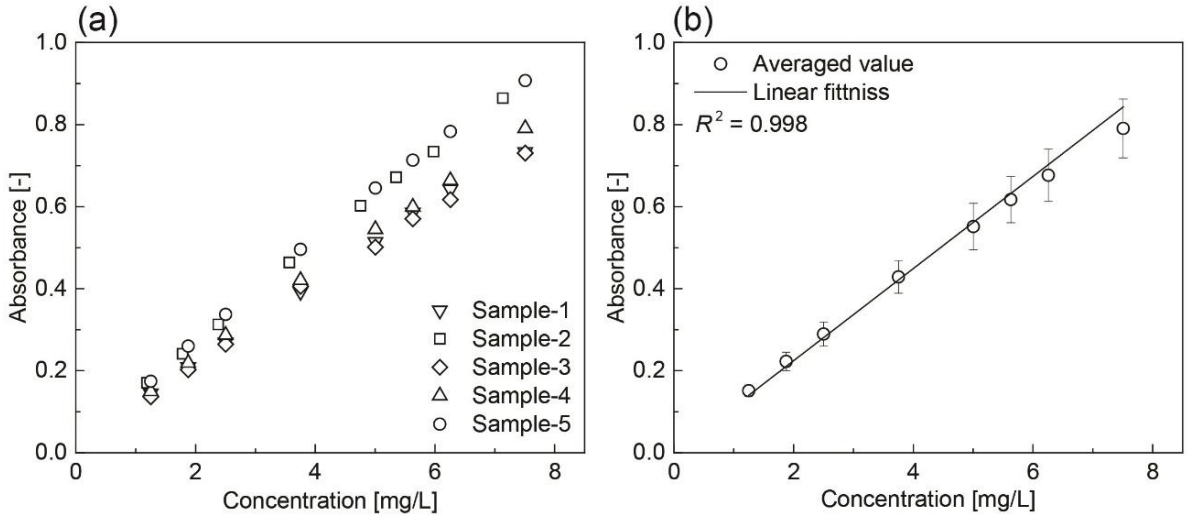

Fig. 6.14 The UV-Vis absorbance *vs*. the drug concentration. (a) The UV-Vis absorbance *vs*. the drug concentration of five samples. (b) The average data and linear fitting.

Table 6.4 Results of the linear fitting.

Intercept		Slope		Statistics
Value	Standard Error	Value	Standard Error	Adj. R-Square
0.02245	0.00363	0.10524	0.00137	0.99841

6.2.4 Gel particles and non-encapsulated drug for UV-Vis test

Four kinds of hydrogel particles containing just the drug and one kind of hydrogel particle comprising both the drug and cellulose fibers were created and the release mechanism of encapsulated drugs was tested by UV-Vis spectroscopy. **Table 6.5** shows the specifics of the prepared hydrogels. For Type 1 hydrogels, a 0.1 g of Irgarol® was introduced to 20 g of 3 wt% Na-alginate solutions (Disperse #1) and collection time for prepared microgels was 30 mins. A 0.05 g of the Irgarol powder was dispersed in 20 g of 3 wt% Na-alginate solutions (Disperse #2) as the second type of gel microcapsules, and the particles were generated for 30 min. The Type 3 microcapsules contained the same composition as the Type 1 microcapsules, but the collection time of gel beads was 60 min. The Type 4 microcapsules had the same amount of water as the Type 2 microcapsules, and the generation period was 60 min. Type 5 hydrogels were loaded with 0.1 g of the Iragrol and 1.0 g of fibers, which were dispersed in 3 wt% Na-alginate solutions (Disperse #3), with a collection time of 60 min. Furthermore, the encapsulated quantity m_e, which is the quantity of encapsulated drug expected given the drug concentration in the initial disperse phase, the flow rate in the dispersion phase, and the collection period, is defined as follows:

$$m_e = C_D \cdot Q_d \cdot t \tag{6-4}$$

where C_D is the initial concentration of drug in disperse phase, Q_d is the flow rate of disperse phase, and t is the producing time gel particles.

Table 6.5 Details of the hydrogel samples for the UV-Vis measurement.

	The type of used disperse phase	Collection time	Encapsulated amount (m_e)
Type 1	Disperse #1	30 min	0.250 mg
Type 2	Disperse #2	30 min	0.125 mg
Type 3	Disperse #1	60 min	0.500 mg
Type 4	Disperse #2	60 min	0.250 mg
Type 5	Disperse #3	60 min	0.500 mg

The non-encapsulated drug samples were dissolved in 20 mL of methanol (3.0 mg or 6.0 mg). Next, 1 mL of the produced solution was taken out by a pipette into a reservoir and allowed to

evaporate for 3 h at 80 °C. Lastly, 50 mL of deionized water was put into the reservoir to reach a concentration of 6.0 mg/L (Non-encapsulated drug sample 1) or 3.0 mg/L (Non-encapsulated drug sample 2).

6.2.5 Fourier-transform infrared (FTIR) spectra measurement

The FTIR spectrophotometer was used to measure the attenuated total reflection (ATR)-FTIR spectra. At 32 scans, spectra were recorded in the region of 4000 cm^{-1} to 400 cm^{-1} at 2 cm^{-1}.

6.2.6 Mechanical strength of hydrogel particles

The mechanical strength of two kinds of gel microcapsules containing either the Iragrol alone or both the Irgarol and fibers were compared. Type 3 microcapsules were chosen for the fiber-free sample, while Type 5 microcapsules were chosen for the fiber-containing sample. these hydrogel particles were sandwiched individually between two glass plates and the forces were added on the top slide glass (**Fig. 6.15**). The height deformation of the prepared gel layer was captured using a digital camera and measured with ImageJ. (NIH, MD, USA).

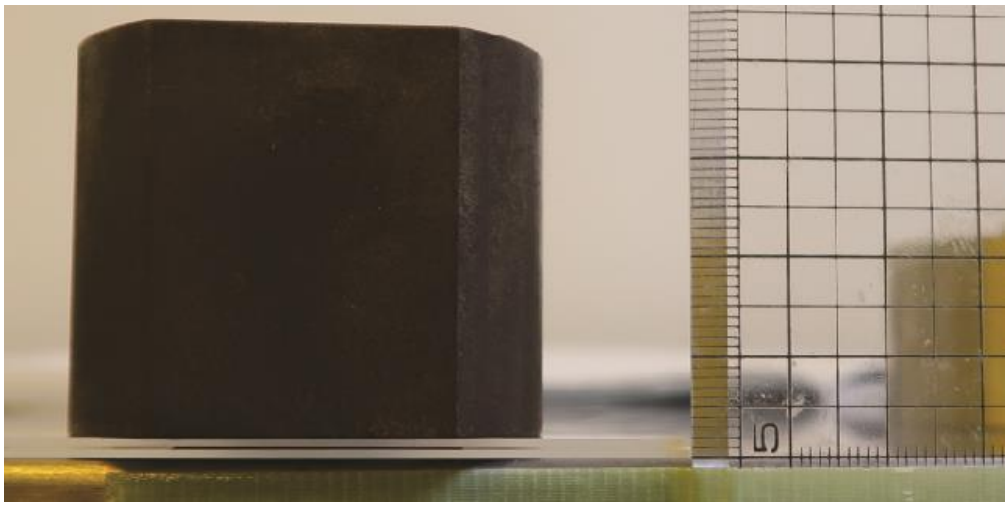

Fig. 6.15 A photograph from the side showing the particles' deformation measurement.

6.3 Results and discussion

6.3.1 Ca-alginate microcapsules containing drugs

6.3.1.1 Generation of droplets loaded with drugs

The disperse phase was prepared according to the **Table. 6.2**. Two Na-alginate solutions containing the drug Irgarol at different concentrations were used. And the drug was homogeneously dispersed in the Na-alginate solution by the mechanical homogenizer.

At the device's upstream cross-junction, the creation of Na-alginate droplets carrying black drug crystals was presented. **Figure 6.16** depicts a normal procedure of droplet production containing the drugs in a dripping regime. Droplets of uniformed sizes were created sequentially, with a production frequency of ~8 drops/s. The average diameter of these droplets was determined using the formation rate of the droplets and the total flow rate of disperse phase. The diameter of the droplets loaded with the Iragrol crystal was about 188 μm. Satellite droplets with small sizes (average diameter: ~49 μm) were sometimes generated as a result of the very viscous disperse phase (approximately 1500 mPa·s; **Fig. 6.16**, t = 48 ms). After passing through the next junction, the droplets reacted with the reactant emulsion (**Fig. 6.16**, time = 109 ms).

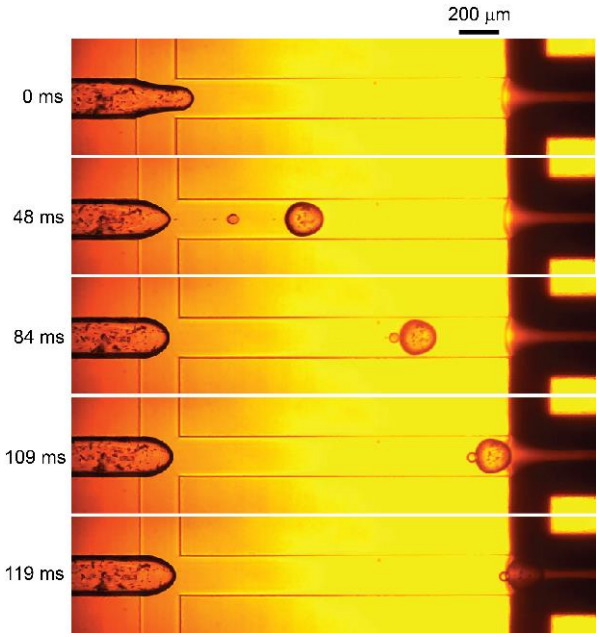

Fig. 6.16 Images of the production procedure of a droplet carrying the Irgarol. Flow rates of the Na-alginate solution (Q_d), corn oil (Q_c), and water-in-oil emulsion (Q_e) are 0.1, 2.0, and 20.0 mL/h, respectively.

This was consistent with the earlier investigation in **Chapter 2, Section 3**, in which droplets with an average diameter of 190 m and a CV of 2.2% were prepared using the equal Q_c (2.0 mL/h) and Q_d (0.1 mL/h). This uniformity in experimental data shows that the existence of the drug had no significant effect on the process of droplet production or droplet size. When used properly, the microfluidic system did not encounter gel blockage throughout the experiments.

6.3.1.2 Prepared Ca-alginate microcapsules loaded with drug

The Q_d, Q_c, and Q_e were set at 0.1, 2.0, and 20.0 ml/h respectively for the following experiments. Reactant W/O emulsion with the optimal mass proportion of aqueous solution (W = 0.26) was used. The produced hydrogel particles were dispersed in pure water for observation and measurement. **Figure 6.17a** depicts images of the produced microgel beads while the Irgarol was added in the Na-alginate solution (Disperse #1). The microspheres had a very spherical morphology, and drug crystals were contained in the hydrogels, as seen by these photos. These particles had an average roundness of 0.97. The particles had an average diameter of 160 μm and a CV value of 3.5% (**Fig. 6.17b**). **Figure 6.18** shows a micrograph of the obtained hydrogel particles when 0.05 g drug Irgarol was added in 20 g Na-alginate solution (Disperse #2). Compared with **Fig. 6.17**, the drug amount in each hydrogel particle was decreased suggesting that the drug amount in each particle can be decreased by simply reducing its total amount in the Na-alginate solution.

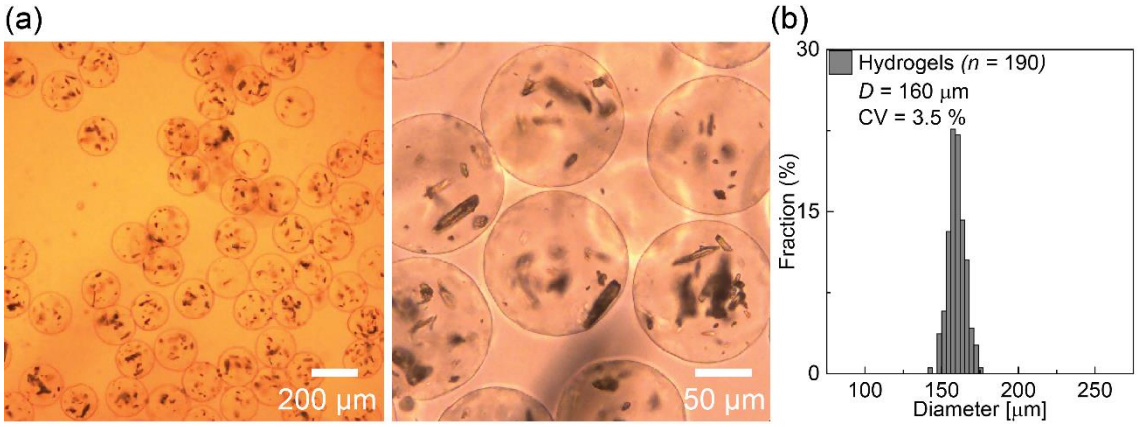

Fig. 6.17 Produced Ca-alginate (Disperse #1) in pure water. (a) Images of hydrogel microbeads in water. (b) The size distribution of hydrogels.

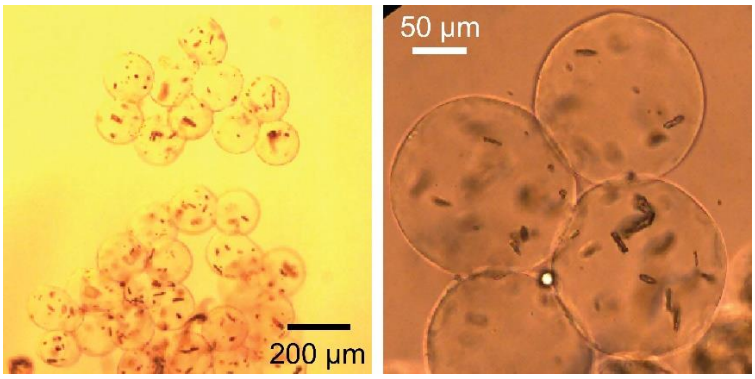

Fig. 6.18 Produced Ca-alginate (Disperse #2) in pure water.

The hydrogel particles were stored at normal temperature (~ 23 °C) for 24 h. Then they were examined by the SEM. The images are shown in **Fig. 6.19.** As shown in the SEM picture of the dehydrated gel beads the resulting microcapsules retained a spherical morphology and the surfaces of the microspheres were smooth. However, the surfaces of certain microgel beads were deformed that is due to the existence of encapsulated drug crystals.

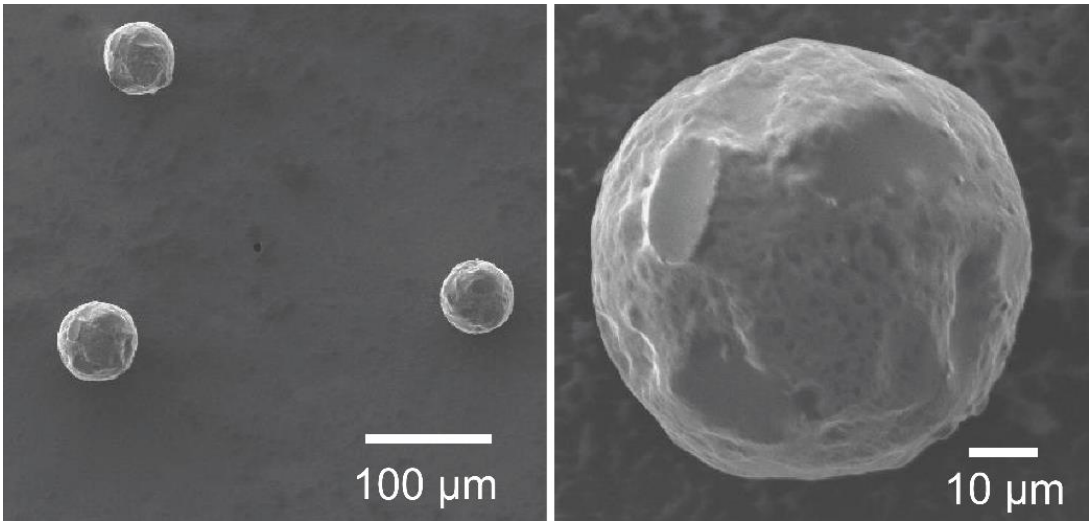

Fig. 6.19 SEM images of gel microcapsules containing drug Irgarol inside.

The cross-sectional SEM images indicated the densely packed polymer network of obtained gel microcapsules in which Irgarol crystals were embedded (**Fig. 6.20**). In prior works (**Chapter 2, Section 3**), monodispersed highly spherical microgel beads with an average diameter of 160 µm (CV: 2.4%) were formed at the same Q_c, Q_d, and Q_e (2.0 mL/h, 0.1 mL/h, and 20.0 mL/h, respectively). Thus, drug encapsulation had no significant effect on the size, size distribution, shrinkage proportion, or shape of the produced microgel particles.

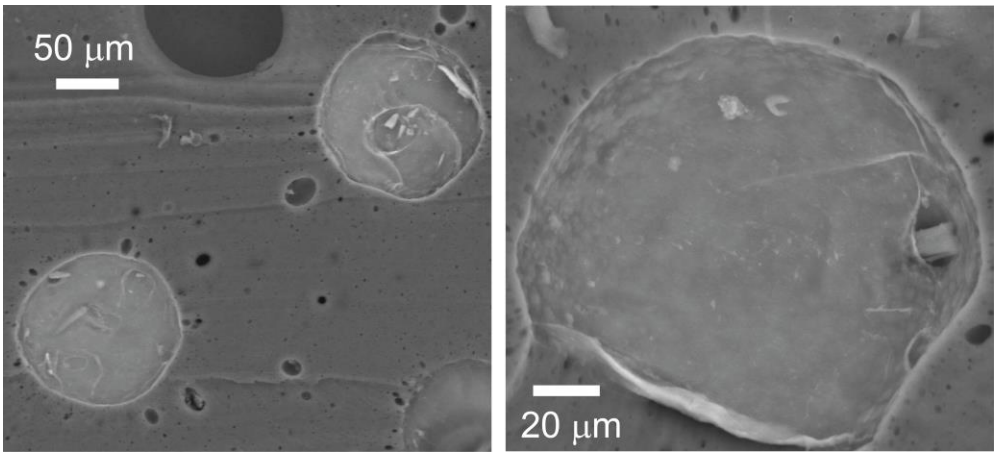

Fig. 6.20. SEM images of the cross-section of the Ca-alginate hydrogel particles.

Moreover, the ATR-FTIR spectra of the produced Ca-alginate microcapsules filled with drugs were examined (**Fig. 6.21**).

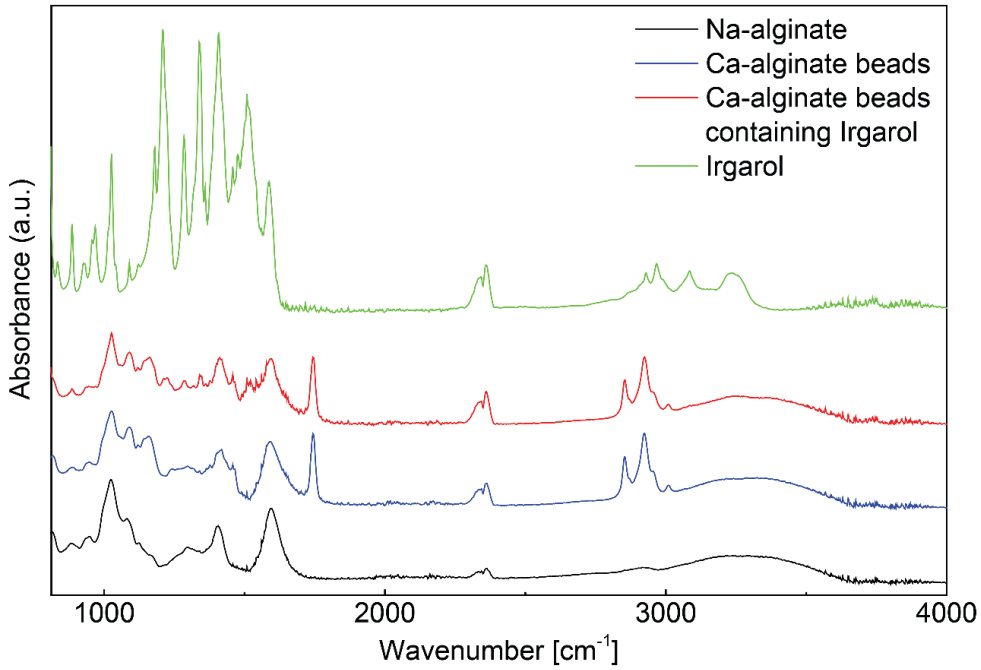

Fig. 6.21 ATR-FTIR spectra of Na-alginate crystals, synthesized Ca-alginate particles, Ca-alginate particles containing Irgarol, and Irgarol powder.

For the spectra of Ca-alginate particles, compared with the Na-alginate powder, the asymmetric stretching peak of $–COO^-$ at 1590 cm^{-1} is gradually replaced by a new absorption peak at 1624 cm^{-1}, which is caused by the interaction of Ca^{2+} with the $–COO^-$ groups of Na-alginate [32]. Further, the spectrum of the Ca-alginate beads with Irgarol shows more absorption

peaks than the Ca-alginate beads without Irgarol in the wavenumber ranging from 1552 cm^{-1} to 1198 cm^{-1}, suggesting the presence of Irgarol. The absorption peaks at 2925 cm^{-1} and 2854 cm^{-1} of the hydrogel samples were caused by the residual corn oil [33].

6.3.2 Release of encapsulated drug

6.3.2.1 Measurement of encapsulated drug samples

The rate of release of the encapsulated Irgarol from four kinds of microcapsules was studied. For simplicity, deionized water was used as the outer aqueous environment during the measurement; however, in the industrial field, the produced gel microcapsules will be distributed in wet coating paints for usage in air, aquatic, and freshwater environments. Four samples with three distinct encapsulated drug mass m_e were prepared by mixing two kinds of dispersion phase (Disperse #1 and #2) and two distinct collection durations (30 and 60 min) (**Table 6.5**). For each sample, three parallel tests were carried out to generate an average value and standard deviation. **Figure 6.22** shows the findings of time-lapse measurements of the release amount of encapsulated drug.

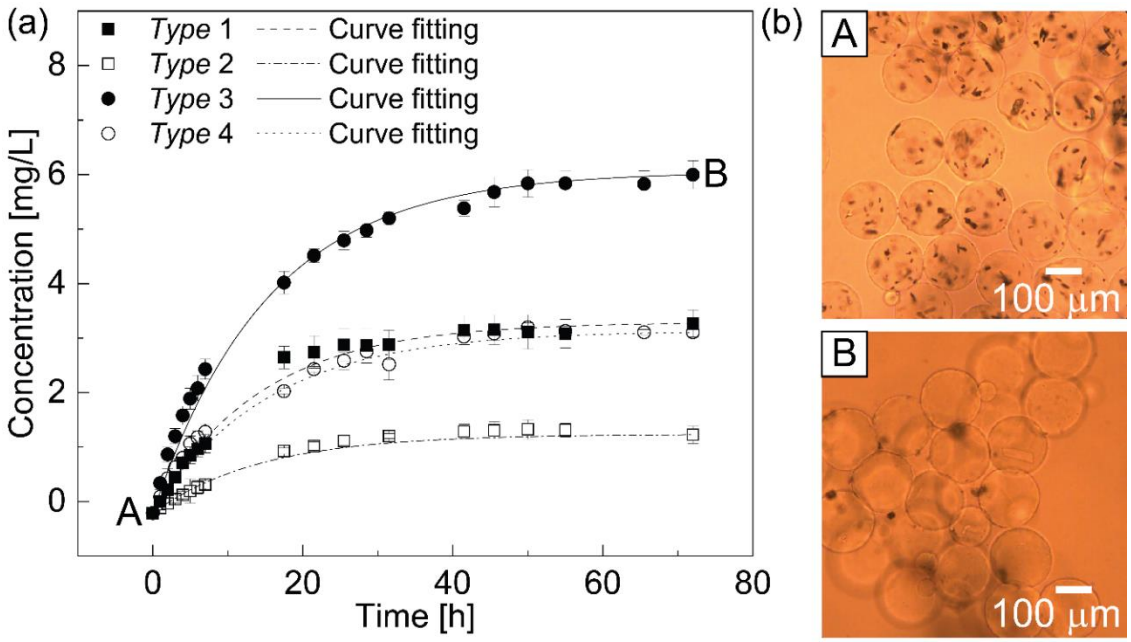

Fig. 6.22 Release mechanism of encapsulated drug Irgarol. (a) The concentration of released drug Irgarol from four kinds of microcapsules changes with time. (b) Images of gel microcapsules containing drug Irgarol in deionized water at (A) t = 0 h and (B) t = 72 h.

The released amount of encapsulated drug Irgarol in the tested solutions grew progressively over time. After 31 h, the concentration of encapsulated drug Irgarol in the solution using Type 2 microcapsules plateaued at about 1.3 mg/L. After 41 h, the concentration of encapsulated drug Irgarol in the solutions containing Type 1 and Type 4 gel microcapsules reached a plateau of about 3.2 mg/L. Finally, after 50 h, the concentration of encapsulated drug Irgarol in the tested solution using Type 3 microcapsules plateaued at about 6.0 mg/L. There was no significant deformation or deterioration of the gel beads throughout this experiment.

6.3.2.2 *Noyes-Whitney* equation

The *Noyes-Whitney* equation was used to fit a curve to the UV-Vis measurement findings to study the release speed and quantity of loaded drug in hydrogel microcapsules that liberated from the microcapsules [34]:

$$\frac{dm}{dt} = A\frac{D}{d}(C_s - C_b) \tag{6-5}$$

where dm/dt is the solute dissolution rate ($kg \cdot s^{-1}$), m is the mass of dissolved material (kg), t is the time (s), A is the surface area of the solute particle (m^2), D is the diffusion coefficient ($m \cdot s^{-1}$), which is related, in part, to the viscosity of the solvent, d is the thickness of the concentration gradient (m), C_s is the particle surface (saturation) concentration (kg) and C_b is the concentration in the bulk solvent/solution (kg). As a result, the simplified version of the Noyes-Whitney equation can be written as:

$$\frac{dC}{dt} = k(C_s - C) \tag{6-6}$$

where the dissolution rate is proportional to the difference of dissolved drug concentration C at time t from the solubility level C_s and k are the dissolution rate constant. The *Noyes-Whitney* equation is illustrated in **Fig. 6.23**.

The *Noyes-Whitney* equation gives a wealth of useful information on the dissolving process. When the differential type of *Noyes-Whitney* equation was solved, it will become:

$$\frac{dC}{dt} = k(C_s - C) \tag{6-7}$$

$$\frac{dC}{(C_s - C)} = k \cdot dt \tag{6-8}$$

$$-ln(C_s - C) = kt \tag{6-9}$$

As a result, if the initial condition is $C(0) = 0$, the solution of this equation will be:

$$C = C_s(1 - e^{-kt}) \quad (6\text{-}10)$$

In the measurements, the released amount m_r was utilized to indicate the total quantity of medication efficiently released from the gel particles, which is equal to:

$$m_r = V \cdot C_s, \quad (6\text{-}11)$$

where V denotes the total volume of the tested solution (0.05 L).

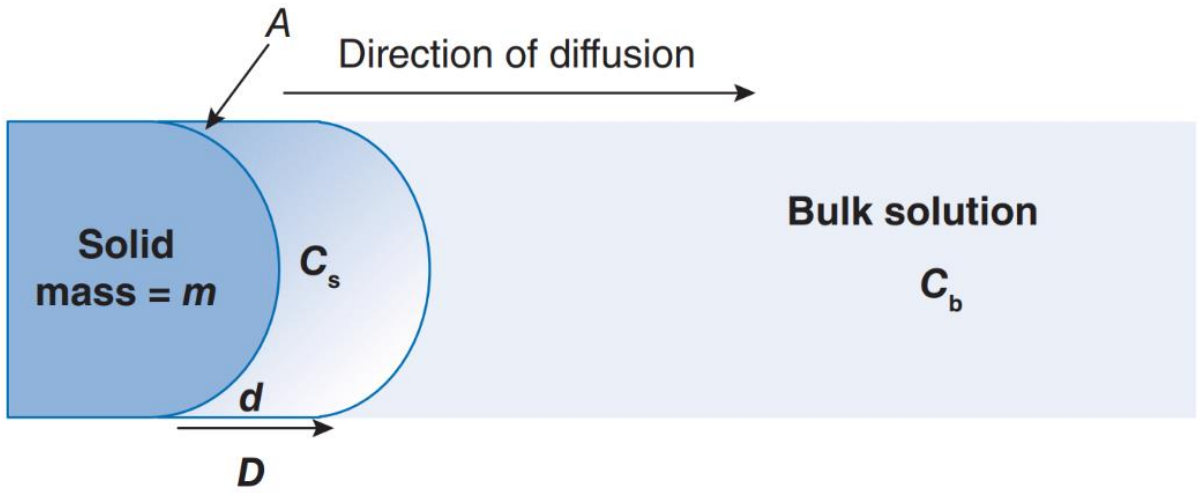

Fig. 6.23 Factors of *Noyes-Whitney* equation to describe the release speed [34].

6.3.2.3 Analysis of UV-Vis measurement

Table 6.6 displays the analysis of the curve fitting in **Fig. 6.19**. The time constant k of the release function of Type 1 hydrogel particles was 14.23. The quantity of drug released (m_r) by Type 1 hydrogel particles was 0.164 mg. Because the encapsulated quantity m_e was 0.250 mg, following filtering, 65.6% of the encapsulated drug left in the hydrogel particles. The k value for Type 2 hydrogel particles was 14.37, and the m_r value was 0.072 mg, while the m_e value was 0.125 mg. That means, after filtering, 57.6% of the drug was left in the hydrogel beads. The k value for Type 3 hydrogel particles was 15.39, the m_r value was 0.303 mg, and the m_e value was 0.500 mg, suggesting that 60.6% of the drug was kept prior to measurement. Finally, the time constant k of Type 4 hydrogel particles' release function was 15.31, the m_r value was 0.157 mg, and the m_e value was 0.250 mg. As a result, prior to measurement, 62.8% of the drug was retained in the microcapsule.

Table 6.6. Parameter study of drug release from hydrogel microparticles

	Type 1	Type 2	Type 3	Type 4
Function	$C = C_s(1 - e^{-x/k})$			
C_s	3.29	1.24	6.06	3.14
k	14.23	14.37	15.39	15.31
Released amount (m_r)	0.164 mg	0.072 mg	0.303 mg	0.157 mg
Encapsulated amount (m_e)	0.250 mg	0.125 mg	0.500 mg	0.250 mg
Encapsulation efficiency (EE)	65.6%	57.6%	60.6%	62.8%

The average value of the time constants *k* of the four fitting curves in the gel microcapsules only containing drugs inside (Types 1 to 4) was 14.83±0.53. The tiny fluctuation in the quantity of drug released at certain periods, as well as the small departure in the *k* value, demonstrated that the encapsulated drug's release rate was steady. Furthermore, using the *Noyes-Whitney* equation and the stable *k* value, the released quantity of the encapsulated drug may be readily predicted and regulated. During the measurement, the quantity of drugs effectively released from the hydrogel particles was lower than the quantity of encapsulated drugs in all four samples. The average drug encapsulation efficiency value was 61.7±2.9%. The drug quantity was presumably reduced due to dissolving and the loss of gel particles during the filtering process.

Figure 6.22b shows the microcapsules containing drugs inside in deionized water at 0 and 72 h. The drug crystals were initially spotted within the gel particles (0 h, **Fig. 6.22b-A**). Whereas, after 72 h, the majority of the drug crystals in the microcapsules had vanished (**Fig. 6.22b-B**), indicating that the drug had dissolved in the outer water environment.

For the realistic formulation of the coating matrix, the aqueous phase in both microcapsule suspension and wet coating paints should be eliminated as much as feasible during the practical manufacture of antifouling coating paints to minimize unwanted difficulties (such as heterogeneous distribution and agglomeration) [25]. The drug release rate from microcapsules to the outer dry coating layer is expected to be much slower than that of microparticles directly contacting with an aqueous environment in the study. A number of parameters, such as the thickness of the coating matrix, the diffusivity within the coating, and the fraction of aqueous phase in the coating matrix, would further influence the release of antifouling compounds from the coating layer to the outer aquatic environment [25]. The regulated release of biocides from a

coating prepared with the alginate microcapsules in this work would be accomplished by taking into account the penetration through both the microcapsule barrier and the dry coating matrix.

6.3.3 Comparison of encapsulated and non-encapsulated drugs

The drug's release rates with and without encapsulation were examined (**Fig. 6.24**). Two non-encapsulated drug samples were prepared with varying amounts of the drug. For each sample, three parallel tests were carried out to generate an average value and standard deviation. The drug concentration of the tested solution containing non-encapsulated drug sample 2 attained a plateau at about 3.2 mg/L after 7 h. After 25 h, the drug concentration in the tested solution containing non-encapsulated drug sample 1 plateaued at about 6.0 mg/L.

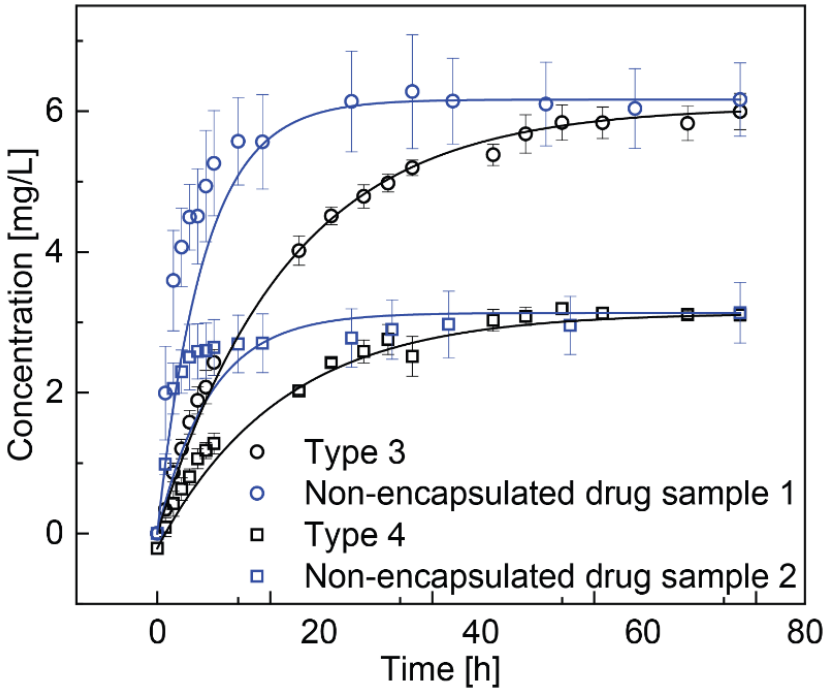

Fig. 6.24 Concentration of the dissolved non-encapsulated drug compared with the released drug from the obtained microcapsules changing with time.

Table 6.7 shows the analysis of the parameters of the curve fitting in **Fig. 6.24**. The *k* value of their release function was 5.73 for non-encapsulated drug sample 1, and the actual quantity of the released drug was 0.309 mg. The *k* value of their release function for non-encapsulated drug sample 2 was 6.54, and the actual quantity of medication released was 0.157 mg.

Table 6.7 Parameter analysis of the release of the encapsulated and non-encapsulated samples.

	Type 3	Non-encapsulated drug sample1	Type 4	Non-encapsulated drug sample 2
Function	$C = C_s(1 - e^{-x/k})$			
C_s	6.06	6.17	3.14	3.14
k	15.39	5.73	15.31	6.54
Released amount (m_r)	0.303 mg	0.309 mg	0.157 mg	0.157 mg
Encapsulated amount (m_e)	0.500 mg	0.500 mg	0.250 mg	0.250 mg
Encapsulation efficiency	60.6%	61.8%	62.8%	62.8%

There are two significant discrepancies in the data of non-encapsulated and encapsulated samples of the same saturation concentration (Type 3 and Type 4). First, the non-encapsulated drug sample released the drug quicker than the encapsulated one. After encapsulation, the average k value rose from 6.14 to 14.83. Because of its relatively wide pore size, Ca-alginate hydrogel materials are not a good substitute for the controlled release of small-molecular-weight chemicals [35]. As a consequence, persistent release from the microcapsules in the above experiments was most likely due to the partial coating of the crosslinking polymer structure on the drug particles, resulting in retarted disintegration. Second, the variation of the non-encapsulated drug's released quantity at each specific moment was greater than that of the encapsulated drug. This smaller release variation is thought to be due in part to the hydrophilic coats of hydrogel microbeads, which created a homogeneous touching surface of the hydrophobic Irgarol particles with the outer deionized water environment.

6.3.4 Microcapsules containing both cellulose fibers and drug

The antifouling drug-loaded hydrogel microcapsules are designed to be blended with wet coating paints. To prevent hydrogel microcapsules from breaking during the production process, cellulose fibers were mixed into the hydrogel beads to increase their mechanical robustness.

6.3.4.1 Droplet generated inside the microchannel

The cellulose fiber which is water-insoluble inside the hydrogel particles was encapsulated

to support the cross-linking structure especially when the particles are dried. The drug and fiber were homogeneously dispersed in the Na-alginate solution through the mechanical homogenizer at 30000 rpm for 5 minutes. The contents of the disperse phase are shown in **Table 6.2**. The photographs of disperse phase, obtained hydrogel beads are shown in **Fig. 6.25**.

Fig. 6.26 illustrates a normal procedure of generation of a droplet carrying both drug and fiber inside when the Q_c and Q_d were set at 2.0 and 0.1 ml/h respectively. Droplets of uniformed sizes were generated in the dripping mechanism at a generation frequency comparable to that of droplets laden with simply the Irgarol crystals (8 drops/s). The droplet generation frequency revealed that the created droplets filled with both the drug and cellulose fibers had a diameter of 188 μm. Following the primary droplet, satellite droplets with a diameter of 39 μm were sometimes formed (**Fig. 6.25**, t = 36 ms). The droplet flowed to the second junction and reacted the reactant W/O emulsion (**Fig. 6.25**, t = 117 ms).

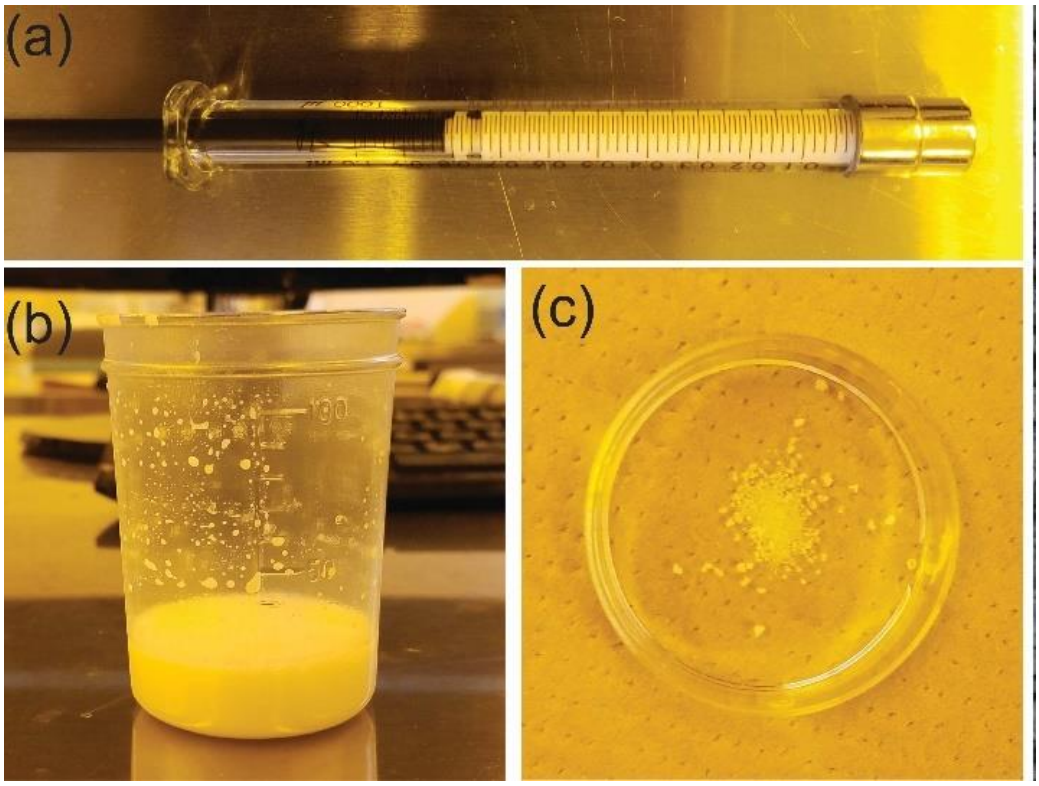

Fig. 6.25 The disperse phase in (a) a syringe and (b) a disposable cup. (c) The produced hydrogel particles in pure water.

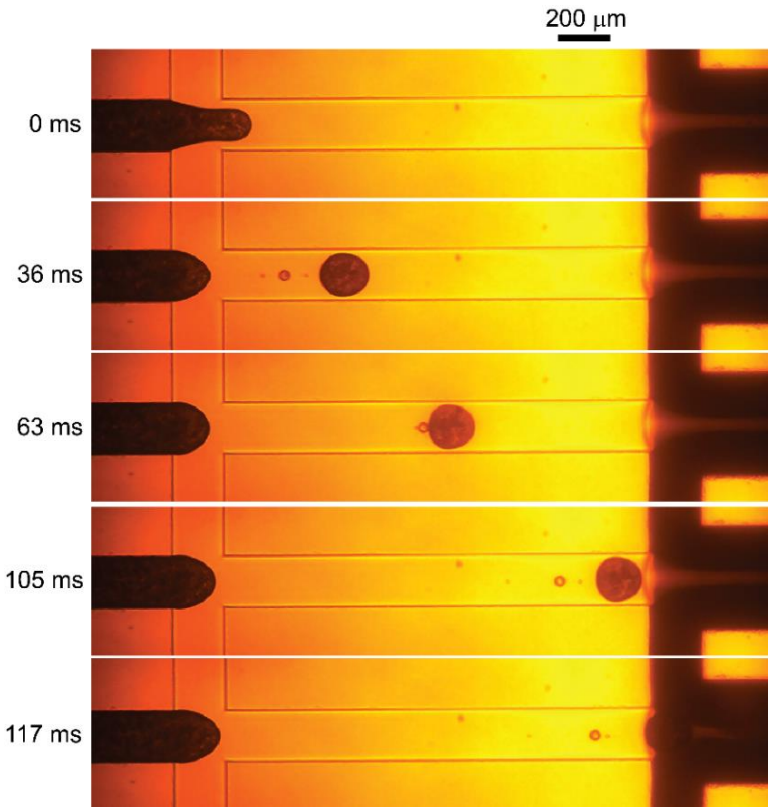

Fig. 6.26 Images of generation of a droplet carrying drug and fiber. The Q_d and Q_c were 0.1 and 2.0 mL/h respectively.

6.3.4.2 Generated hydrogels carrying both drugs and fibers

The Q_d, Q_c, and Q_e were set at 0.1, 2.0, and 20.0 mL/h respectively for the following experiments. The reactant W/O emulsion was prepared at the best proportion of aqueous solution (W = 0.26). The produced hydrogel particles were dispersed in pure water for observation and measurement. The obtained hydrogels had a black color under the microscope due to the encapsulated fiber (**Fig. 6.27a**). Besides, the obtained gel particles were highly spherical (average roundness ~0.93). The average diameter of gel particles was around 163 μm with a CV of 3.9% (**Fig. 6.27b**).

The SEM image of the dried aerogel particles, which contain both Irgarol crystals and fiber, indicates that the microparticles could keep their spherical morphology after the water phase totally evaporated. However, when compared to the surface of the dried gel beads that had just encapsulated drugs inside, the surfaces of the particles were creased and had a fiber-like formation (**Fig. 6.28**).

Compared with hydrogel particles made without fibers, the shapes of the microcapsules containing fibers had more deformation, their average roundness decreasing from 0.97 to 0.93, but the average diameter and CV value of obtained particles increased, increasing from 160 μm to 163 μm and from 3.5% to 3.9%, respectively. The presence of cellulose fibers caused these differences because the concentration of alginate molecules in a single droplet was reduced, resulting in inadequate gelation. These droplets with poor crosslinking have the potential to create hydrogel microparticles with bigger sizes and distorted morphologies (**Fig. 6.28**).

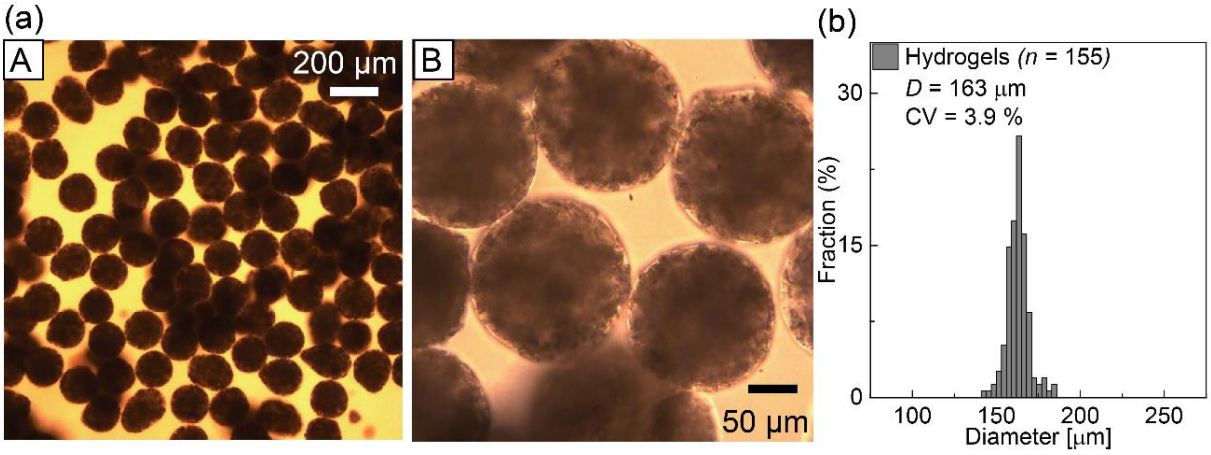

Fig. 6.27 Prepared hydrogel particles containing drugs and fibers. (a) Images of the hydrogel microparticles in deionized water were observed at different magnifications: (A) 10 × and (B) 40 ×. (b) Size distribution of the obtained hydrogel microbeads.

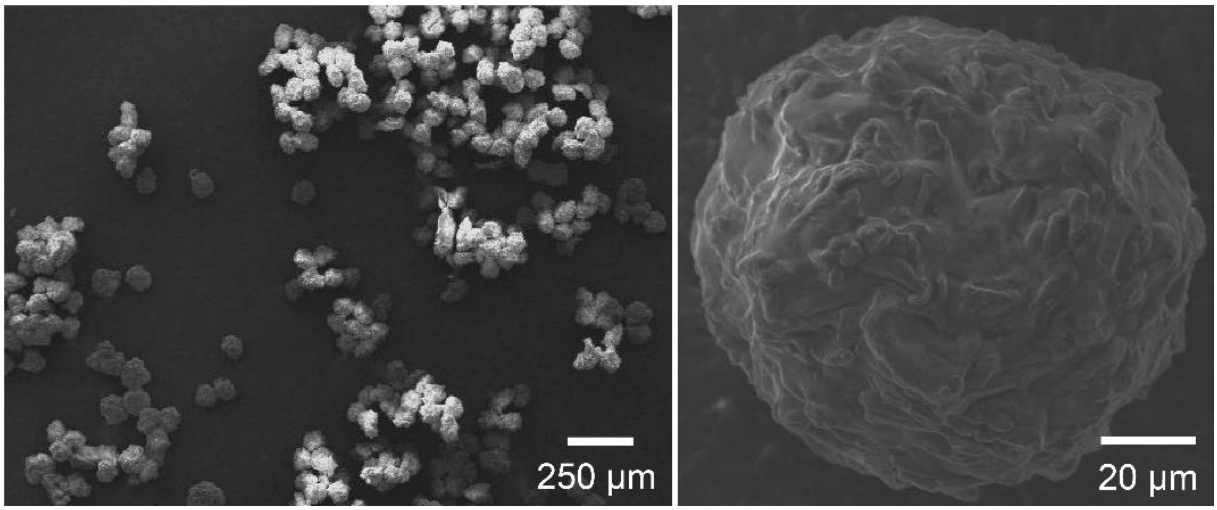

Fig. 6.28 SEM images of hydrogel particles with drug and fiber inside.

6.3.4.3 UV-Vis measurement

Figure 6.29 shows the released amount of encapsulated drugs at each moment assessed by UV-Vis spectroscopy in three paralleled tests. The released drug amount from the gel microcapsules containing both the Irgarol crystals and fibers steadily increased over time, reaching a plateau at about 6.0 mg/L (t = 50 h). **Table 6.8** shows the analysis of the curve fitting in **Fig. 6.29**. The k value of the release function of the gel microcapsules containing both the Irgarol crystals and cellulose fibers was 15.34, the m_r value was 0.309 mg, and the m_e value was 0.500 mg, indicating that almost 61.0% of the drug left in the capsules before measurement. The k value of the fitting curve (15.34) and encapsulation efficiencies (61.0%) of the hydrogel particles containing both drug crystals and fiber and the hydrogel particles loaded with drug only (Type 3) were similar, indicating that the encapsulation of the cellulose fiber had no effect on the release speed and efficiency.

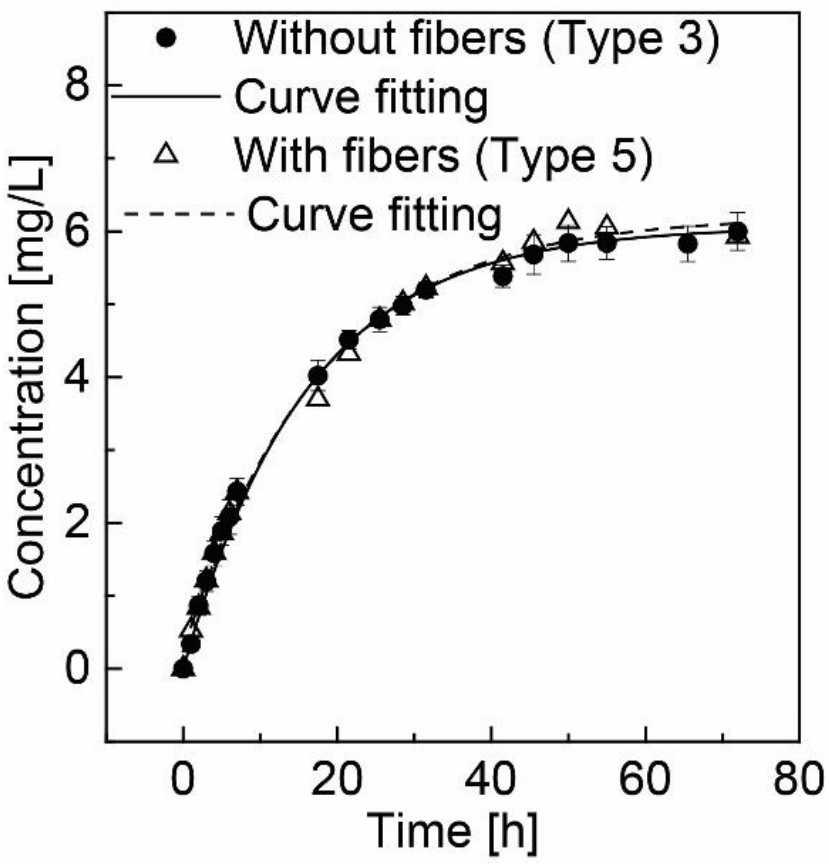

Fig. 6.29 The release of encapsulated drug from hydrogel microspheres with or without cellulose fibers changing with time.

Table 6.8 The drug release parameters of microcapsules carrying cellulose fibers.

	With Fiber (Type 5)
Function	$C = C_s(1 - e^{-x/k})$
C_s	6.17
k	15.34
Released amount (m_r)	0.309 mg
Encapsulated amount (m_e)	0.500 mg
Encapsulation efficiency (EE)	61.0%

6.3.4.4 Mechanical property of gel particles containing fiber

The cellulose fibers can largely enhance the mechanical properties of the gel microparticles. **Figure 6.30** depicts the proportion of deformation of two types of hydrogel layers under various external stresses. The following equation was used to express the distortion ratio of the layer of gel particles between the two glass slides:

$$D = \frac{\Delta T}{T_0} \times 100 \tag{6-12}$$

Where D is the deformation percentage, ΔT is the deformation amount, and T_0 is the original thickness of the prepared hydrogel layer. Three parallel experiments were performed for each sample to produce an average value and standard deviation.

The mean distortion ratio of the pure hydrogel layers and hydrogel layer containing fibers was 0.93% and 21.21%, respectively, when 0.74 N of force was added. The distortion of hydrogel layers grew when the force was raised to 1.52 N. The layer of microcapsules containing cellulose fibers had a mean distortion ratio of 18.52%, whereas the layer of pure gel particles had a distortion ratio of 37.27%. The deformation of measured hydrogel layers reached a peak when the force was raised to 11.76 N and 16.66 N that means hydrogel layers were overloaded. The layer of gel capsules containing cellulose fibers had a maximum deformation percentage of around 50%, whereas the layer of pure gel microbeads had a maximum deformation percentage of about 71%. The majority of the water phase in the hydrogel layers is supposed to be squeezed out under this condition.

By including cellulose fibers, the mechanical performance of the hydrogel microspheres might be increased. The increased mechanical strength has the ability to disperse the hydrogel

microparticles into a paint coating matrix, ensuring that the microspheres remain an unbroken structure with a sustained-release capability.

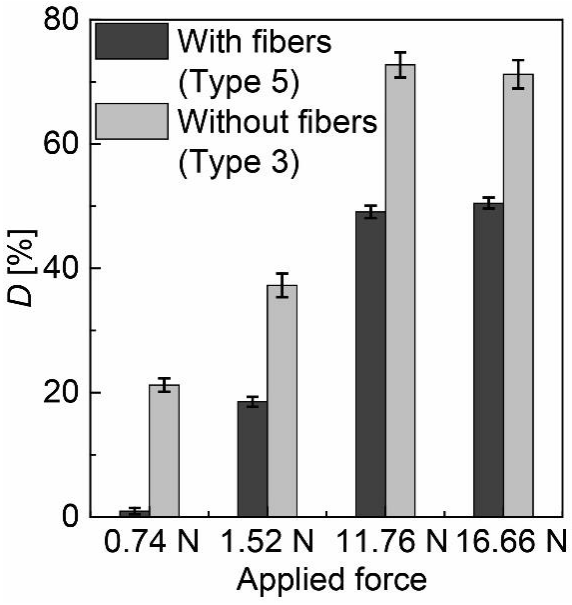

Fig. 6.30 Distortion ratio of the layer of pure gel particles and gel particles containing cellulose fibers

6.3.5 Antifouling functionality of encapsulated drug

Irgarol is well-known for its ability to limit photosynthesis in a wide variety of marine and aquatic plant species. The antifouling activity of the encapsulated medicine was proven in our investigation utilizing water grass (*Bacopa monnieri*) (**Fig. 6.31**). The tested grass samples were viable initially, with green leaves. Nevertheless, after 4 days of cultivation in a beaker containing Type 3 microcapsules, the majority of the leaves of the grass withered. Furthermore, the water in the beaker became dark and had a terrible odor, suggesting that the grass sample had practically died out. In contrast, the water grass in the reservoir containing Type 4 microcapsules was still alive with green leaves, even though the water in the glass reservoir had become muddy. There were no unusual smells detected. After 6 days of cultivation, the majority of the water grass in the beakers containing the antifouling drug wilted, and the water within the beaker got darker and smelled strongly of rottenness.

The antifouling agent impeded the photosynthesis of water grass, causing the samples to wither and decay. As a result, the encapsulated drug could be released from the gel

microcapsules over time and display antifouling properties. Furthermore, according to **Table 6.7**, the m_r value of Type 3 and Type 4 microcapsules was 0.303 mg and 0.157 mg, respectively. As a result of the greater drug concentration, the water grass with Type 3 microcapsules wilted quicker than the water grass with Type 4 microcapsules.

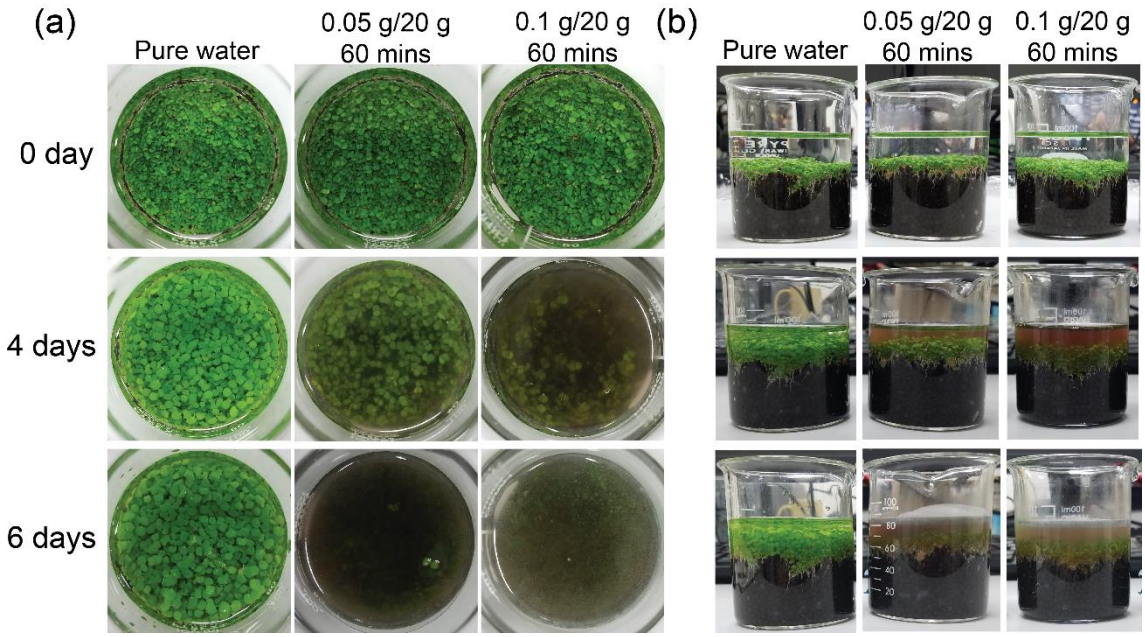

Fig. 6. 31 Images of cultured grass (*Bacopa monnieri*) from (a) top and (b) side views.

6.4 Conclusion

Section 6.1. Introduction

This section describes the background, previous researches, and objectives of this thesis.

Section 6.2. Materials and methods

This section describes the peripheral equipment, our microfluidic device, and the materials that used in our experiments.

Section 6.3. Results and discussion

In this section, a microfluidic approach was developed for the preparation of hydrophilic gel microcapsules of an antifouling chemicals. Hydrogel beads encapsulated with Irgarol had an average diameter of 160 μm, had a CV of 3.8%, a roundness of 0.97, and an encapsulation efficiency of 61.7±2.9%. Irgarol was used to encapsulate the beads. The use of UV-Vis spectroscopy revealed that a steady and regulated release was achieved by encapsulation. It has been shown that the incorporation of cellulose fiber with a biocide improves the mechanical properties of monodisperse microbeads with an average diameter of 163 μm, CV of 3.7%, and roundness of 0.93. In the last experiment, water grass was used to illustrate the antifouling effect of the medication released from the gel microcapsules (*B. monnieri*).

References

[1] Shirakawa, M.A.; Tavares, R.G.; Gaylarde, C.C.; Taqueda, M.E.S.; Loh, K.; John, V.M. Climate as the most important factor determining anti-fungal biocide performance in paint films. *Sci. Total Environ.* **2010**, *408*, 5878–5886.

[2] Viitanen, H.; Ritschkoff, A.C. Strategies-remediation: Coating and surface treatment of wood. In Fundamentals of mold growth in indoor environments and strategies for healthy living; Adan, O.C.G.; Samson, R.A., Ed.; Wageningen Academic Publisher: Netherlands, 2011; pp 463–484.

[3] Faÿ, F.; Gouessan, M.; Linossier, I.; Rehel, K. Additives for efficient biodegradable antifouling paints. *Int. J. Mol. Sci.* **2019**, *20*, 2–20.

[4] Kyei, S.K.; Darko, G.; Akaranta, O. Chemistry and application of emerging ecofriendly antifouling paints: a review. *J.Coat. Technol. Res.* **2020**, *17*, 315–332.

[5] Almeida, E.; Diamantino, T.C.; Sousa, O. Marine paints: The particular case of antifouling paints. *Prog. Org. Coatings* **2007**, *59*, 2–20.

[6] Bergek, J. Evaluation of biocide release from modified microcapsules. Ph. D. Thesis, Chalmers University of Technology, 2017.

[7] Watermann, B.; Eklund, B. Can the input of biocides and polymeric substances from the antifouling paints into the sea be reduced by the use of non-toxic hard coatings. *Mar. Pollut. Bull.* **2019**, *144*, 146–151.

[8] Kamtsikakis, A.; Kavetsou, E.; Chronaki, K.; Kiosidou, E.; Pavlatou, E.; Karana, A.; Papaspyrides, C.; Detsi, A.; Karantonis, A.; Vouyiouka, S. Encapsulation of antifouling organic biocides in poly(lactic acid) nanoparticles. *Bioengineering* **2017**, *4*, 81–99.

[9] Han, X.; Wu, J.; Zhang, X.; Shi, J.; Wei, J.; Yang, Y.; Wu, B.; Feng, Y. Special issue on advanced corrosion-resistance materials and emerging applications. The progress on antifouling organic coating: from biocide to biomimetic surface. *J. Mater. Sci. Technol.* **2021**, *61*, 46–62.

[10] Paijens, C.; Bressy, A.; Frere, B.; Moilleron, R. Biocide emissions from building materials during wet weather: identification of substances, mechanism of release and transfer to the aquatic environment. *Environ. Sci. Pollut. Res.* **2020**, *27*, 3768–3791.

[11] Trojer, M.A.; Movahedi, A.; Blanck, H.; Nydén, M. Imidazole and triazole coordination chemistry for antifouling coatings. *J. Chem.* **2013**, *2013*, 1–23.

[12] Urbanczyk, M.M.; Bester, K.; Borho, N.; Schoknecht, U.; Bollmann, U.E. Influence of pigments on phototransformation of biocides in paints. *J. Hazard. Mater.* **2019**, *364*, 125–133.

[13] Andersson, M. Imidazole containing polymers complexed with Cu^{2+} and Zn^{2+}: Materials properties and coordination chemistry as studied using vibrational spectroscopy, DSC and EPR. Ph. D. Thesis, Chalmers University of Technology, December 2009.

[14] Dahlberg, G.; Jansson, P.; Lindblad, L.; Arrhenius, A.; Backhaous, T.; Blanck, H.; Granmo, A.; Hilvarsson, A.; Nordstierna, L.; Nyden, M.; et al. Marine paint: final report; University of Gothenburg; Chalmers University of Technology: Gothenburg, February 2012.

[15] Kavouras, P.; Trompeta, A.F.; Larroze, S.; Maranhao, M.; Teixeira, T.; Beltri, M.; Koumoulos, E.P.; Charitidis, C.A. Correlation of mechanical properties with antifouling efficacy of coatings containing loaded microcapsules. *Prog. Org. Coat.* **2019**, *136*, 105249.

[16] Bergek, J.; Trojer, M.A.; Mok, A.; Nordstierna, L. Controlled release of microencapsulated 2-n-octyl-4-isothiazolin-3-one from coatings: Effect of microscopic and macroscopic pores. *Colloids Surfaces A Physicochem. Eng. Asp.* **2014**, *458*, 155–167.

[17] Zheng, L.; Lin, Y.; Wang, D.; Chen, J.; Yang, K.; Zheng, B.; Bai, W.; Jian, R.; Xu, Y. Facile one-pot synthesis of silver nanoparticles encapsulated in natural polymeric urushiol for marine antifouling. *RSC Adv*. **2020**, *10*, 13936–13943.

[18] Li, Y.; Wang, G.; Guo, Z.; Wang, P.; Wang, A. Preparation of microcapsules coating and the study of their bionic anti-fouling performance. *Materials* **2020**, *13*, 1669.

[19] Faÿ, F.; Linossier, I.; Legendre, G.; Vallée-Réhel, K. Micro-encapsulation and antifouling coatings: development of poly(lactic acid) microspheres containing bioactive molecules. *Macromol. Symp.* **2008**, *272*, 45–51.

[20] Pisani, E.; Ringard, C.; Nicolas, V.; Raphael, E.; Rosilio, V.; Moine, L.; Fattal, E.; Tsapis, N. Tuning microcapsules surface morphology using blends of homo- and copolymers of PLGA and PLGA-PEG. *Soft Matter* **2009**, *5*, 3054–3060.

[21] Long, Y.; Vincent, B.; York, D.; Zhang, Z.; Preece, J.A. Organic-inorganic double shell composite microcapsules. *Chem. Commun.* **2010**, *46*, 1718–1720.

[22] Andersson, M.; Mohamed, A.; Eastoe, J. A highly hydrophobic anionic surfactant at oil-water, water-polymer and oil-polymer interfaces: Implications for spreading coefficients, polymer interactions and microencapsulation via internal phase separation. *Colloid and Surfaces A: Physicochem. Eng. Aspects* **2013**, *436*, 1048–1059.

[23] Nordstierna, L.; Movahedi, A.; Nydén, M. New route for microcapsule synthesis. *J. Dispers. Sci. Technol.* **2011**, *32*, 310–311.

[24] Lavergne, F.M.; Cot, D.; Ganachaud, F. Polymer microcapsules with "foamed" membranes. *Langmuir* **2007**, *23*, 6744–6753.

[25] Trojer, M.A.; Nordstierna, L.; Bergek, J.; Blanck, H.; Holmberg, K.; Nyden, M. Use of microcapsules as controlled release devices for coatings. *Adv. Colloid Interface Sci.* **2015**, *222*, 18–43.

[26] Cunningham, M.F.; Campbell, J.D.; Fu, Z.; Bohling, J.; Leroux, J.G.; Mabee, W.; Robert, T. Future green chemistry and sustainability needs in polymeric coatings. *Green Chem.* **2019**, *21*, 4919–4926.

[27] Liu, Y. and Nisisako, T. Microfluidic encapsulation of hydrophobic antifouling biocides in calcium alginate hydrogels for controllable release. ACS Omega **2020**, *5*, 25695-25703.

[28] Rehman, S.W.U.; Wang, H.; Yao, W.; Deantes-Espinosa, V.M.; Wang, B.; Huang, J.; Deng, S.; Yu, G.; Wang, Y. Ozonation of the algaecide irgarol: kinetics, transformation products, and toxicity. *Chemosphere* **2019**, *236*, 124374.

[29] Zhang, A.Q.; Zhou, G.; Lam, M.H.W.; Leung, K.M.Y. Toxicities of the degraded mixture of Irgarol 1051 to marine organisms. *Chemosphere* **2019**, *225*, 565-573.

[30] Wikipedia. Cellulose fiber. https://en.wikipedia.org/wiki/Cellulose_fiber (accessed Dec 27, 2021).

[31] Ocean Optics. Modular Spectroscopy Setups for Absorbance, Reflection, Emission & More. https://oceanoptics.com/knowledge-support/example-setups/ (accessed Jan 19, 2019).

[32] Saarai, A.; Kasparkova, V.; Sedlacek, T.; Saha, P. On the development and characterization of crosslinked sodium alginate/gelatine hydrogels. *J. Mech. Behav.*

Biomed. **2013**, *18*, 152–166.

[33] Setyaningrum, D.L.; Riyanto, S.; Rohman, A. Analysis of corn and soybean oils in red fruit oil using FTIR spectroscopy in combination with partial least square. *Int. Food Res. J.* **2013**, *20*, 1977–1981.

[34] Noyes, A.; Whitney, W. The rate of solution of solid substances in their own solutions. *J. Am. Chem. Soc.* **1897**, *19*, 930-934.

[35] Utech, S.; Prodanovic, R.; Mao, A.S.; Ostafe, R.; Mooney, D.J.; Weitz, D.A. Microfluidic generation of monodisperse, structurally homogeneous alginate microgels for cell encapsulation and 3D cell culture. *Adv. Healthc. Mater.* **2015**, *4*, 1628–1633.

Chapter 7

Conclusion and outlook

7.1 Conclusion

Chapter 1 Introduction

This chapter briefly introduces the definition and background of hydrogel materials. The conventional and previous microfluidic methods for preparing hydrogel particles are compared and discussed. Then the objectives of this thesis and layout from chapter 2 to chapter 6 are described.

Chapter 2 Microfluidic emulsion-based synthesis of calcium-alginate hydrogel particles

A novel microfluidic external emulsion-based gelation using $CaCl_2$ emulsion as the reactant is reported for preparing highly spherical Ca-alginate hydrogel particles. The quartz glass microfluidic chip consists of two cross-junctions connected serially was used. The primary conclusions are summarized as follows:

- Roundness

1). The concentration of surfactant (SY-Glyster) in the $CaCl_2$ emulsion phase influenced the roundness of obtained hydrogel beads. The best concentration of surfactant in this condition was 0.1wt%.

2). The fraction of the aqueous phase in the reactant $CaCl_2$ emulsion is important. The best fraction of the aqueous phase was 0.26.

3). The flow rate of continuous phase (corn oil) effects. A high flow rate of the continuous phase ($\geq$ 1.5 mL/h) will result in hydrogels with bullet shape.

- Sizes

By controlling the relationship between the flow rate of disperse phase and continuous phase, the sizes of obtained hydrogel beads could be adjusted.

It is concluded that the homogeneous spatial distribution of $CaCl_2$ emulsions around precursor Na-alginate droplets is essential to obtain highly spherical hydrogels. By optimizing

the parameters above, monodisperse hydrogels with a diameter of 147–176 μm and roundness of 0.90–0.96 could be produced.

Chapter 3 Functional Janus calcium-alginate hydrogel

Unpublished contents

Chapter 4 Surface coating on calcium-alginate hydrogel particles

Based on **Chapter 2**, the microfluidic external emulsion-based gelation was used for the production of highly spherical Ca-alginate hydrogels with corresponding surface coatings. The primary conclusions are summarized as follows:

1). Highly spherical Ca-alginate hydrogels that had whole Fe3O4 nanoparticles coating with an average diameter of 160 μm, a CV value of 3.8%, and a roundness around 0.90 were prepared. The manipulation of obtained particles under the exterior magnetic field was also demonstrated.

2). Ca-alginate hydrogel beads that had whole fluorescent polystyrene microspheres coating with an average diameter of 165 μm, a CV value of 3.4%, and a roundness around 0.95 were generated. It is confirmed that the obtained hydrogels had a clear fluorescence under the fluorescent microscopy.

3). The Ca-alginate microgels that had both fluorescent and magnetic coating with an average diameter of 156 μm, a CV value of 2.5%, and roundness around 0.97 were synthesized.

The prepared hydrogels with different coatings might have great potential in applications like drug delivery and release, high-resolution imaging, sorting, and separation.

Chapter 5 Mass production of calcium-alginate hydrogel particles

Unpublished contents

Chapter 6 Microencapsulation of hydrophobic antifouling biocide

As a practical application of highly spherical Ca-alginate hydrogel beads in **Chapter 2**, the environment-friendly hydrophilic encapsulation of a hydrophobic antifouling biocide in hydrogels by applying a microfluidic emulsion-based external gelation was demonstrated. The primary conclusions are summarized as follows:

1). Irgarol-encapsulated monodisperse hydrogel beads with an average diameter of 160 μm, CV of 3.8%, the roundness of 0.97 were prepared, and the encapsulation efficiency of 61.7 ± 2.9%.

2). Cellulose fiber incorporated with the biocide enhanced the mechanical strength of the monodisperse microcapsules having an average diameter of 163 μm, CV of 3.7%, and roundness of 0.93.

3). The encapsulated antifouling biocide (Irgarol 1071) had a stable and controlled release in an aqueous environment both with or without cellulose fiber inside the hydrogel microcapsule.

4). The antifouling effect of the drug released from the hydrogel beads was demonstrated with water grass (*B. monnieri*).

7.2 Outlook

■ **Size and morphology of alginate hydrogel**

(1) Nano-sized calcium chloride ($CaCl_2$) emulsion

The $CaCl_2$ emulsion prepared using a mechanical homogenizer in this thesis had an average diameter of around 2 μm. The size of the reactant emulsion can be further decreased if the homogenizer with a much higher rotating speed is used. In addition, nano-sized $CaCl_2$ emulsion can be prepared by the piezoelectric chip according to the previous research [1]. The piezoelectric chip could be integrated with the microchannels in the same microfluidic module. In this situation, no surfactant is needed in the experiment.

Homogeneous spatial distribution of $CaCl_2$ emulsions around precursor Na-alginate droplets is essential to obtain highly spherical hydrogels. As a result, the nano-sized $CaCl_2$ emulsion provides a possible method to synthesize highly spherical alginate-based hydrogels with much smaller sizes. For example, highly spherical hydrogel particles with a diameter around 20 μm that near the cell sizes may have great potentials in the biology or biomedical field.

(2) Alginate hydrogels with controllable shapes

Different shapes of alginate-based hydrogels like hemispherical shape or blood cells shape could also be synthesized based on this in-situ external gelation method. These hydrogel particles with specific shapes have great potentials in the applications like drug delivery or cells encapsulation. For instance, hydrogel particles with blood cell shape can stay in the blood vessel 5 times longer than the normal spherical hydrogel particles. That means the drug can acquire more release time inside the human blood vessel if these particles are used as the carrier [2].

The primary difficulty will be the choice of aqueous materials combined with alginate. The proper materials should be phase-separated with an alginate aqueous solution. In the meanwhile, it should have suitable viscosity that can form droplets together with the alginate phase.

(3) Core-shell shape alginate microcapsules

By properly designing the microchannel, Ca-alginate microcapsules with controllable shell thickness could be fabricated from core-shell alginate droplets via the microfluidic external emulsion-based gelation presented in this thesis. Efficient production of monodispersed alginate microcapsule with an aqueous liquid core has great potentials in a miniaturized 3D culture of cells which could promote their proliferation and aggregation [3].

(4) Mass production

As described in **Chapter 5**, a novel microfluidic module was designed to prepare highly spherical Ca-alginate hydrogel particles and achieve a maximum production rate of 373 s^{-1}. The paralleled microchannels were from 16 to 128. However, the number of microchannels could be further increased (e.g. 256 or 512) to largely improve the production efficiency. Besides, the geometry of microchannels could be also adjusted for the mass production of alginate microparticles with specific shapes, such as Janus hydrogels or core-shell hydrogels.

(5) Improvement of controllable release ability

The modification of Ca-alginate hydrogel beads like the surface coating (e.g. chitosan or pectin) and integration with other chemicals (e.g. cyclodextrin) will be helpful to achieve a better-controlled release ability. By properly designing the microfluidic geometry and utilizing the external emulsion-based gelation, different kinds of alginate-based microcapsules could be prepared to satisfy the specific requirements.

■ **Other hydrogels synthesized by external emulsion-based gelation**

This microfluidic external emulsion-based gelation is also possible to be used for producing other kinds of hydrogel microparticles instead of Ca-alginate. The key point is to prepare a fine water-in-oil reactant emulsion containing homogeneous small droplets. The example of hydrogel materials are as follows:

(1) Phytic acid(PA)-alginate hydrogel

The alginate aqueous solution could form alginate hydrogel when it contacts with PA aqueous solution [4]. Based on this, the PA-alginate microparticles could be prepared using the microfluidic device used in this thesis. The PA-alginate hydrogel has better mechanical

properties and a more stable cross-linking structure than the Ca-alginate hydrogel. To the best of our knowledge, the generation of PA-alginate hydrogel microbeads has not been reported yet.

(2) Condensed-protein materials

According to the previous research, an aqueous protein solution could form water-rich but water-segregated, gelled liquid materials when it contacts with anionic and cationic surfactants that contain a hydrophobic alkyl chain and polyethylene glycol (PEG) [5]. This microfluidic device and gelation strategy could be utilized to prepare these gelled-like protein microparticles by reaction between aqueous protein droplets and surfactants containing water-in-oil emulsion.

■ More applications of alginate hydrogels

(1) Controlled release of alginate microcapsules

(A) Formulation of antifouling coating paints

In **Chapter 6**, Ca-alginate microcapsules containing hydrophobic antifouling biocides were prepared. This application could be further researched by mixing the Ca-alginate microcapsules into water-based and/or solvent-based paints with the alginate capsules and to evaluate the release rates of the biocide from the coated surfaces.

(B) Release in a different environment

In **Chapter 6**, the release mechanism of alginate microcapsules in pure water was investigated. However, for practical use, the investigation of the release mechanism of alginate microcapsules in a more complicated environment is important. For example, the different pH values would largely affect the size and shape of alginate hydrogels and further influence the release of carried drugs. Also, the release of encapsulated drugs in seawater or the human body will be different from their release in pure water.

(2) Biological research

In **Chapters 3 and 5**, mammal cells was simply encapsulated in the alginate hydrogel beads. Further investigation of cell culturing in alginate beads is meaningful. Other biological researches such as tissue engineering and the comparison of hydrogels prepared by other methods and the highly spherical alginate hydrogels in cells researches are also interesting

topics that could demonstrate the superiorities of the Ca-alginate beads prepared in this thesis.

References

[1] Kanda, T.; Harada, T.; Tominaga, Y.; Suzumori, K.; Ono, T.; Iwabuchi, S.; Ito, K.; Ogawara, K.; Higaki, K. and Yoshizawa, Y. Design and evaluation of emulsion generation device using ultrasonic vibration and microchannel. *Jpn. J. Appl. Phys.* **2011,** 50, 07HE24.

[2] Merkel, T.J.; Jones, S.W.; Herlihy, K.P.; Kersey, F.R.; Shields, A.R. Napier, M.; Luft, J.C.; Wu, H.; Zamboni, W.C.; Wang, A.Z.; Bear, J.E. and DeSimone, J.M. Using mechanobiological mimicry of red blood cells to extend circulation times of hydrogel microparticles. *PNAS* **2011**, 108, 586–591.

[3] Agarwal, P.; Zhao, S.; Bielecki, P.; Rao, W.; Choi, J.K.; Zhao, Y.; Yu, J.; Zhang, W. and He, X. One-step microfluidic generation of pre-hatching embryo-like core-shell microparticles for miniaturized 3D culture of pluripotent stem cells. *Lab Chip* **2013**, 13, 4525–4533.

[4] Nita, L.E.; Chiriac, A.P.; Ghilan, A.; Rusu, A.G.; Tudorachi, N. and Timpu, D. Alginate enriched with phytic acid for hydrogels preparation. *Int. J. Biol. Macromol.* **2021**, 181, 561–571.

[5] Nojima, T. and Iyoda, T. Water-rich fluid material containing orderly condensed proteins. *Angew. Chem. Int. Ed.* **2017**, 56, 1308–1312.

Appendix

A.1 Microfabrication

A.1.1 Quartz glass chip

(1) Fabrication

Microgrooves and through-holes were fabricated on a quartz glass chip (15 mm × 15 mm, 2 mm thick) using mounted wheels of three different diameters 0.2 mm, 0.4 mm, and 1 mm (AAR72, AAR07, and AAR29, FSK, Japan, **Fig. A.1**) through computer numerical control (CNC) machining (LB2000 EXII, OKUMA, Japan, **Fig. A.2**). The fabricated microgrooves were sealed by fusion bonding with another planer quartz glass piece of the same size. The parameters of the microfabrication process of CNC machining are shown in **Table A.1**.

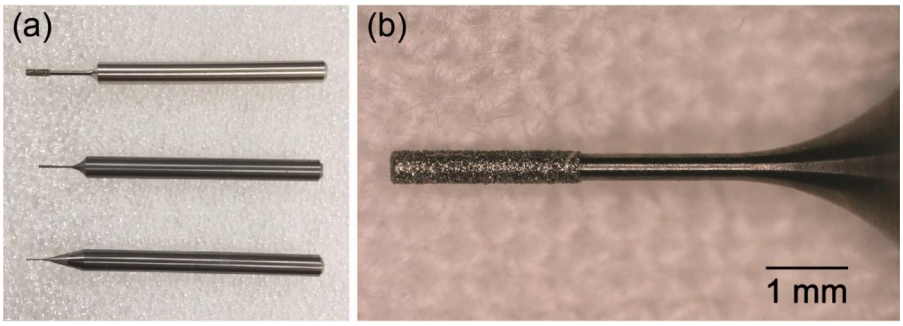

Fig. A.1 (a) Mounted wheels with diameters of 0.2 mm, 0.4 mm, and 1 mm. (b) Mounted wheel with a diameter of 0.4 mm.

Fig. A.2 The computer numerical control machining (LB2000 EXII, OKUMA, Japan).

Table A.1 The fabrication data of CNC machining.

Type (mm)	Wheel type (mm)	Rotation speed (rpm)	Feed speed (mm/min)
Hole (diameter 0.5)	Diameter 1.0	20000	1
Channel (depth 0.4 and width 0.4)	Diameter 0.4	40000	10
Channel (depth 0.4 and width 0.2)	Diameter 0.2	40000	10
Channel (depth 0.2 and width 0.2)	Diameter 0.2	40000	10

(2) Surface modification

The microfluidic chip underwent surface modification that changed the glass surface from hydrophilic to hydrophobic for generating W/O droplets. First, a 2 M aqueous solution of sodium hydroxide (NaOH) was infused into the dried microchannel for washing. After rinsing the residual NaOH solution away with pure water, the channel was flushed with toluene. Next, a 1 wt% octadecyl trichlorosilane (ODS, Shin-Etsu Chemical, Japan) in toluene was used as a surface-modifying agent and infused through the five inlets of the microfluidic chip at a flow rate of 2 μl/min for 1.5 hours. Then, pure toluene was infused again for removing the residual ODS inside channels. Finally, the channels were washed with acetone and ethanol repeatedly.

A.1.2 Polydimethylsiloxane (PDMS) chip

Up to now, manifold manufacturing technologies have been utilized to fabricate micro/nanostructures, such as wet etching, dry etching, laser beam machining, mechanical machining, and soft lithography. However, these technologies have their specific advantages in processing different materials (e.g. glass, silicon wafer, and polymers)

In this thesis, soft lithography technology was used to fabricate the PDMS chip [1]. Soft lithography is a family of techniques for fabricating or replicating structures using “elastomeric stamps, molds, and conformable photomasks”. Soft lithography is generally used to construct features measured on the micrometer to nanometer scale.

(1) Fabrication of SU-8 mold

The schematic illustration of the SU-8 mold fabrication is shown in **Fig. A.3**.

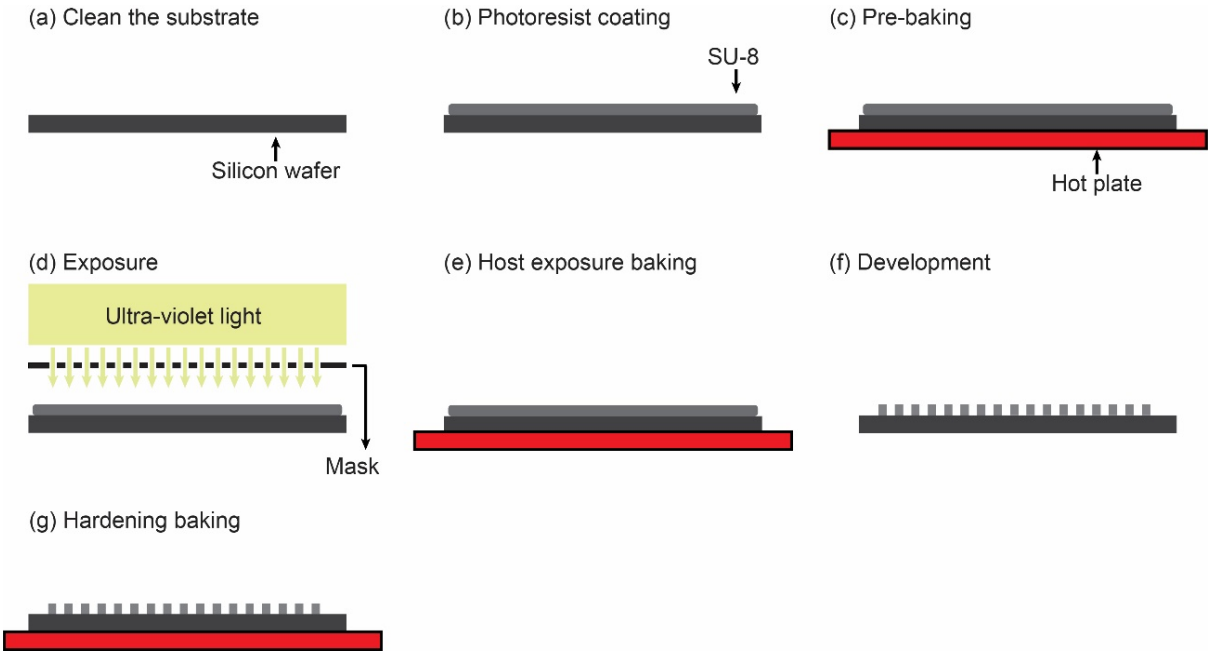

Fig. A.3. Schematic illustration of SU-8 mold fabrication.

(a) Substrate cleaning

Wash the silicon wafer with acetone, ethanol, and pure water sequentially in the ultrasonic machine (2510, Branson, Kanagawa, Japan) for 5 minutes. After that, dry the wafer on the hot plate.

(b) Photoresist coating

The negative photoresist SU8-3050 (Nippon Chemical Industrial, Tokyo, Japan) was homogeneously coated on the silicon wafer by spin coater (1H-D7, Mikasa, Hiroshima, Japan). The parameters of spin coating are shown in **Table A.2**. For a better adhesion between the photo-mask and silicon wafer during the exposure process, the photoresist around the wafer edge should be removed.

(c) Pre-baking

To evaporate the extra solution, the silicon wafer is put on the hot baker at 65 ℃ for around 5 mins and 95 ℃ for around 40 mins. After that, the silicon wafer should be cooled down to room temperature before the UV exposure.

(d) Exposure

The silicon wafer coated with SU-8 photoresist and the film mask (thickness: 0.175 mm; resolution: 0.001 mm; Unno Giken, Tokyo, Japan) taped on a glass plate are fixed on the mask aligner (MA-10, Misaka, Hiroshima, Japan) for the UV exposure with total energy around 150 mJ.

(e) Post-exposure baking

The silicon wafer should be put on the hot baker at 65 ℃ for around 1 min and 95 ℃ for around 15 mins after UV exposure.

(f) Development

For the pattern development, the silicon wafer is soaked in the SU-8 developer (Nippon Chemical Industrial, Tokyo, Japan) and waved on the mechanical shaker (Wave-SI slim, Taitec, Saitama, Japan) for 40 mins. The isopropyl alcohol is used to clean the extra SU-8 developer on the wafer.

(g) Hardening baking

Finally, the wafer is put on the hot baker at 150 ℃ for around 10 mins for hardening.

Table A.2 Parameters of the spin coating

	Rotation speed	Time
First	500 rpm	10 s
Second	1400 rpm	30 s

(2) Fabrication of PDMS microchannel

The schematic illustration of the PDMS microchannels fabrication is shown in **Fig. A.4**.

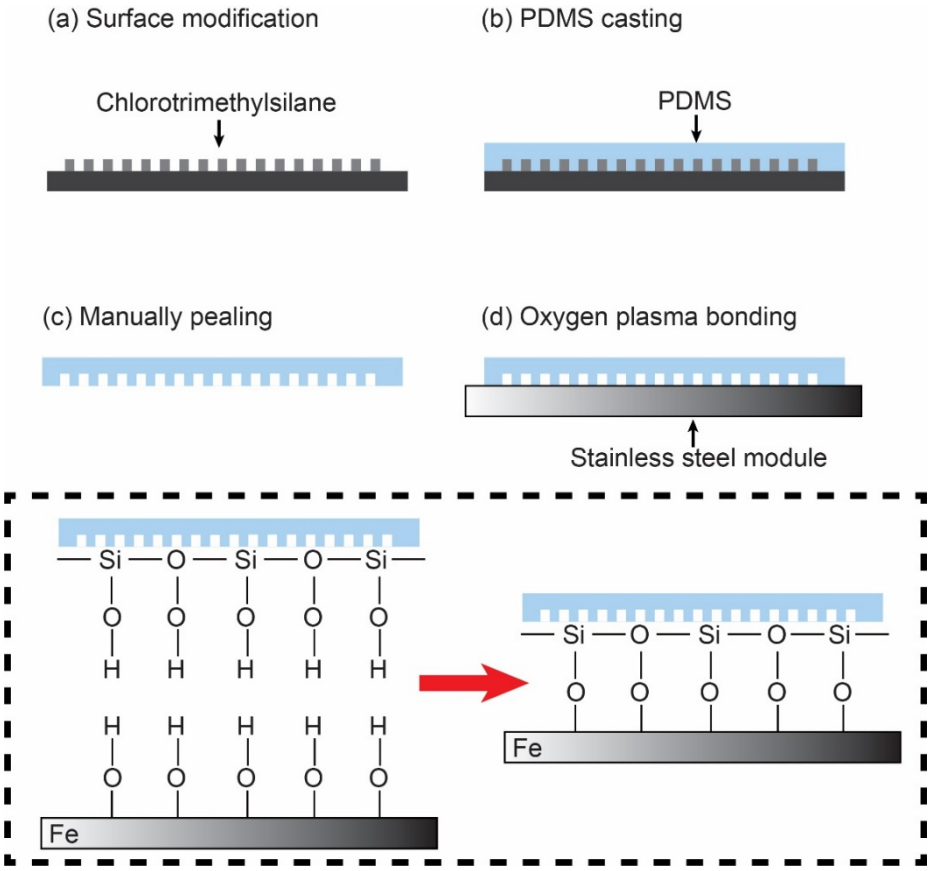

Fig. A.4 The schematic illustration of the PDMS microchannels fabrication.

(a) Surface modification

For the hydrophobic modification of the prepared SU-8 mold surface. The silicon wafer is put in a glass petri dish, and 0.5 mL of chlorotrimethylsilane (Shin-Etsu Chemical, Tokyo, Japan) is dropped around the wafer. The silicon wafer is put at room temperature for 10 mins and on the hot plate at 120 ℃ for 5 mins.

(b) PDMS casting

The PDMS base liquid (SILPOT 184 Silicon Elastomer Base, DuPont Toray Specialty Materials K.K., Tokyo, Japan) and hardening agent (SILPOT 184 Silicon Elastomer Curing agent, DuPont Toray Specialty Materials K.K.) are mixed at the ratio of 10:1 w/w. The mixture is put inside the vacuum desiccator (MVD-100, AS-ONE, Osaka, Japan) to remove the bubbles. After that, the PDMS mixture is poured onto the SU-8 mold and put on the hot plate at 80 ℃ for 1 hour for hardening.

(c) Manually pealing

The hard PDMS layer can be manually peeled from the SU-8 mold. The useless part (containing no micro-patterns) could be easily cut out.

(d) Oxygen plasma bonding

The oxygen plasma treatment is used to achieve an irreversible bonding between the PDMS chip and stainless-steel module (SUS304). The PDMS chip and stainless-steel module are firstly treated by the oxygen plasma using the plasma equipment (BP-1, Samco Inc., Kyoto, Japan). After that, the PDMS chip is attached to the stainless-steel module and heated on the hot plate at 110 ℃ for 12 hours. The condition of plasma treatment is shown in **Table A.3**.

Table A.3 The condition of plasma treatment

	Oxygen flow rate	Power	Chamber pressure	Time
Value	20 ccm	20 W	1000 mTorr	30 s

A.2 Cell culturing and encapsulation

A.2.1 Cell preparation

A hypotriploid human cell line, HEK 293, which derived from Riken BRC (Ibaraki, Japan), were used in **Chapter 3** and **5** (**Fig. A.5**). The thawed primary cells were maintained in Dulbecco's Modified Eagle Medium (DMEM, Wako Pure Chemical Industries, Japan) supplemented with 10% (v/v) fetal bovine serum (10270, Gibco, Thermo Fisher Scientific, USA.) and 1% penicillin-streptomycin solution (X100, Wako Pure Chemical Industries, Japan), using disposable cell culture flask (Nunc EasYFlask, 75 cm^2, Thermo Fisher Scientific, USA.) coated with 0.1% (w/v) gelatin solution (Wako Pure Chemical Industries, Japan). Then the cells were stored in a CO_2 incubator (E-22, AS ONE, Osaka, Japan) at 37℃ under a 5% CO_2 atmosphere.

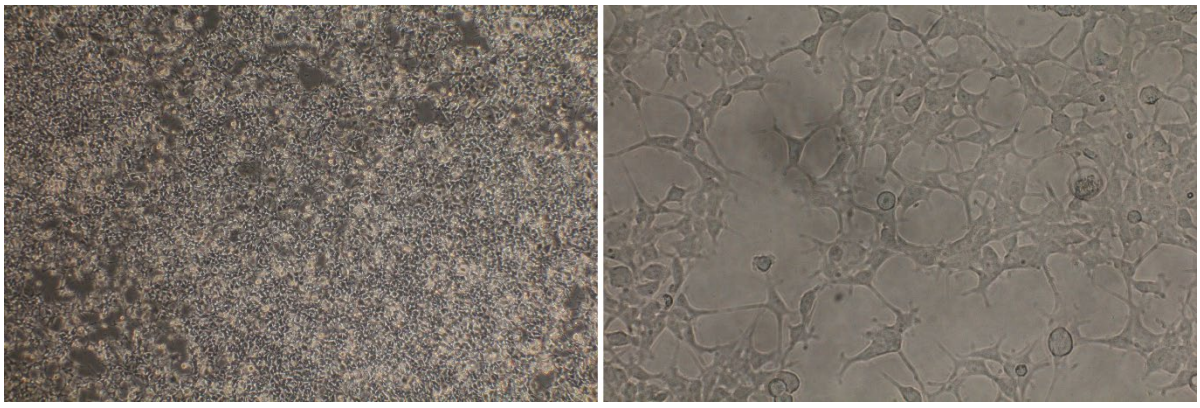

Fig. A.5 Microphotographs of human cell line: HEK 293 at different magnification.

A.2.2 Cell encapsulation

Before encapsulation, the living cells were stained by calcein-AM (excitation/emission wavelength: 490/515 nm, Dojindo, Japan) for fluorescence imaging (**Fig. A.6**). Firstly, 5 μL of the calcein-AM solution was uniformly dissolved in 5 mL of phosphate-buffered saline (PBS) as the staining mixture. Then the cells were detached from the culturing flask using by adding 0.25% (w/v) trypsin-ethylenediaminetetraacetic acid (trypsin-EDTA). The cells were homogeneously distributed in 0.70 ml of PBS plus 0.35 ml of prepared staining mixture and further stored in CO_2 incubator at 37℃ under a 5% CO_2 atmosphere for 15 mins (Around 2.5 ×

10^6 cells/mL in **Chapter 3** and 5.0×10^6 cells/mL in **Chapter 5**).

Afterward, about 1 mL of above cells suspension was added to Na-alginate solution with 150 mM sodium chloride (NaCl) to make the final concentration of Na-alginate at 3wt% and concentration of cells at 2.5×10^5 cells/mL in **Chapter 3** and 5.0×10^5 cells/mL in **Chapter 5** respectively. For the filtration of gel beads, hexadecane and deionized water were added in turn to wash out the $CaCl_2$ emulsion. The obtained Ca-alginate particles encapsulating cells were collected in a petri dish with PBS solution for observation.

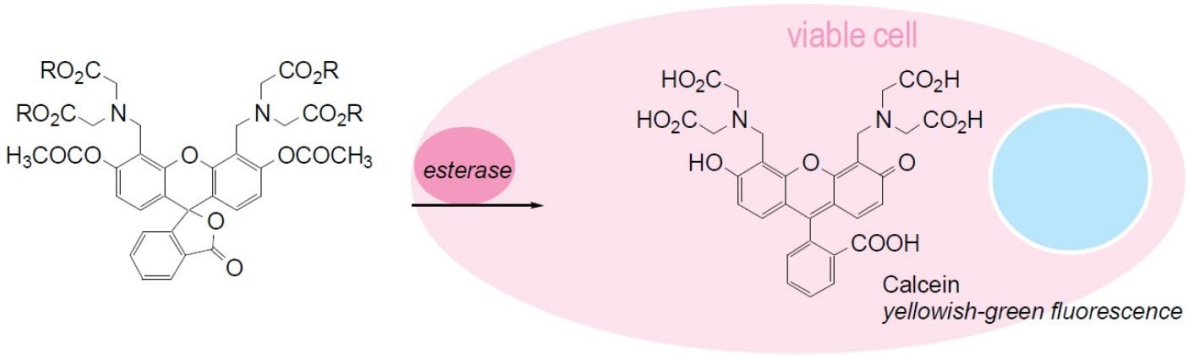

Fig. A.6 The staining mechanism of the calcein-AM agent.

A.3 Flow simulation

A.3.1 Software and computer

The flow simulation was achieved by the flow simulation software (ANSYS Fluent R19.0, ANSYS Inc. USA). The used computer has the following hardware: Inter®Core(TM) i7-9700 CPU @3.00 GHz 3.00 GHz; RAM (8.0 GB); OS Microsoft Windows 10 Professional 64 bit.

A.3.2 Simulation parameter

The physical parameters of used liquids are shown in **Table A.4**. The simulation parameters of the software are shown in **Table A.5**. The boundary condition for the inlet and outlet channel was set at constant velocity and free outlet, respectively.

Table A.4 Physical properties of used samples

	Material	Density [kg/m^3]	Viscosity [mPa·s]	Interfacial tension [N/m]	Contact angle [°]
Disperse phase	Na-alginate (3wt%)	1002	1500	0.032	140
Continuous phase	Corn oil	851	57		

Table A.5 Analysis condition using ANSYS

Time step size	3.3×10^{-5} to 1.0×10^{-4}
Number of time step	5000
Inlet boundary condition	Constant velocity
Wall boundary condition	No-slip
Outlet boundary condition	Free outlet

A.4 Peripheral equipment

A.4.1 Experimental setup

The schematic illustration of the experimental setup is shown in **Fig. A.7**. Gastight glass syringe was filled with the liquids and mounted on syringe pumps. The glass microfluidic chip was assembled in a stainless supporting holder and linked to syringes through polytetrafluoroethylene (PTFE) tubes and connectors. An optical microscope and a high-speed video camera were combined for flow observation.

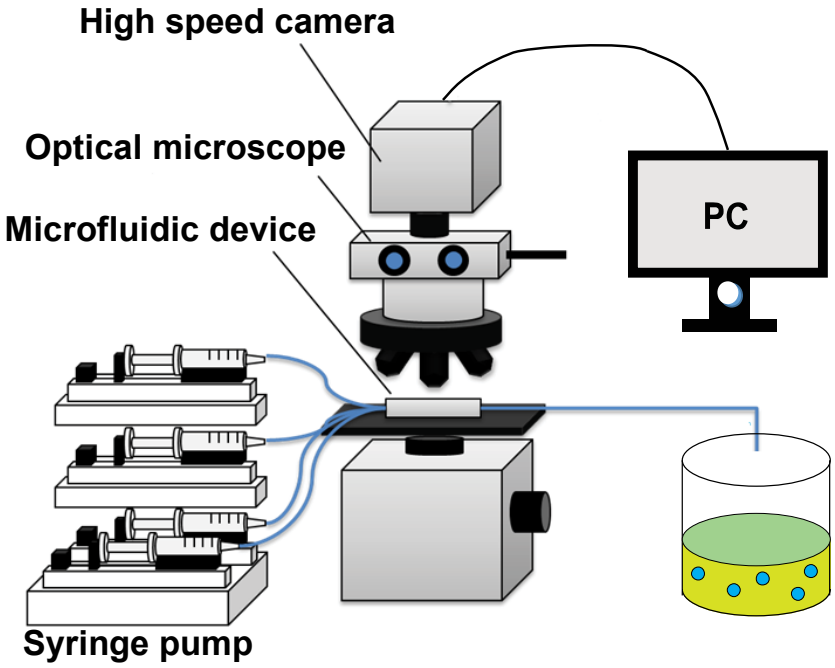

Fig. A.7 Schematic illustration of an experimental setup

A.4.2 Peripheral equipment of microchannel

(1) Connectors and tubes

The polytetrafluoroethylene (PTFE) connectors and tubes (FLON Industry, Tokyo, Japan) which are pervasively used in the high-performance liquid chromatography (HPLC) process were used to connect the syringes and stainless supporting holder. For the supporting holder used in **Chapters 2,3,4**, the connector with a screw size of No. 10-32UNF was used for linking the supporting holder. Whereas for the supporting holder used in **Chapter 5**, the connector with a screw size of 1/4-28UNF was used. The connectors with Luer-lock adaptor (screw size: No.

1/4-28UNF) were used for linking the syringes (**Fig. A.8**).

The input PTFE tubes had two sizes: one with an inner diameter of 0.5 mm and outer diameter of 1.59 mm (F-8008-002, **Chapter 2,3,4**), the other with an inner diameter of 2.0 mm and an outer diameter of 3.0 mm (F-8006-009, **Chapter 5**) and the output PTFE tubes with an inner diameter of 0.8 mm and outer diameter of 1.59 mm (F-8008-003).

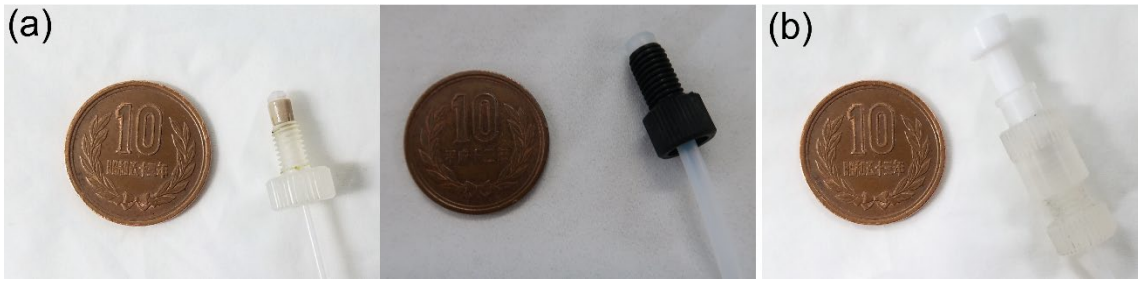

Fig. A.8 HPLC connectors for linking the (a) holder and (b) syringes.

(2) Supporting holder

The assembled microfluidic device consists of a glass chip, supporting holder and PTFE connectors and tubes are shown in **Fig. A.9**. The stainless supporting holder is comprised of SUS304. Screws (sizes: NO. 10-32UNF) fitting the HPLC connectors were fabricated on the side of the holder and connected with the vertical holes (Φ1) which were fabricated from the top side. A backup ring comprised of PTFE (2.5 mm outer diameter, 1.0 mm inner diameter, 1.0 mm thickness) was used to adjust the alignment between the through-holes of the supporting holder and microfluidic chip. The chip and holder were connected tightly under the pressure added by the screw.

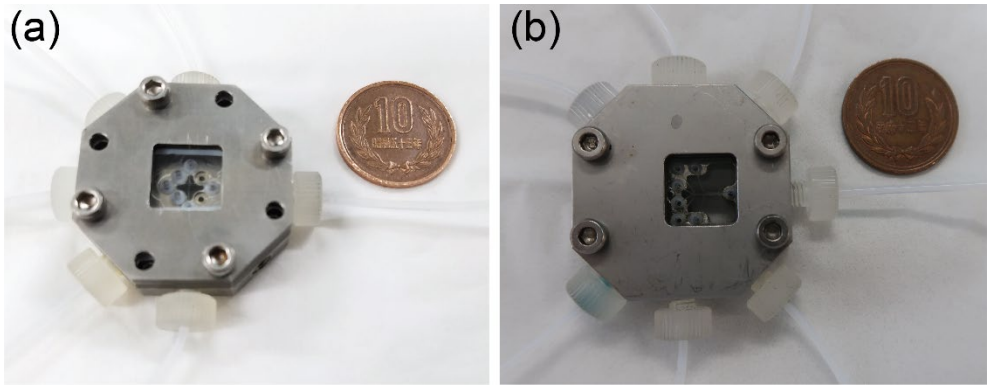

Fig. A.9 Assembled microfluidic device. (a) A microfluidic device used in **Chapters 2,3,4**. (b) A microfluidic device used in **Chapter 5**.

A.4.3 Fluid infusion system

(1) Glass syringe

Gastight glass syringe (1000 series, Hamilton Company, NV, USA) are shown in **Fig. A.10**. Two glass syringe types with a total volume of 1 mL and 10 mL with Luer-lock adaptor were used here. A syringe of 1 mL volume type to infuse the disperse phase and a 10 mL volume type was used to infuse the continuous phase and reactant emulsion phase.

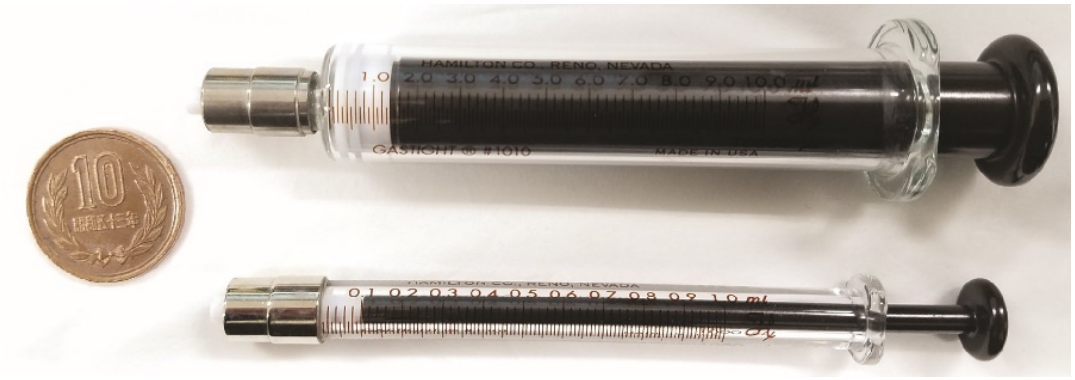

Fig. A.10 Gastight glass syringe of total volume 1 mL (bottom) and 10 mL (top).

(2) Plastic syringe

The plastic syringe (SS-20ESZ and SS-50ESZ, Terumo, Tokyo, Japan) are shown in **Fig. A.11**. Two plastic syringe types with a total volume of 20 mL and 50 mL were used. A syringe of 20 mL type was used to wash and modify the surface condition of the microchannels and a 50 mL type to infuse the reactant $CaCl_2$ emulsion phase in **Chapter 5**.

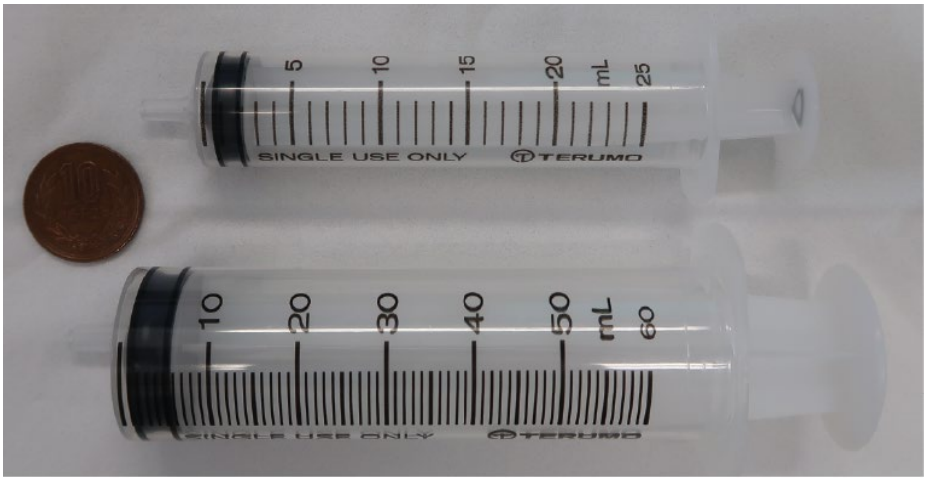

Fig. A.11 Plastic syringe of total volume 20 mL (top) and 50 mL (bottom).

(3) Syringe pump

Syringe pumps (KDS 200 and KDS LEGATO 200, KD Scientific Inc., PA, USA) were used to infuse the fluid. The specifications are shown in **Table A.6**.

Table A.6 The specifications of syringe pumps

	KDS 200	**KDS LEGATO 200**
Pump type	Push	Push
Syringes	10 μl ~ 140 ml	0.5 μl ~ 140 ml
Dimensions	28×23×15 cm	27.94×25.4×8.89 cm
Weight	4 kg	4.9 kg
Power	176 N (18 kgf)	332 N (34 kgf)
Max. step rate	1600 (0.5 step)/sec	26 μsec/μstep
Min. step rate	1 (0.0625 step)/120 secs	27.5 sec/μstep
Accuracy	±1 %	±0.35 %
Reproducibility	±0.1 %	±0.05 %
Max. flow rate	8700 ml/h (140 ml syringe)	13258 ml/h (140 ml syringe)
Min. flow rate	0.001 μl/h (10 μl syringe)	0.0003 μl/h (0.5 μl syringe)

A.4.4 Observation system

(1) Optical microscope

An upright optical microscope (BX-51, Olympus, **Fig. A.12**) was used for observation. The light source was a halogen lamp (U-LH100-3, Olympus).

(2) High-speed camera

A high-speed video camera (Fastcam Mini AX50, Photron) was mounted on the optical microscope for flow observation. Software ImageJ was used to calculate the size and roundness of precursor droplets and hydrogels. Below is the calculation process:

While taking the pictures of droplets and hydrogels, the resolution of the high-speed camera was set as 640×640, the pixel size is 20 μm×20 μm. So, the actual length L (μm) of each pixel is according to the equation:

$$L = 20/(0.5 \times \mathrm{a}) \qquad (2\text{-}1)$$

0.5 is the ratio of adapter between the high-speed camera and microscope, a is the ratio of microscope lens.

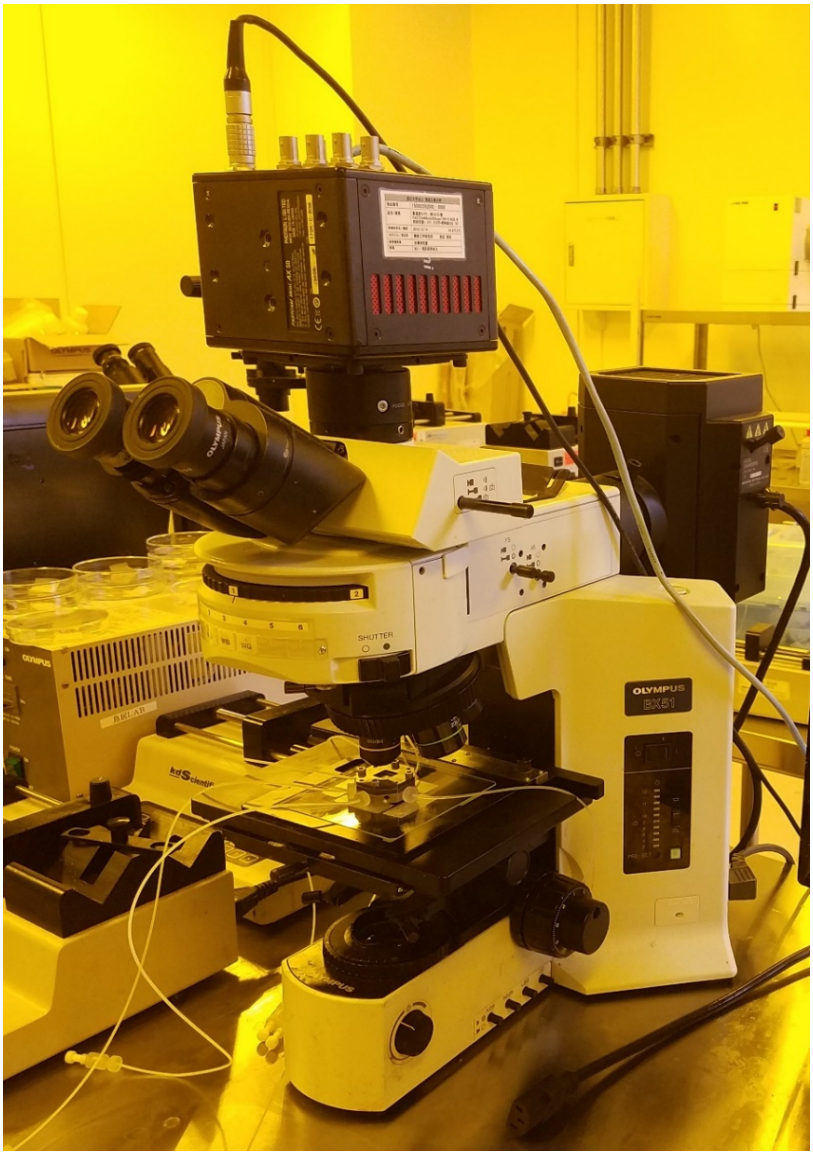

Fig. A.12 Optical microscope (BX-51, Olympus)

A.4.5 Other equipment

(1) Mechanical homogenizer

The reactant $CaCl_2$ emulsion was prepared by a homogenizer (T10 basic ULTRA-TURRAX, IKA, Germany, **Fig. A.13**) at 30000 rpm for 3 minutes.

Fig. A.13 Mechanical homogenizer (T10 basic ULTRA-TURRAX, IKA, Germany)

(2) Laser scattering particle size distribution analyzer

A laser scattering particle size distribution analyzer (Partica LA-960, HORIBA, Japan, **Fig. A.14**) was used to analyze the sizes of $CaCl_2$ emulsion droplets.

Fig. A.14 Laser scattering particle size distribution analyzer (Partica LA-960, HORIBA, Japan)

(3) Filtration system

A glass mesh holder (Glass Type KG-25, ADVANTEC, Japan, **Fig. A.15**) was assembled with a nylon mesh (42 μm×42 μm, Tokyo Screen, Japan) to separate hydrogels from $CaCl_2$ emulsion. Pure water was added to flush out the $CaCl_2$ emulsion in the glass holder. Hexane was subsequently added to wash out the residual corn oil. Then pure water was used to wash the hexane away. Finally, the hydrogels were dispersed in water in a petri dish for observation.

Fig. A.15 Glass mesh holder (Glass Type KG-25, ADVANTEC, Japan)

(4) Viscometer

The viscosities of the liquids were measured at 293 K by using a rotational viscometer (BL-type, Toki Sangyo, Tokyo, Japan, **Fig. A.16**).

Fig. A.16 Rotational viscometer (BL-type, Toki Sangyo, Tokyo, Japan)

(5) Contact angle meter

The surface tension between two immiscible liquids was measured by a contact angle meter (B100, Asumi Giken, Tokyo, Japan, **Fig. A. 17**).

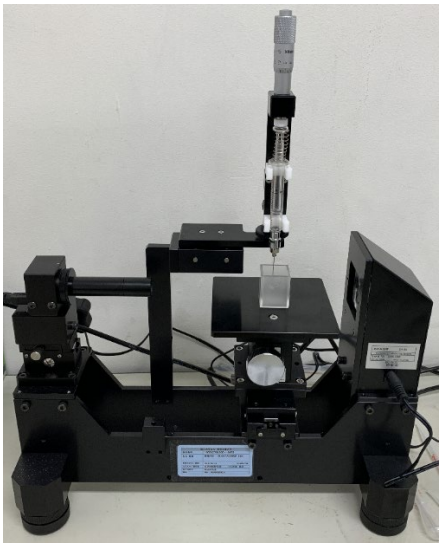

Fig. A. 17 Contact angle meter (B100, Asumi Giken, Tokyo, Japan)

(5) Scanning electron microscope

Scanning electron microscope (SEM, JSM-6610LA, JEOL, Japan, **Fig. A.18**) at 東京工業大学−技術部−すずかけ台分析部門 was used to observe the fabricated microchannel and dried hydrogel particles.

Fig. A.18 Scanning electron microscope (SEM, JSM-6610LA, JEOL, Japan)

(7) Plasma kit

The bonding between the PDMS chip and stainless module was achieved by the basic plasma kit (BP-1, Samco Inc., Kyoto, Japan, **Fig. A.19**)

Fig. A.19 Basic plasma kit (BP-1, Samco Inc., Kyoto, Japan)

(6) UV-Vis spectroscopy

Sustained release of encapsulated drug Irgarol was measured by UV-Vis spectroscopy. The UV-Vis spectroscopy setup (**Fig. A.20**) consists of a light source (DT-Mini-2, Ocean Optics, UK), a spectrometer (USB2000+, Ocean Optics, UK), a cuvette holder, and a glass cuvette (Z27667-7, Aldrich Chemical, Germany).

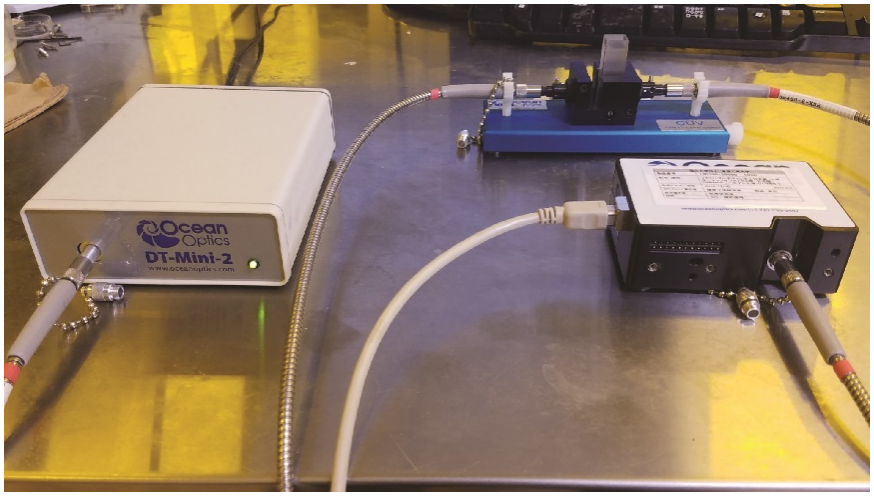

Fig. A.20 Assembled UV-Vis spectroscopy measurement equipment.

(8) Fourier transform infrared (FTIR) spectrophotometer

The FTIR spectrophotometer (IRAffinity-1, Shimadzu, Tokyo, Japan, **Fig. A.21**) at 東京工業大学−機械系分析室 was used to identify, analyze and define the synthesized materials in **Chapter 6**.

Fig. A.21 FTIR spectrophotometer (IRAffinity-1, Shimadzu, Tokyo, Japan)

(9) Oil bath

The oil bath (OB-200A, AS ONE, Osaka, Japan, **Fig. A. 22**) was used to warm up the bio-reagents to room temperature.

Fig. A. 22 Oil bath (OB-200A, AS ONE, Osaka, Japan)

(10) Centrifuge

The centrifuge (CN-2060, AS ONE, Osaka, Japan, **Fig. A. 23**) was used to separate the cells from the culture medium in 15 mL centrifuge tubes.

Fig. A. 23 Centrifuge (CN-2060, AS ONE, Osaka, Japan)

(11) Autoclave

The autoclave (NCC-1701B, AS ONE, Osaka, Japan, **Fig. A. 24**) was used to sterilize the equipment that used in cell culturing.

Fig. A. 24 Autoclave (NCC-1701B, AS ONE, Osaka, Japan)

(12) Carbon dioxide (CO_2) incubator

The CO_2 incubator (E-22, AS ONE, Osaka, Japan, **Fig. A. 25**) was used to culture the cells at 37℃ under a 5% CO_2 atmosphere.

Fig. A. 25 CO_2 incubator (E-22, AS ONE, Osaka, Japan).

(13) Clean bench

The cell culturing operation was done inside the clean bench (CT-600UVAD, AS ONE, Osaka, Japan, **Fig. A. 26**) to ensure a germ-free environment.

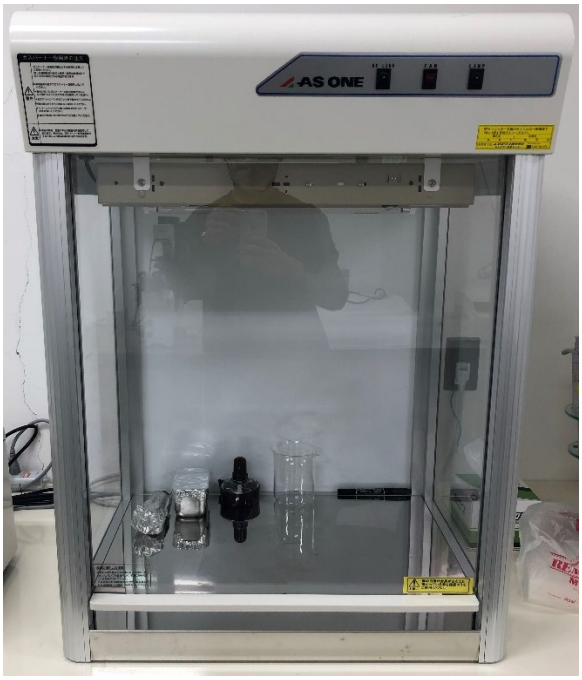

Fig. A. 26 Clean bench (CT-600UVAD, AS ONE, Osaka, Japan).

A.5 Reference

[1] Duffy D.C. Rapid prototyping of microfluidic system in poly(dimethylsiloxane). *Anal. Chem.* **1998,** 70, 4974–4984.

Acknowledgments

Working as a Ph.D. student at Tokyo Institute of Technology was a magnificent as well as challenging experience for me. In these priceless years as a Master and Doctor student in Nisisako lab. I feel so much indebted to many people who have instructed and favored me not only in terms of studying and researching but also in my daily life. It was hardly possible to thrive in my doctoral work without the precious support of these personalities.

My deepest gratitude goes first and foremost to Professor. Nisisako Takasi, my supervisor, for his valuable guidance, cheerful enthusiasm and, ever-friendly nature that I was able to complete my research work in a respectable manner. He has let me walk through all the stages of the writing of this thesis. Without his consistent and illuminating instruction, this thesis could not have reached its present form. I will never forget the kind suggestions, helpful comments, and also useful advice for my life in Japan during this period of my obtaining the doctor degree. In addition, I always appreciate his guidance that helps me cultivate critical and logical thinking which is precious to my future research life.

Secondly, I would like to express my heartfelt gratitude to Assistant Professor Tottori Naotomo, who helped me not only in his doctor degree period but also in the two years as Assistant Professor. Great thanks to his help and guidance in seminars, conferences, and everyday experiments.

Third, I would like to thank the Semiconductor and MEMS Process Division, Design and Manufacturing Division, Open Facility of Tokyo Tech. for the device fabrication. Also the Materials Analysis Division, Open Facility of Tokyo Tech. for the sample analysis.

Furthermore, my great thanks will give to the following professors who provide priceless advice and guidance when I prepare this thesis and presentation (in alphabetical order):

Tokyo Tech. Institute of Innovative Research, Prof. Hatsuzawa Takeshi.

Tokyo Tech. School of Mechanical engineering, Assoc. Prof. Ishida Tadashi.

Tokyo Tech. Institute of Innovative Research, Prof. Shinshi Tadahiko.

Tokyo Tech. Institute of Innovative Research, Prof. Yanagida Yasuko.

I also want to thank all the students of Nisisako lab for their help in daily life.

Last my thanks would go to my beloved parents for their loving accompanies, considerations, and great confidence in me all through these years. Especially to my dad who passed away in

2020. I deeply regret that I was not by your side at that moment. Without your persistence and encouragement, I might give up my study three years ago. I will keep going and hope that I can meet your expectations one day.

January 2022

Tokyo, Japan

Achievements

Peer-Reviewed Journals (3)

Yingzhe Liu, Takasi Nisisako
Microfluidic generation of monodispersed Janus alginate hydrogels using calcium chloride emulsion reactant
(**accepted for publication**)

Yingzhe Liu, Takasi Nisisako
Microfluidic Encapsulation of Hydrophobic Antifouling Biocides in Calcium Alginate Hydrogels for Controllable Release
ACS Omega 5, pp. 25695-25703 (2020).

Yingzhe Liu, Naotomo Tottori, Takasi Nisisako
Microfluidic synthesis of highly spherical calcium-alginate hydrogels based on external gelation using emulsion reactant
Sensors and Actuators B-Chemical. 283, pp. 802-809 (2019).

International Conferences (5)

(Oral Presentation)
Liu Yingzhe, Takasi Nisisako
Functional Janus Alginate Hydrogels Synthesized via a Microfluidic Emulsion-based External Gelation
The 18th International Conference on Precision Engineering (ICPE), H-1-3, Online, November 24-26, 2020.

(Oral Presentation)
Liu Yingzhe, Takasi Nisisako
Microfluidic emulsion-based external gelation to design magnetic Janus hydrogels
International Chemical Engineering Symposia 2020, No. 419, T313, Osaka, Japan, March 15-

17, 2020.

(Oral Presentation)

Liu Yingzhe, Takasi Nisisako

Hydrogel microparticles for anti-fouling application synthesized via in-situ microfluidic method.

The 8th International Conference of Asian Society for Precision Engineering and Nanotechnology (ASPEN), D32, Matsue, Japan, November 12-15, 2019.

(Oral Presentation)

Takasi Nisisako, **Yingzhe Liu**

Microfluidic synthesis of spherical calcium-alginate hydrogels for antifouling herbicide application.

7th International Conference on Small Science (ICSS), Hawaii, USA, March 26-30, 2019.

(Poster Presentation)

Yingzhe Liu, Naotomo Tottori, Takasi Nisisako

Microfluidic external gelation of shape-controlled calcium-alginate hydrogels for drug encapsulation and sustained release.

22nd International Conference on Miniaturized Systems for Chemistry and Life Sciences(MicroTAS2018), pp.2183-2184, Kaohsiung, Taiwan, November 11-15, 2018.

Domestic Meetings (3)

(Oral Presentation)

Yingzhe Liu, Takasi Nisisako

Microfluidic synthesis of highly spherical hydrogels for encapsulation and sustained release of antifouling drug.

2019 年度精密工学会春季大会，東京電機大学千住キャンパス（東京），3/13-15 (2019).

劉英哲，鳥取直友，西迫貴志

Spherical calcium alginate microgels synthesized using a microfluidic chip.

2018 年度精密工学会春季大会，H21，p. 487-488，中央大学後楽園キャンパス（東京），

3/15-17 (2018).

(Poster Presentation)

Yingzhe Liu, Naotomo Tottori, Takasi Nisisako

Spherical calcium alginate microgels synthesized via in-situ emulsion-based external gelation.

化学とマイクロ・ナノシステム学会第 37 回研究会（CHEMINAS37th）, 2P26, p.58，

産業技術総合研究所つくばセンター（つくば），5/21-22 (2018).